Impurity Effects in Antiferromagnetic Quantum Spin-1/2 Chains

Sebastian Eggert

University of British Columbia, Vancouver, Canada

1994

Abstract

We calculate the effects of a single impurity in antiferromagnetic quantum spin-1/2 chains with the help of one-dimensional quantum field theory and renormalization group techniques in the low temperature limit. We are able to present numerical evidence from exact diagonalization, numerical Bethe ansatz, and quantum Monte Carlo methods, which support our findings. Special emphasis has been put on impurity effects on the local susceptibility in the chain, because of the experimental relevance of this quantity. We propose a muon spin resonance experiment on quasi one-dimensional spin compounds, which may show some of the impurity effects.

Table of Contents

Acknowledgements

I would like to give my special thanks to my advisor, Ian Affleck for his patience in many long and helpful discussions. Without him and his extraordinary ability to pass on his vast knowledge this thesis would not have been possible. I am also very grateful for interesting discussions with Eugene Wong, Rob Kiefl, Bill Buyers, and Philip Stamp which were helpful in preparing this thesis. Special thanks also go to a number of people in the physics department with whom I had the pleasure to interact with in the past years: Junwu Gan, Arnold Sikkema, Jacob Sagi, Gordon Semenoff, Erik Sørensen, Birger Birgerson, and Michel Gingras.

At this point I would also like to acknowledge some of my former advisors, mentors, and teachers which made a special contribution in my course of studies: Herr Unger, Ebs Hilf, Alexander Rauh, Glen Rebka, Lee Schick, and Ramarao Inguva.

Chapter 1

Introduction

Considerable attention has been focused on spin-1/2 chains since Bethe's original work more than 60 years ago[1]. The large interest in these relatively simple many-body quantum mechanical systems is no surprise, since they exhibit many fascinating cooperative phenomena which may be shared by more complex models. The Bethe ansatz has been refined over the years[2], and thermodynamic quantities can be calculated exactly for a wide parameter range[3]. With the advent of conformal field theory and more computing power, we are now able to understand the model even on a more detailed level as presented in this thesis. Another goal of this thesis is to link this theoretical knowledge to real experimental systems with special emphasis on impurity effects.

1.1 The Hamiltonian

We can model the magnetic properties of insulators very well by describing the exchange coupling between orbital spins in terms of an anisotropic Heisenberg coupling. It is possible to have quasi one-dimensional spin systems, in which the spins form "chains" along one crystal axis in the sense that the exchange coupling is much stronger between neighboring spins within the chain compared to the coupling $J_\perp$ between spins of different chains. If we neglect this interchain coupling we can describe the model by the Hamiltonian

$$H = \sum_{i=1}^{l-1} [\frac{J}{2} (S_i^+ S_{i+1}^- + S_i^- S_{i+1}^+) + J_z S_i^z S_{i+1}^z], \tag{1.1}$$

where S_i^+, S_i^- are the usual spin-1/2 raising and lowering operators at site i, l is the total number of sites, and J is taken to be positive. We may choose open boundary conditions where the ends at the 1^{st} and l^{th} site are free, or we may impose periodic boundary conditions where the ends are coupled with the same coupling constants, J and J_z.

Some materials are known to exist for spin-1/2 which exhibit this one-dimensional behavior to various degrees (e.g. $KCuF_3$[4] and CPC[5]). The ratio $J/J_\perp$ is a measure of the one-dimensional properties of the material since three dimensional Néel ordering will occur for low temperatures $T < T_N$, $T_N \propto J_\perp$[6]. In some materials a spin-Peierls transition to a dimer phase may occur instead if the phonon-spin coupling is strong. Typically the exchange coupling J is of the order of $20 - 1000K$, while the ordering temperature T_N is at least one order of magnitude smaller. Experimental results in $KCuF_3$[4] and CPC[5] are reported to agree well with the prediction of the Hamiltonian in equation (1.1) at the isotropic point $J \approx J_z$. Both J and $J_\perp$ arise from an exchange integral since the dipole-dipole interaction is only in the mK range. We also neglected the spin-orbit coupling which is generally also much smaller than the exchange coupling. The effect of a spin-orbit coupling can be described by a single-ion anisotropy of the form $(S^z)^2$ in the Hamiltonian, which reduces to a trivial c-number for spin-1/2.

1.2 Impurities

The main goal of this thesis is to provide a good understanding of impurity effects in spin-1/2 chains. The study of impurities has always been a large part of solid state physics, because there are many cases where impurities produce very interesting effects and may even dominate the behavior of the system. The best known examples may be semiconductor doping, the Kondo effect, and high temperature superconductors.

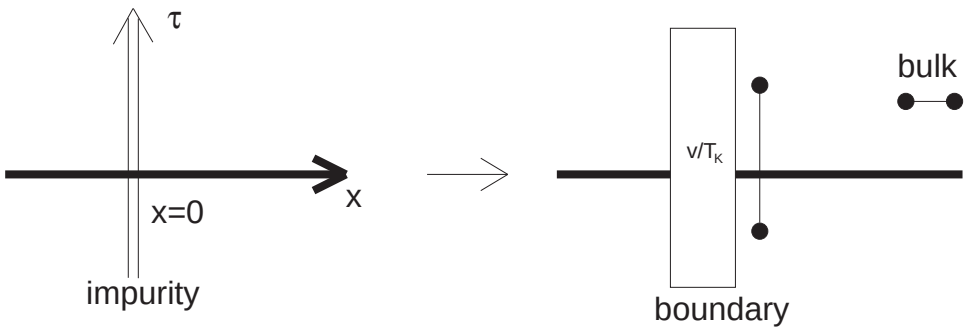

Figure 1.1: An impurity breaks conformal invariance and renormalizes to a boundary condition.

Recently, there has been an increased theoretical interest in quantum impurity problems which can be described by (1+1) dimensional conformal field theories. The resulting theory of boundary critical phenomena proved to be very successful in treating a variety of problems[8], with the Kondo problem being probably the most famous. It turns out that our model system can be regarded as one example of this technique, so it is instructive to present the central ideas of this approach at this point (see also reference [8]).

Let us start with some gapless, scale invariant system that can be described by a conformally invariant field theory. We may introduce a local, time-independent perturbation as shown in figure 1.1, which represents the impurity in the system and breaks the conformal invariance. It also creates a new energy scale in the system, which depends on the initial strength of the perturbation and on the scaling dimensions of the perturbing operators in the field theory. This energy scale is defined as the temperature where we expect a breakdown of perturbation theory, which is often called T_K in analogy with the Kondo effect. It is reasonable to assume that the system will still be described by the conformal field theory far away from the impurity, i.e. outside a "boundary layer" which is defined by the new energy scale in the system i.e. with width v/T_K, where v is the

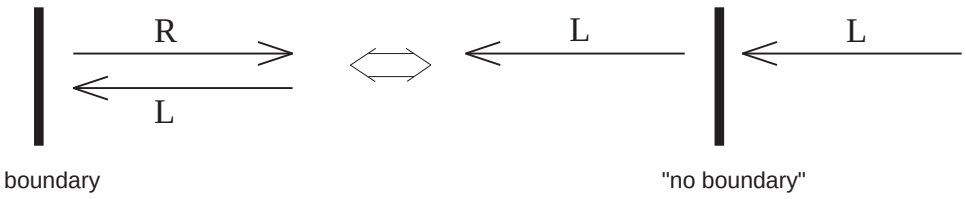

Figure 1.2: An analytic continuation of left movers in terms of right movers to the negative half axis effectively removes the boundary and restores conformal invariance.

effective speed of light of the field theory.

The system outside the boundary layer may still be affected by the impurity in a universal way, however, since it may effectively introduce a boundary condition on the system. The effective boundary conditions are created quite naturally, because the usual renormalization group ideas of perturbations in scale invariant systems apply. We expect a relevant impurity perturbation to renormalize from a weak coupling limit to a strong or intermediate coupling limit as the temperature is lowered. The weak coupling limit recovers the original boundary condition of the unperturbed system, while the strong (infinite) coupling limit can most likely be described by some other (e.g. fixed) boundary condition as indicated in figure 1.1. In this case we expect to find universal correlation functions for points close to the impurity compared to their relative distance (but outside the boundary layer v/T_K as shown in figure 1.1). These boundary correlation functions are in general different from the correlation functions in the bulk. The cross-over temperature between the two boundary conditions is simply given by the original energy scale T_K that has been created by the perturbation.

One important point of the theory is the fact that a fixed boundary condition is still consistent with conformal invariance, although it seems to break translational invariance. As an example consider a fixed boundary condition where some quantum field has been set to zero $\phi(0) = \phi_L(0) + \phi_R(0) \equiv 0$. An analytic continuation to the negative half axis

of the left moving field in terms of the right moving field allows us to effectively get rid of this boundary condition for the newly defined left moving field $\phi_L(-x) \equiv \phi_R(x),\ x > 0$ as shown in figure 1.2.

Although we will *not* use the theory of boundary critical phenomena to its full extent, we will recover the same results in our analysis of impurities. The reader may understand some of the presented ideas better once they are explained with the example of the spin-1/2 chain later in this thesis.

As will be shown in chapter 4, we can understand the effect of impurities in these systems very well with the help of the field theoretical analysis. In all cases, we find that any impurity renormalizes to an effective boundary condition on the bulk system at zero temperature. An effectively *decoupled* spin may be left over and there might be impurity corrections to thermodynamic quantities. While extensive quantities generally scale with the size of the system, the impurity contributions are independent of the length l of the chain. These findings are analogous to those of the Kondo effect to some extent.

1.3 Experimental Relevance

To detect these impurity effects in experimental systems, we have to overcome some difficulties. Since the predicted corrections to thermodynamic quantities scale with the impurity density, we will generally need a macroscopic number of defects, and even then it will be difficult to extract the part of the signal which is due to the impurities. Moreover, we expect that impurities will affect each other in a strongly correlated system like the spin-1/2 chain[7]. Instead of making a global measurement on thermodynamic quantities, we would therefore ideally like to make a measurement only locally, close to an isolated impurity. In this case, we expect a strong effect since the impurity will effectively play the role of a boundary condition on an otherwise unperturbed system at low temperatures.

Correlation functions will be changed drastically in this case as we will see later.

Out of the motivation to make a *local* measurement and perturbation, we developed the idea of a Muon Spin Resonance (μSR) experiment on quasi one-dimensional spin compounds. In this case the electric charge of the muon creates a defect in the material, while the muon also makes a measurement of the *local* susceptibility in its vicinity. The idea of the experimental setup will be discussed in more detail in section 5.4.

Even assuming that we are able to create an idealized impurity system, we still have the serious problem that our field theory predictions are strictly valid only at low temperatures where experimental materials might already behave three dimensionally. This problem can be overcome only to some extent by selecting materials that have very pronounced one-dimensional behavior (i.e. a large ratio $J/J_\perp$).

To give a more complete prediction of the outcome of the μSR experiments and to link theoretical calculations to the experimentally accessible temperature range, we performed extensive quantum Monte Carlo simulations. We can recover the predicted scaling at low temperatures, which we can link to the predicted experimental signal at higher temperatures. This gives some very encouraging results for the possible μSR experiment. The presented setup for the μSR experiment is of course only one possible way of detecting the predicted effects of impurities, which will be present in any quasi one-dimensional compound. This thesis will provide some interesting Monte Carlo data for the local susceptibility near an impurity. The reader is encouraged to use this data to develop other experimental methods to probe the predicted effects.

1.4 Outline

This thesis is organized as follows: A review of the derivation of the quantum field theory treatment for spin-1/2 chains is given in chapter 2 which is largely based on previous

references. We are able to extend this analysis to derive some results for finite size systems in chapter 3. Some renormalization group ideas will also be presented in chapter 3 in connection with finite size scaling. We use the field theory treatment to study the effects of impurities in the chain as discussed in chapter 4 in some detail, which is based on some of my previous work with Ian Affleck in reference [9]. Some finite size scaling results from numerical exact diagonalization studies are also presented to confirm our results.

The most recent results of our field theory analysis are predictions for the local and the bulk susceptibility of the spin chain in chapter 5. The impurity contributions to the susceptibility will be discussed in the language of boundary critical phenomena as described above. In the last chapter 6, we present the promising data from our Monte Carlo simulations, which also establishes our predictions for the μSR experiments. The results are discussed in the context of the expectations from the field theory.

Chapter 2

Theoretical Background

To establish our notation, we will review the field theoretical treatment of the spin-1/2 chain in this chapter. While we attempt to give a complete outline, it might be necessary to refer to reference [10] or appendix A in some cases, since it is not the primary goal of this thesis to present research on this aspect. We consider the antiferromagnetic spin-1/2 xxz chain with l sites, which is described by the Hamiltonian in equation (1.1).

2.1 From the Lattice Model to the Quantum Field Theory

We first apply the Jordan-Wigner transformation by expressing the spin operators in terms of spinless fermion annihilation and creation operators at each site[11]:

$$\begin{aligned} S_i^z &= \psi_i^\dagger \psi_i - \frac{1}{2} \\ S_i^- &= (-1)^i \psi_i \exp\left(i\pi \sum_{j=1}^{i-1} \psi_j^\dagger \psi_j\right) \end{aligned} \tag{2.2}$$

The exponential string operator cancels for nearest neighbor interactions on a chain, and we are left with a local Hamiltonian for interacting Dirac fermions by direct substitution into equation (1.1):

$$H = \sum_{i=1}^{l-1} [-\frac{J}{2} (\psi_i^\dagger \psi_{i+1} + h.c.) + J_z (\psi_i^\dagger \psi_i - \frac{1}{2})(\psi_{i+1}^\dagger \psi_{i+1} - \frac{1}{2})] \tag{2.3}$$

For $J_z = 0$, this is just a Hamiltonian for free fermions on a lattice. For this case, we obtain a cosine dispersion relation, and the ground state is a half-filled band with the Fermi points at $k_F = \pm\pi/2$. Expanding around this ground state, we can restrict

ourselves to low energy excitations by only considering those fermions which have wave-vectors close to $k_F = \pm\pi/2$:

$$\psi(x) \approx e^{ix\pi/2}\psi_L(x) + e^{-ix\pi/2}\psi_R(x) \tag{2.4}$$

The coordinate x is measured in units of the lattice spacing, and ψ_L and ψ_R contain only long wavelength Fourier modes.

We now take the continuum limit, and, up to terms with higher order derivatives, we are left with a (1+1) dimensional relativistic field theory of left- and right-moving fermions. The resulting Hamiltonian for the case $J_z = 0$ is:

$$H = v\int dx\left[\psi_R^\dagger i\frac{d}{dx}\psi_R - \psi_L^\dagger i\frac{d}{dx}\psi_L\right] \tag{2.5}$$

The J_z-interaction can be reintroduced in terms of the fermion currents $J_I = :\psi_I^\dagger\psi_I:$, $I = L, R$ by use of equation (2.4):

$$J_z\sum_i^{l-1} :\psi_i^\dagger\psi_i: :\psi_{i+1}^\dagger\psi_{i+1}: \rightarrow J_z\int dx[J_L^2 + J_R^2 + 4J_LJ_R - \{(:\psi_L^\dagger\psi_R:)^2 + h.c.\}] \tag{2.6}$$

Because of Fermi statistics, we can drop the last term for now. The first two terms can be rewritten to first order with the help of Wick's formula:

$$\begin{aligned} J_L(x)J_L(x+\delta) &\approx :J_L(x)J_L(x): + \text{const.} \\ &\quad + \frac{i}{2\pi\delta}[\psi_L^\dagger(x+\delta)\psi_L(x) - \psi_L^\dagger(x)\psi_L(x+\delta)] \\ &\approx -\frac{i}{\pi}\psi_L^\dagger\frac{d}{dx}\psi_L + \text{const.} \\ J_R(x)J_R(x+\delta) &\approx \frac{i}{\pi}\psi_R^\dagger\frac{d}{dx}\psi_R + \text{const.} \end{aligned} \tag{2.7}$$

With the use of those relations, we can rewrite the complete Hamiltonian in terms of the Fermion currents with a renormalized "speed of light" v:

$$H = v\pi\int dx[J_R^2 + J_L^2 + \frac{4J_z}{\pi v}J_LJ_R] \tag{2.8}$$

This model can now be transformed using the usual abelian bosonization rules[10]:

$$\begin{aligned} J_L &= \frac{1}{\sqrt{4\pi}}(\Pi_\phi - \frac{\partial\phi}{\partial x}) \\ J_R &= -\frac{1}{\sqrt{4\pi}}(\Pi_\phi + \frac{\partial\phi}{\partial x}) \\ \psi_R &= \text{const.}\exp(i\sqrt{4\pi}\phi_R) \\ \psi_L &= \text{const.}\exp(-i\sqrt{4\pi}\phi_L), \end{aligned} \tag{2.9}$$

where the constant of proportionality can be taken to be real, but cut-off dependent. The fields ϕ_L and ϕ_R are the left and right-moving parts of ϕ which can be defined in an infinite system as

$$\begin{aligned} \phi_L(x) &= \frac{1}{2}\phi(x) + \frac{1}{2}\int_{-\infty}^{x}\Pi_\phi(y)dy \\ \phi_R(x) &= \frac{1}{2}\phi(x) - \frac{1}{2}\int_{-\infty}^{x}\Pi_\phi(y)dy, \end{aligned} \tag{2.10}$$

where Π_ϕ is the momentum variable conjugate to ϕ. Left moving operators are functions of only $x+vt$, while right moving operators are functions of only $x-vt$. A dual field $\tilde{\phi}$ can also be defined in terms of those components:

$$\tilde{\phi} \equiv \phi_L - \phi_R \tag{2.11}$$

The resulting Hamiltonian is a non-interacting boson theory

$$\mathcal{H} = \frac{v}{2}\left[(1-\frac{2J_z}{\pi v})\Pi_\phi^2 + (1+\frac{2J_z}{\pi v})\left(\frac{\partial\phi}{\partial x}\right)^2\right]. \tag{2.12}$$

However, the boson operators now have to be transformed by a canonical transformation to obtain a conventionally normalized theory:

$$\begin{aligned} \phi &\rightarrow \frac{\phi}{\sqrt{4\pi}R} \\ \Pi_\phi &\rightarrow \sqrt{4\pi}R\,\Pi_\phi \end{aligned} \tag{2.13}$$

$$R^2 = \frac{1}{4\pi}\sqrt{\frac{\pi v + 2J_z}{\pi v - 2J_z}} \approx \frac{1}{4\pi} + \frac{J_z}{2v\pi^2}. \tag{2.14}$$

This gives us the usual free boson Hamiltonian:

$$\mathcal{H} = \frac{v}{2}\left[(\Pi_\phi)^2 + (\frac{\partial\phi}{\partial x})^2\right] = v\left[T_L + T_R\right]. \tag{2.15}$$

Here $T_{L,R}$ are the left- and right-moving parts of the free Hamiltonian

$$T_{R,L} \equiv \left(\frac{\partial\phi_{R,L}}{\partial x}\right)^2 = \frac{1}{4}\left(\frac{\partial\phi}{\partial x} \pm \Pi_\phi\right)^2. \tag{2.16}$$

By combining the spin to fermion and fermion to boson transformations, we obtain the continuum limit representation for the spin operators:

$$\begin{aligned} S^z_j &\approx \frac{1}{2\pi R}\frac{\partial\phi}{\partial x} + (-1)^j \text{const. } \cos\frac{\phi}{R} \\ S^-_j &\propto e^{-i2\pi R\tilde{\phi}}\left[\cos\left(\frac{\phi}{R}\right) + \text{const.}(-1)^j\right]. \end{aligned} \tag{2.17}$$

Altogether, this is a very nice result, because we are now in the position to calculate any expectation value of spin operators in terms of free boson Green's functions.

Note, that all physical operators are invariant under a shift of the boson

$$\begin{aligned} \phi &\equiv \phi + 2\pi R \\ \tilde{\phi} &\equiv \tilde{\phi} + 1/R. \end{aligned} \tag{2.18}$$

Therefore, the boson ϕ must be thought of as a periodic variable measuring arc-length on a circle of radius R.

So far, we have treated the J_z interaction perturbatively so that the rescaling equations (2.14) are only accurate to lowest order in J_z/J. Fortunately, the "boson radius" R and the "spin-wave velocity" v have been analytically determined with the help of the Bethe ansatz[12, 13]. After defining a new variable θ,

$$\cos\theta \equiv \frac{J_z}{J}, \tag{2.19}$$

the two quantities are conveniently expressed as

$$\begin{aligned} v &= \frac{J\pi \sin\theta}{2\theta} \\ R &= \sqrt{\frac{1}{2\pi} - \frac{\theta}{2\pi^2}}, \end{aligned} \tag{2.20}$$

which agrees to first order in $J_z/J \approx \pi/2 - \theta$ with the perturbative field theory calculations in equation (2.14).

2.2 Symmetries

There are two independent discrete symmetries of the spin chain which we can identify in the continuum limit. The first one is translation by one site, T. This appears as a discrete symmetry independent of translation in the continuum limit, simply interchanging even and odd sublattices. By comparing with equation (2.17) we see that it corresponds to:

$$T : \phi \to \phi + \pi R,\ T : \tilde{\phi} \to \tilde{\phi} + 1/2R. \tag{2.21}$$

The second one is site parity, P_S, i.e. reflection of the whole chain about a site. Note, that this *does not* interchange even and odd sub-lattices. Thus it must map the spin operators into themselves. Since parity interchanges left and right, ϕ and $\tilde{\phi}$ transform oppositely. We see that the correct transformation is

$$P_S : \phi \to -\phi,\ P_S : \tilde{\phi} \to \tilde{\phi}. \tag{2.22}$$

There is a third discrete symmetry, link parity, P_L, i.e. reflection about a link. However, this is not independent, but is a product of P_S and T. It corresponds to

$$P_L : \phi \to -\phi + \pi R,\ P_L : \tilde{\phi} \to \tilde{\phi} + 1/2R. \tag{2.23}$$

2.3 Correlation Functions

One of the first[13] and most important results of the field theory treatment is the calculation of spin correlation functions, which is not possible with Bethe ansatz methods. Using equation (2.17) and some results from appendix A it is straight forward to express the S^z Green's function as

$$\begin{aligned} G^z(x,t) &\equiv \langle S_0^z(0) S_x^z(t)\rangle \\ &= \frac{1}{4\pi^2 R^2} < \frac{\partial\phi(0,0)}{\partial x}\frac{\partial\phi(x,t)}{\partial x}\rangle \;+\; \text{const. } (-1)^x \langle \cos\frac{\phi(0,0)}{R}\cos\frac{\phi(x,t)}{R}\rangle \\ &= \frac{-1}{16\pi^3 R^2}\left(\frac{1}{(x+vt)^2}+\frac{1}{(x-vt)^2}\right) \;+\; \text{const. } \frac{(-1)^x}{(x^2-v^2t^2)^{1/4\pi R^2}}. \end{aligned} \tag{2.24}$$

The separation into uniform and alternating parts is taken from equation (2.17), which also implies that the spin operators can be separated into uniform and alternating parts. This seems to be a valid assumption in the long wave-length limit, but the separation is not unique on small length scales. Note, that the cross terms of the alternating and uniform parts of S^z in equation (2.17) have a vanishing expectation value as they should. In a scale invariant system we can define a scaling dimension $d \equiv d_L + d_R$ of an operator $\mathcal{O} = \mathcal{O}_L\mathcal{O}_R$ by the auto-correlation function

$$\langle \mathcal{O}(x,t)\mathcal{O}(0,0)\rangle = \langle \mathcal{O}_L(x+vt)\mathcal{O}_L(0)\rangle\langle \mathcal{O}_R(x-vt)\mathcal{O}_R(0)\rangle \propto \frac{1}{|x+vt|^{2d_L}}\frac{1}{|x-vt|^{2d_R}}. \tag{2.25}$$

According to equation (2.24) the scaling dimension of the uniform part of the S^z operator is always one, while the exponent of the alternating part decreases with anisotropy. At the isotropic point the alternating scaling dimension is $d = 1/2$, while we recover $d = 1$ at the xx point (free fermions).

Likewise, we can calculate the $S^{\pm}$ Green's function:

$$G^{\pm}(x,t) \equiv \langle S_0^+(0) S_x^-(t)\rangle \tag{2.26}$$

$$\propto \quad (x^2 - v^2t^2)^{-(1/R-2\pi R)^2/4\pi} \left(\frac{1}{(x+vt)^2} + \frac{1}{(x-vt)^2} \right) + \text{const.} \; \frac{(-1)^x}{(x^2 - v^2t^2)^{\pi R^2}}$$

Now the uniform scaling dimension decreases from $d = 5/4$ at the xx-model, to $d = 1$ at the Heisenberg point, while the alternating dimension increases from 1/4 to 1/2. At the Heisenberg point, the expressions for the two Green's functions G^z and $G^{\pm}$ are identical, as expected.

The scaling dimensions at the xx-point (free fermions) agree with previous results from rigorous methods[14]. Extensive numerical studies at the Heisenberg point show that the predicted exponents are correct there as well[15, 16] up to logarithmic corrections. The constant of proportionality of the alternating part in equation (2.24) has been estimated numerically to be const. ≈ 0.5[16].

Chapter 3

Scaling and Finite Size Effects

So far we have treated the spin chain with a theory which used the implicit assumption that we are in the limit of infinite length and very low temperatures. It is now useful to extend this theory to make useful predictions on finite size systems.

3.1 Boundary Conditions

To identify possible fixed points, we need to uncover the corresponding boundary conditions on the boson in the continuum limit.

3.1.1 Periodic boundary conditions

To get periodic boundary conditions, we can define $\vec{S}_0 \equiv \vec{S}_l$ and let the sum in equation (1.1) run from 0 to l. For the fermions, this condition translates into periodic or antiperiodic boundary conditions, depending on the total number of fermions[11]. It is clear from equation (2.17) that the boundary conditions on the boson are given by

$$\begin{aligned} \phi(l) &= \phi(0) + 2\pi R\mathcal{S}^z \\ \tilde{\phi}(l) &= \tilde{\phi}(0) + m/R, \end{aligned} \tag{3.27}$$

where m and $\mathcal{S}^z$ have to be integer for even length l and half-odd-integer for odd length l. We can identify $\mathcal{S}^z$ to be the z-component of the total spin by integrating equation(2.17):

$$\mathcal{S}^z \equiv \sum_i S_i^z = \frac{1}{2\pi R}(\phi(l) - \phi(0)) \tag{3.28}$$

As expected, $\mathcal{S}^z$ is integer or half-odd-integer for an even or odd length chain, respectively. There is no immediate physical interpretation for m other than that it represents a conserved quantity with integer or half-odd-integer value [see also equation (3.42) later].

3.1.2 Open boundary conditions

The case of free ends is slightly more subtle. One way of dealing with it is to introduce two additional "phantom sites" at 0 and $l+1$ and let the sum of the first term in equation (2.3) run from 0 to l, and then impose vanishing boundary conditions on ψ_0 and ψ_{l+1}. This imposes conditions on the continuum limit left and right moving Fermion fields:

$$\begin{aligned} \psi_L(0) + \psi_R(0) &= 0 \\ \psi_L(l+1) + (-1)^{l+1}\psi_R(l+1) &= 0 \end{aligned} \tag{3.29}$$

Using equations (2.4) and (2.9) and taking into account the correct commutation relations in equation (A.106), we conclude that the correct boundary conditions on the bosons are

$$\begin{aligned} \phi(0) &= \pi R/2 \\ \phi(l+1) &= \pi R/2 + 2\pi R\mathcal{S}^z, \end{aligned} \tag{3.30}$$

where $\mathcal{S}^z$ is integer for l even or half-odd-integer for l odd. As expected, this condition is *not* compatible with site (link) parity for an even (odd) number of sites.

At first sight, these conditions do not seem to correspond to conformally invariant boundary conditions because they break translational invariance, but we can rewrite them in terms of left- and right-movers

$$\phi_L(0,t) = \pi R/2 - \phi_R(0,t). \tag{3.31}$$

Since ϕ_L is a function only of $x+vt$ and ϕ_R only of $x-vt$, we can define ϕ_L for negative values of x by regarding ϕ_R as an analytic continuation:

$$\phi_L(-x,t) \equiv -\phi_R(x,t) + \pi R/2, \qquad x > 0. \tag{3.32}$$

The condition at $l+1$ then becomes

$$\phi_L(l+1,t) = -\phi_R(l+1,t) + \pi R/2 + 2\pi R\mathcal{S}^z = \phi_L(-l-1,t) + 2\pi R\mathcal{S}^z. \tag{3.33}$$

We therefore recover the usual periodic or antiperiodic boundary conditions, depending on whether l is even or odd. This is in complete agreement with the discussion in section 1.2 and figure 1.2. The right moving channel ϕ_R has been replaced by an analytical continuation of the left moving field ϕ_L to the negative half axis. Since ϕ_L has now twice the range $2l$ we have the same degrees of freedom as before, but the left moving field has the usual periodic (conformally invariant) boundary conditions. It appears as if we have gotten rid of the fixed boundary condition altogether.

One may ask at this point how the boundary correlation functions can be different after we have effectively recovered periodic boundary conditions and translational invariance. The reason is that all physical operators that were previously expressed in terms of left and right movers are now written in terms of left-movers only. The spin operators therefore become non-local expressions because they will be a function of both $\phi_L(x)$ and $\phi_L(-x)$. To understand the effect on the boundary scaling dimensions, it is instructive to consider the staggered part of the spin-spin correlation function at the Heisenberg point as an example. This is most easily calculated for S^- by using

$$S^-(x) \propto (-1)^x e^{-i\sqrt{2\pi}[\phi_L(x,t)+\phi_L(-x,t)]}. \tag{3.34}$$

The two-point Green's function for $\langle S^-S^+\rangle$ now becomes a four-point function for the left-moving boson, giving, according to equation (A.105):

$$\langle S^+(t_1,x_1)\cdot S^-(t_2,x_2)\rangle \propto (-1)^{x_1-x_2}\sqrt{\frac{x_1x_2}{[(x_1-x_2)^2-t_{12}^2][(x_1+x_2)^2-t_{12}^2]}}, \tag{3.35}$$

where we have set the spin-wave velocity to one and $t_{12} \equiv t_1 - t_2$. Note, that far from the boundary, when $x_1x_2 \gg |(x_1-x_2)^2 - t_{12}^2|$, we recover the bulk correlation

function $1/\sqrt{(x_1 - x_2)^2 - t_{12}^2}$, corresponding to a scaling dimension of $d = d_L + d_R = 1/2$ for the staggered spin operator. This also fixes the constant of proportionality in equation (3.35) to be const. ≈ 2[16] as mentioned at the end of section 2.3. However, the correlation function near the boundary (i.e. when $|t_{12}| \gg x_1, x_2$) takes the form $\sqrt{x_1 x_2}/|t_{12}|^2$, corresponding to a scaling dimension of $d = 1$ for the staggered boundary spin operator. In this case the scaling dimensions of the original left and right movers no longer add, since they are no longer independent as $x_1, x_2 \to 0$. In this case the different scaling dimension can formally be derived by the operator product expansion[17, 18].

3.2 Scaling and Irrelevant Operators

Although we were able to arrive at a free Hamiltonian in equation (2.15), it is important to realize that we neglected all terms which involved higher order derivatives or powers of fermions. These terms are irrelevant at low temperatures and long wavelengths, but they will give some corrections with characteristic scaling relations.

We can study these corrections systematically by classifying operators in the Hamiltonian density by their scaling dimension. We see that the free Hamiltonian density has a scaling dimension of $d = 2$ as it should since its integral has to have units of energy. This is assuming that in a scale invariant theory the scaling dimension d in equation (2.25) is the only quantity that determines the units of the corresponding operator. If we want to consider perturbing operators with scaling dimension other than $d = 2$, we need to consider that this operator must contain the appropriate powers of the ultraviolet cutoff Λ in so that its overall units work out to that of the Hamiltonian density. We may choose to define a dimensionless coupling constant $\lambda\Lambda^{d-2}$ by absorbing the appropriate powers of the cutoff. The renormalized coupling constant of an operator with scaling dimension $d \neq 2$ is therefore proportional to $\lambda\Lambda^{d-2}$, where λ is the original coupling parameter in

the Hamiltonian density. We therefore conclude that operators with dimension $d > 2$ are irrelevant when the cutoff is lowered, while operators with $d < 2$ will be relevant. If relevant operators are present we expect a breakdown of perturbation theory, and the system either develops a mass gap or renormalizes to a different fixed point. The ultraviolet cutoff Λ may be reduced to the larger of the temperature T or the inverse system size v/l. We expect that this results in an effective Hamiltonian that describes the macroscopic physics correctly and only depends on the energy scale T or v/l and the renormalized coupling constants.

Since the coupling constants always appear in the combination $\lambda\Lambda^{d-2}$ it is sufficient in most cases to only consider the perturbing operator with the lowest scaling dimension d (the "leading" operator). This determines the leading correction to the spectrum and other quantities which will be proportional to T^{d-2} or l^{2-d} to first order in perturbation theory. This can be generalized to higher orders in $\lambda\Lambda^{d-2}$ if higher order perturbation theory should be necessary to calculate the corrections.

We still need to consider the special case of perturbing operators with scaling dimension $d = 2$, which are marginal and can be categorized into three different cases. Sometimes we may absorb the operator exactly into the free Hamiltonian as we did with the J_z interaction in equations (2.6-2.8). We then refer to the operator as exactly marginal. If we cannot absorb the operator in the free Hamiltonian, we can calculate the rescaling equations from perturbation theory. If we have only one marginal coupling constant λ, the so called β-function has the generic form

$$\frac{d\lambda}{d\log\Lambda} = b\lambda^2, \tag{3.36}$$

where b is determined by the perturbation expansion. We see that whether the perturbation is relevant or irrelevant depends on the sign of b and λ. In particular, assuming

b is positive, we see that λ decreases when the cutoff is lowered, making a positive coupling λ marginally irrelevant and a negative coupling λ marginally relevant. It therefore depends on the initial sign of the bare coupling constant if the perturbation is relevant or irrelevant. Integrating equation (3.36) gives

$$\lambda = \frac{\lambda_0}{1 - \lambda_0 b \log \Lambda}, \tag{3.37}$$

where $\lambda_0 \equiv \lambda(\Lambda = 1)$. For the irrelevant case $\lambda_0 b > 0$, the renormalized coupling λ becomes smaller when the cutoff is lowered and "universal" logarithmic corrections of order $-1/b \ln \Lambda$ arise which are independent of λ_0 as $\Lambda \to 0$. If $\lambda_0 b < 0$, however, the perturbation is relevant and we expect a breakdown of perturbation theory when $\lambda_0 b \ln \Lambda \to 1$ (i.e. $T_K \propto e^{1/b\lambda_0}$ in terms of the cross-over energy scale).

Since the above arguments rely on the dimensional analysis of the operators, we can immediately deduce that a δ-function increases the scaling dimension by one. Therefore local operators are regarded to be marginal for $d = 1$ and irrelevant for $d > 1$. Likewise a derivative will always increase the effective scaling dimension of operators by one.

Let us study these renormalization group concepts with the example of the spin-1/2 chain. One perturbing operator comes from the last term in the J_z interaction of equation (2.6), which represents an Umklapp process for the fermions. We expect this to be the leading irrelevant operator, because it is the only four-Fermion operator, which we have not taken into account which does not include higher derivatives. After direct substitution of the bosonization formulas in equation (2.9) and the rescaling in equation (2.14), this operator is given by $\lambda \cos(2\phi/R)$ with some non-universal coupling constant λ. According to equation (A.104) its scaling dimension is given by $d = 1/\pi R^2$, which decreases with J_z and becomes $d = 2$ at the isotropic ("Heisenberg") point $J_z = J, \quad R = 1/\sqrt{2\pi}$, corresponding to a marginal irrelevant operator. For $J_z > J$, the operator will be relevant and drive the system into the Néel ordered phase.

Since the operator is marginally *irrelevant* at the Heisenberg point, the effective coupling constant $\lambda_{\text{eff}}(l)$ scales to zero only logarithmically slowly with length l, and logarithmic corrections arise[19]. This seems to make an accurate determination of the critical behavior from numerical finite-size scaling essentially hopeless, unless exponentially large chains can be studied. However, it is known from numerical studies that the marginal coupling constant λ can be decreased by adding a positive next-nearest-neighbor coupling J_2

$$H \rightarrow \sum_i (J\vec{S}_i \cdot \vec{S}_{i+1} + J_2 \vec{S}_i \cdot \vec{S}_{i+2}). \tag{3.38}$$

The coupling λ passes through 0 at a critical point, which has been estimated numerically to be at $J_2/J \approx 0.24$[20]. For larger J_2/J the operator is marginally *relevant* and the system renormalizes to a spontaneously dimerized phase. In particular, at $J_2/J = 1/2$, the exact ground-states are the nearest neighbor dimer states. Right at the critical point, the marginal operator is absent, and hence finite-size scaling becomes very accurate even with chains of modest lengths $l < 30$ since corrections drop off at least as fast as $1/l$. The model with the critical value of J_2/J represents the critical point to which the nearest neighbor model and all models with J_2 less than the critical value flow logarithmically slowly under renormalization. Therefore, we expect the behavior to be the same for the nearest neighbor model up to logarithmic corrections.

Now that we have managed to get rid of the leading irrelevant operator, we can consider higher order corrections. Since translational symmetry is broken for open boundary conditions, the local *energy* boundary operators $T_L(0)$ and $T_L(l)$ are allowed as a perturbation with some unknown coupling constant c

$$c\, T_L(0) = c \left(\frac{\partial \phi_L}{\partial x} \right)^2 (0) \;=\; \frac{c}{4} \left(\frac{\partial \phi}{\partial x}(0) - \Pi_\phi(0) \right)^2, \tag{3.39}$$

with an analogous expression for $T_L(l)$. Here, we have also used the analytic continuation in equation (3.32), which allows a description in terms of left-movers only. Local operators

are multiplied by a δ-function in the Hamiltonian density and will therefore be marginal for scaling dimension $d = 1$ and relevant for $d < 1$. The operator in equation (3.39) has dimension $d = 2$ for all values of J_z and should give corrections of order $1/l$ to the finite size spectrum, which will be discussed in the next section.

There is no such local operator for periodic boundary conditions, and the lowest dimension bulk operator is $T_L T_R$ of dimension $d = 4$, where $T_{L,R}$ have been defined in equation (2.16). Corrections to the finite size spectrum of the periodic chain should therefore be at least of order $1/l^2$. Note that the operator $\cos 4\phi/R$ is also allowed by the original symmetries of the Hamiltonian, but its scaling dimension of $d = 4/\pi R^2$ makes it much more irrelevant for all values of J_z.

3.3 Finite-size Spectrum

As discussed above, there are four different fixed points to consider, corresponding to the four different possible boundary conditions: periodic or open with even or odd length (i.e. $\mathcal{S}^z$ integer or half-odd-integer).

3.3.1 Periodic boundary conditions

We first consider the case of periodic boundary conditions on a spin-chain. This implies periodic boundary conditions on ϕ as in equation (3.27) and determines the mode expansion:

$$\phi(x,t) \;=\; \phi_0 + \hat{\Pi}\frac{vt}{l} + \hat{Q}\frac{x}{l} + \sum_{n=1}^{\infty} \frac{1}{\sqrt{4\pi n}} \left[e^{-\frac{2\pi i}{l} n(vt+x)} a_n^L \;+\; e^{-\frac{2\pi i}{l} n(vt-x)} a_n^R + \; h.c. \right]. \quad (3.40)$$

This implies that $\tilde{\phi}$ has the mode expansion

$$\tilde{\phi}(x,t) \;=\; \tilde{\phi}_0 + \hat{Q}\frac{vt}{l} + \hat{\Pi}\frac{x}{l} + \sum_{n=1}^{\infty} \frac{1}{\sqrt{4\pi n}} \left[e^{-\frac{2\pi i}{l} n(vt+x)} a_n^L \;-\; e^{-\frac{2\pi i}{l} n(vt-x)} a_n^R + \; h.c. \right]. \quad (3.41)$$

The $a_n^{L,R}$'s are bosonic annihilation operators. $\hat{\Pi}$ and $\hat{Q}$ are canonically conjugate to the periodic variables ϕ_0 and $\tilde{\phi}_0$, respectively. Hence their eigenvalues are quantized

$$\hat{\Pi} = m/R,\ \hat{Q} = 2\pi R\mathcal{S}^z, \tag{3.42}$$

with $\mathcal{S}^z$ and m given in equation (3.27). Note, that $\tilde{\phi}$ is also periodic with radius $1/2\pi R$, as already mentioned in equation (2.18). The Hamiltonian can now be written as[21]

$$\begin{aligned} H &= \int_0^l \mathcal{H}dx = \frac{v}{2}\int_0^l \left[\Pi_\phi^2 + \left(\frac{\partial\phi}{\partial x}\right)^2\right] \\ &= \frac{v}{2}\left[\frac{\hat{\Pi}^2}{l} + \frac{\hat{Q}^2}{l} + \frac{2\pi}{l}\sum_{n=1}^{\infty} n\left(a_n^{L\dagger}a_n^L + a_n^{R\dagger}a_n^R\right)\right], \end{aligned} \tag{3.43}$$

with the resulting excitation spectrum

$$E = \frac{2\pi v}{l}\left[\frac{1}{2}\left(2\pi R^2\left(\mathcal{S}^z\right)^2 + \frac{m^2}{2\pi R^2}\right) + \sum_{n=1}^{\infty} n(m_n^L + m_n^R)\right]. \tag{3.44}$$

The corresponding wave-function is

$$e^{i\left(\mathcal{S}^z 2\pi R\tilde{\phi}_0 + m\phi_0/R\right)}\prod_{n=1}^{\infty}(a_n^{L\dagger})^{m_n^L}(a_n^{R\dagger})^{m_n^R}|0\rangle. \tag{3.45}$$

We see from equation (2.22) and (3.40) that site-parity takes $m \to -m$ and $m_n^L \leftrightarrow m_n^R$. It also multiplies the wave-function in equation (3.45) by $e^{i\pi(\mathcal{S}^z+m)}$.

Here and in what follows, we always measure parity relative to that of the ground-state. The ground-state parity itself for an even length chain is $(-1)^{l/2}$. At the point $J^z = 0$, $R = 1/\sqrt{4\pi}$, this spectrum is that of free fermions with anti-periodic (periodic) boundary conditions for even (odd) particle number. At the Heisenberg point $J^z = J$, $R = 1/\sqrt{2\pi}$, the spin of left and right-movers is separately conserved and the z-components are given by

$$\mathcal{S}_{L,R}^z = (\mathcal{S}^z \pm m)/2. \tag{3.46}$$

$\mathcal{S}_{L,R}^z$ are either both integer or both half-odd-integer for even length l. For odd length one quantum number is half-odd-integer while the other one is integer valued (i.e. $\mathcal{S}_L^z\mathcal{S}_R^z$ is half-odd-integer valued).

$\frac{lE}{\pi v}$	Even periodic	Odd Periodic
0	0^+	$\frac{1}{2}^+$, $\frac{1}{2}^-$
1	0^+, 1^-	
2	1^+, 1^-	$2\times(\frac{1}{2}^+)$, $2\times(\frac{1}{2}^-)$, $\frac{3}{2}^+$, $\frac{3}{2}^-$
3	0^+, 0^-, 1^+, 1^-	
4	$2\times(0^+)$, 0^-, 1^+, $2\times(1^-)$, 2^+	$4\times(\frac{1}{2}^+)$, $4\times(\frac{1}{2}^-)$, $3\times(\frac{3}{2}^+)$, $3\times(\frac{3}{2}^-)$
5	$2\times(0^+)$, 0^-, $2\times(1^+)$, $3\times(1^-)$, 2^+, 2^-	

Table 3.1: Low energy spectrum for periodic boundary conditions. Relative parity and total spin are given.

The energy can then be written as

$$E=\frac{2\pi v}{l}\Big[(\mathcal{S}_L^z)^2+(\mathcal{S}_R^z)^2+\sum_{n=1}^{\infty}n(m_n^L+m_n^R)\Big]. \tag{3.47}$$

This spectrum has $SU(2)_L\times SU(2)_R$ symmetry for this value of R. Note, for instance, that for even l the lowest four excited states have total spin quantum numbers $(s_L,s_R)=(1/2,1/2)$, corresponding to a degenerate triplet and singlet under diagonal $SU(2)$. We can take higher values of $\mathcal{S}_L^z$ and $\mathcal{S}_R^z$ and can always find degenerate states to group the excited states into SU(2) multiplets. It is useful to divide the spectrum into four sectors corresponding to s_L integer or half-odd-integer and s_R integer or half-odd-integer. We the write $(s_L,s_R)=(Z,Z)+(Z+1/2,Z+1/2)$ for l even and $(Z,Z+1/2)+(Z+1/2,Z)$ for l odd where Z represents the integers. Parity interchanges all left and right quantum numbers and multiplies wave-functions by (-1) in the $(Z+1/2,Z+1/2)$ and $(Z+1/2,Z)$ sectors. Although periodic boundary conditions for even or odd length chains give identical equations (3.40 - 3.47), we can clearly distinguish two different fixed points with different excitation energies for the two cases, $\mathcal{S}^z$ integer or half-odd-integer. The states of the first six energy levels have been worked out in table 3.1 for the periodic chain with even and odd length l at the Heisenberg point. We can test the predicted spectrum numerically by exact diagonalization on a finite system with the algorithm in

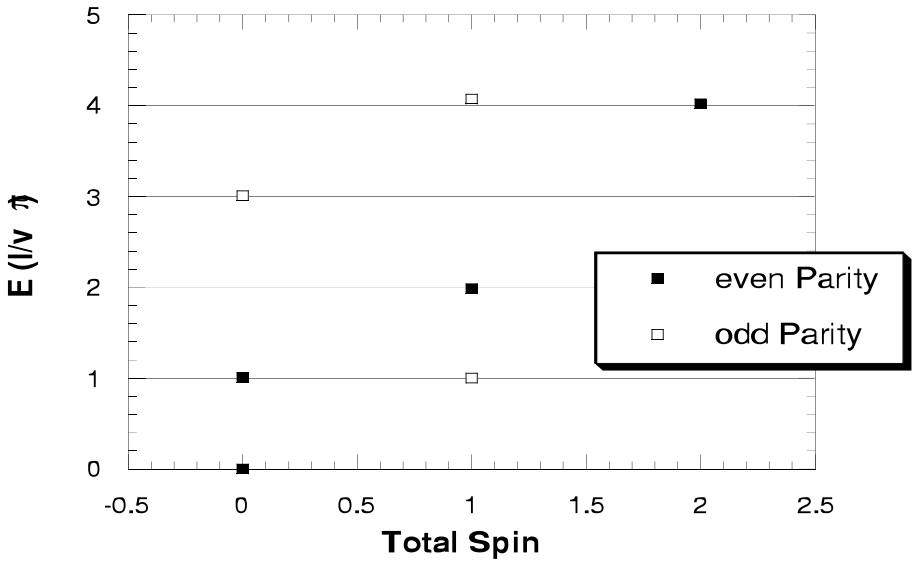

Figure 3.3: Numerical low energy spectrum for periodic, even length $l = 20$ spin chain. The integer values $El/\pi v$ of the numerically accessible states agree with the theoretical predictions. The velocity $v\pi = 3.69$ was used (see figure 3.5).

appendix B. To get rid of the logarithmic correction, we chose a next nearest neighbor coupling of $J_2 = 0.24J$ as discussed above. Figures 3.3 and 3.4 show the excellent agreement for all the states that were accessible with our algorithm (see appendix B). Moreover, we can see in figure 3.5 that for this choice of the Hamiltonian, the corrections to the spectrum $E(l/\pi)v$ drop off exactly as $1/l^2$ as predicted in section 3.2 for periodic boundary conditions.

3.3.2 Open boundary conditions

We now turn to the case of free boundary conditions on the spins corresponding to fixed boundary conditions on ϕ, as in equation (3.30). The mode expansion is now:

$$\phi(x,t) = 2\pi R\left(\frac{1}{2} + \mathcal{S}^z\frac{x}{l}\right) + \sum_{n=1}^{\infty}\frac{1}{\sqrt{\pi n}}\sin(\frac{\pi n x}{l})\left[e^{-i\pi nt/l}a_n + h.c.\right] \qquad (3.48)$$

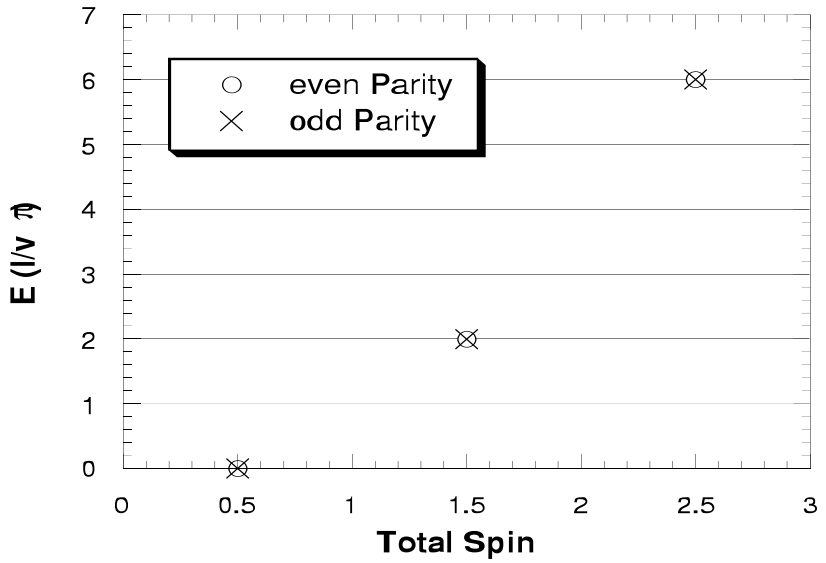

Figure 3.4: Numerical low energy spectrum for periodic, odd length $l = 19$ spin chain ($v\pi = 3.69$).

with $\mathcal{S}^z$ integer (half-odd-integer) for l even (odd). The spectrum now takes the form[22]

$$E = \frac{\pi v}{l}\left[2\pi R^2 \left(\mathcal{S}^z\right)^2 + \sum_{n=1}^{\infty} n m_n\right]. \tag{3.49}$$

These results can also be derived when we consider a single left-moving boson on twice the range $-l$ to l and periodic or antiperiodic boundary conditions as in equation (3.33).

Note, that parity [i.e. $x \to l - x$ for fixed boundary conditions or $x \to -x$ for the single boson] takes $a_m \to (-1)^m a_m$. It also multiplies wave-functions by $(-1)^{\mathcal{S}^z}$ for l even (for odd l we only have site-parity, which does not change the phase of the wave function). Thus

$$P = (-1)^{\sum_{p=0}^{\infty} m_{2p+1} + \mathcal{S}^z} = (-1)^{\sum_{p=1}^{\infty} p m_p + (\mathcal{S}^z)^2} \tag{3.50}$$

for l even. For l odd, $\left(\mathcal{S}^z\right)^2 - 1/4$ is even, so we may write a similar formula:

$$P = (-1)^{\sum_{p=1}^{\infty} p m_p + (\mathcal{S}^z)^2 - 1/4}. \tag{3.51}$$

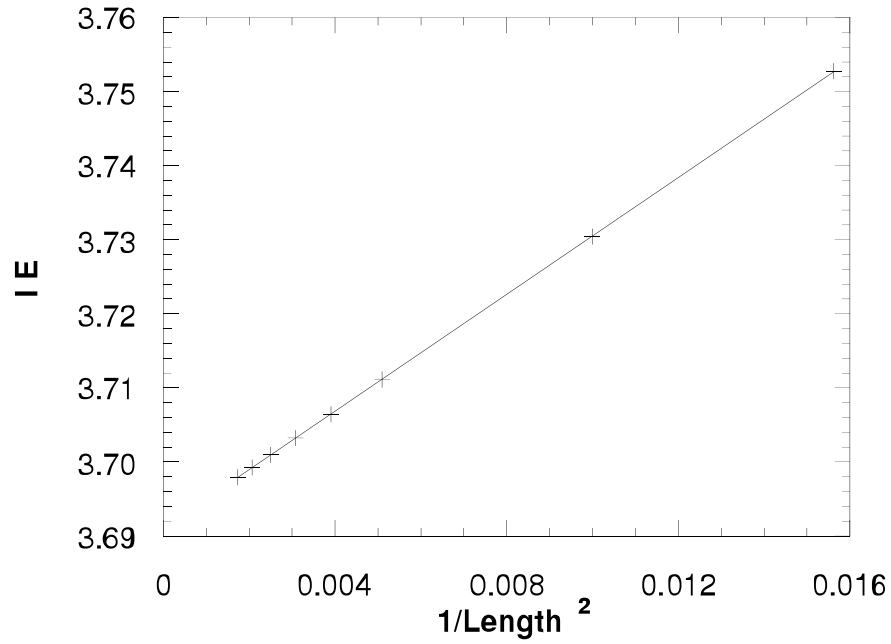

Figure 3.5: Renormalization group flow towards the asymptotic spectrum of the periodic chain. The lowest excitation gap 0^+, 1^- is fitted to $l\ E = a + b/l^2$ for even lengths ($a = 3.69$, $b = 3.94$).

At the Heisenberg point, this can be expressed in terms of the excitation energy

$$P = (-1)^{lE_{ex}/v\pi}, \tag{3.52}$$

where the ground-state energy of $\pi v/4l$, for l odd, is subtracted from E_{ex}; i.e. the energy levels are equally spaced, and the parity alternates. Again we measure parity relative to the ground-state, which is $(-1)^{l/2}$ or $+1$ for an even or odd-length open chain, respectively. There is now a single $SU(2)$ symmetry at the Heisenberg point corresponding to two possible sectors with total spin s integer for l even or s half-odd-integer for l odd.

The states of the first six energy levels have again been worked out in table 3.2 for open boundary conditions at the Heisenberg point. We can test this spectrum numerically with the algorithm in appendix B and find excellent agreement at the critical point $J_2 = 0.24J$

$\frac{lE}{\pi v}$	Even Open	Odd Open
0	0^+	$\frac{1}{2}^+$
1	1^-	$\frac{1}{2}^-$
2	0^+, 1^+	$\frac{1}{2}^+$, $\frac{3}{2}^+$
3	0^-, $2\times(1^-)$	$2\times(\frac{1}{2}^-)$, $\frac{3}{2}^-$
4	$2\times(0^+)$, $2\times(1^+)$, 2^+	$3\times(\frac{1}{2}^+)$, $2\times(\frac{3}{2}^+)$
5	$2\times(0^-)$, $4\times(1^-)$, 2^-	$4\times(\frac{1}{2}^-)$, $3\times(\frac{3}{2}^-)$

Table 3.2: Low energy spectrum for open boundary conditions. Relative parity and total spin are given.

(see figures 3.6 and 3.7). Figure 3.8 shows that corrections to the energy gaps $E(l/\pi v)$ now drop off as $1/l$, as expected for open boundary conditions. Note, however, that this is a length dependent renormalization of the velocity v, since the corrections come from the boundary *energy* operator in equation (3.39). [see also the discussion before equation (5.83)]. Therefore we estimate the velocity as $v\pi = 3.65 - 4.6/l$ in figures 3.6 and 3.7, which gives good results.

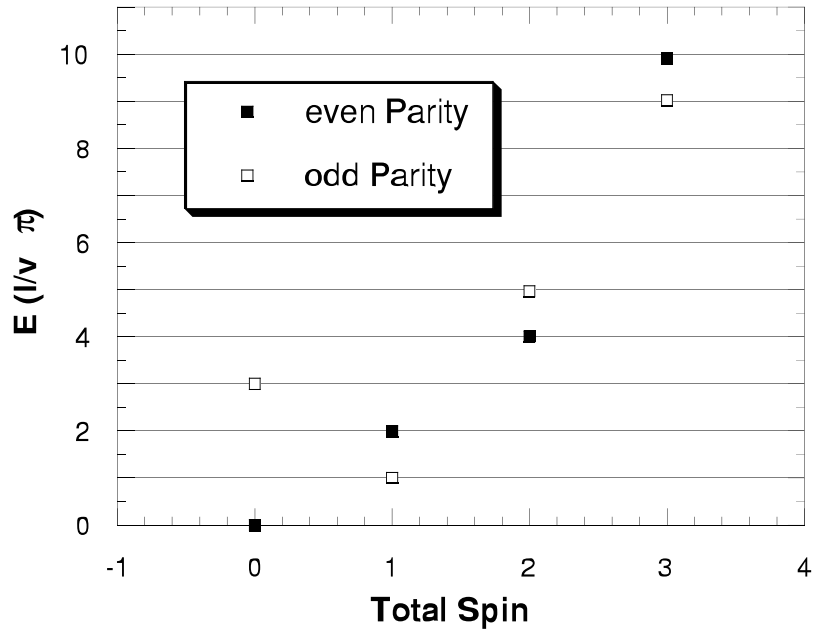

Figure 3.6: Numerical low energy spectrum for the open, even length $l = 20$ spin chain ($v\pi = 3.42$).

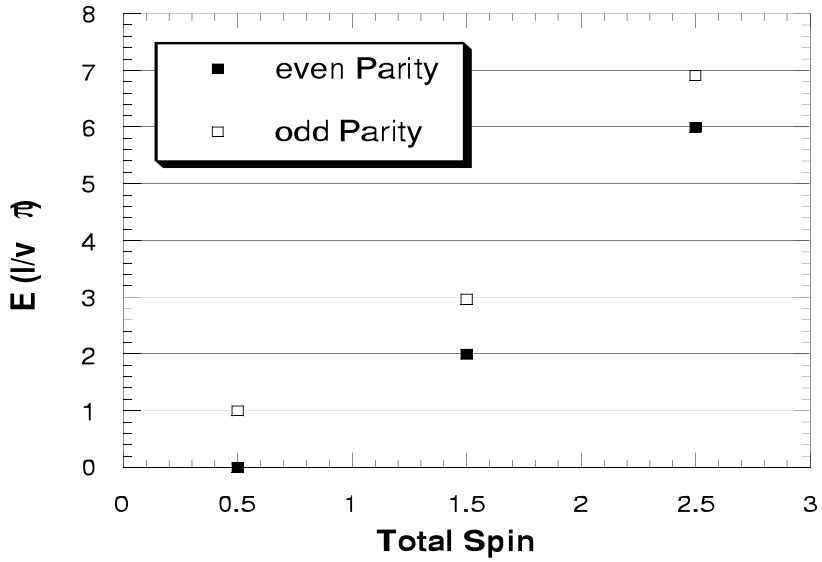

Figure 3.7: Numerical low energy spectrum for the open, odd length $l = 19$ spin chain ($v\pi = 3.42$).

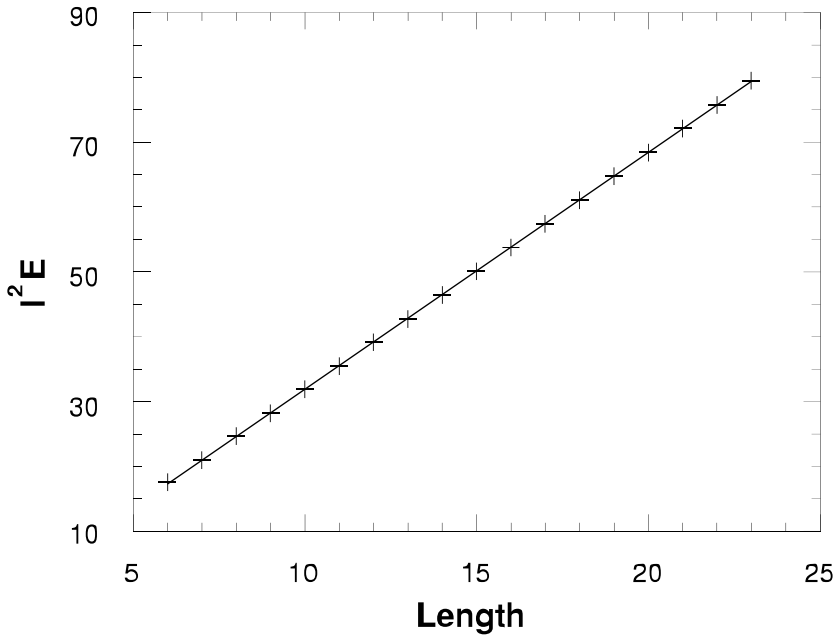

Figure 3.8: Renormalization group flow towards the asymptotic spectrum for the open chain. The lowest excitation gap $E(l/\pi v)$ is fitted to $l\ E = a + b/l$ for *both* even and odd length chains ($a = 3.65$, $b = -4.6$).

Chapter 4

Impurities

We are now in the position to calculate the effect of any perturbation on the chain in terms of our renormalization group and scaling analysis. Since we are able to express perturbing spin operators in terms of the boson fields, we can determine the relevance of the perturbation by looking at the corresponding scaling dimension.

Although a variety of possible perturbations can be considered[9], we will only consider a local change of coupling constants between spins within the chain, which can model many kinds of defects or impurities. We can obtain a more or less complete picture by focusing on two simple cases, which can later be generalized with respect to their symmetry properties: The perturbation of one coupling constant ("link") within the chain and the equal perturbation of two neighboring links. We will mainly consider the isotropic model $J_z = J$ unless otherwise indicated, since it seems to be the most interesting case experimentally[4].

4.1 One Perturbed Link

A generic local lattice distortion in a quasi one-dimensional spin compound could be described by the small perturbation of one link in a periodic chain $J'\vec{S}_m \cdot \vec{S}_{m+1}$, as shown in figure 4.9. Although such a perturbation has special link parity symmetry, we will argue later that the following renormalization group analysis is valid for all local perturbation that are *not* site parity symmetric. The $S^-_m S^+_{m+1} + S^+_m S^-_{m+1}$ part of the interaction is

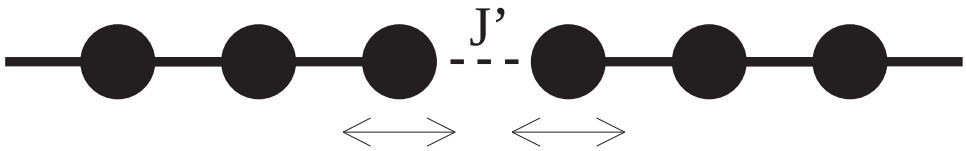

Figure 4.9: A quantum spin chain with one altered link.

given by

$$S_m^- S_{m+1}^+ + S_m^+ S_{m+1}^- \approx i(-1)^m(\psi_L^\dagger \psi_R - h.c.), \tag{4.53}$$

ignoring derivative terms of higher dimension as well as the uniform part which has the same form as the free Hamiltonian density with scaling dimension $d = 2$. Using the bosonization formula of equation (2.9) and rescaling the boson field following equation (2.13), we obtain

$$S_m^- S_{m+1}^+ + S_m^+ S_{m+1}^- \approx (-1)^m \text{const. } \sin\frac{\phi}{R}. \tag{4.54}$$

which has scaling dimension $d = 1/4\pi R^2$ and is therefore more relevant than the uniform contribution for all positive values of J_z.

The uniform part of $S_m^z S_{m+1}^z$ is known to have a scaling dimension of $d = 2$ from the free Hamiltonian. The staggered part, i.e. the cross-term between uniform and staggered parts of S^z can be written in terms of the fermion currents:

$$[J_L + J_R](m)\left[\psi_L^\dagger \psi_R(m+1) + h.c.\right] \; + \; \left[\psi_L^\dagger \psi_R(m) + h.c.\right][J_L + J_R](m+1) \tag{4.55}$$

The individual terms can be written as a completely normal ordered four-Fermion operator together with an additional term from Wick-ordering of the form

$$J_L(m)\psi_L^\dagger \psi_R(m+1) \;\; \rightarrow \;\; :\psi_L^\dagger \psi_L \psi_L^\dagger \psi_R : \; - \frac{i}{2\pi}\psi_L^\dagger \psi_R. \tag{4.56}$$

We can ignore all normal ordered terms since they reduce to irrelevant derivative operators. After combining all remaining terms together, we obtain the same operator as in

equations (4.53) and (4.54), for all values of R

$$S^z_m S^z_{m+1} \approx (-1)^m \text{const. } \sin \frac{\phi}{R}. \tag{4.57}$$

While this follows from symmetry at the Heisenberg point, it is not a priori obvious in the general case. These results can also be obtained by using the bosonic representation of the spin operators of equation (2.17) and the operator product expansion. In the bulk, the operator in equations (4.54) and (4.57) corresponds to a staggered interaction. The scaling dimension is given by $d = 1/4\pi R^2$ and a staggered interaction is therefore relevant for all positive values of J_z Such a staggered interaction may be induced by phonons, which leads to the so called spin-Peierls transition to a spontaneously dimerized, ordered phase.

Since this operator has a scaling dimension of $d = 1/2$ at the Heisenberg point, we conclude that it is relevant even as a local perturbation. Under the presence of such a perturbation, the energy corrections to the periodic chain spectrum should increase as $l\Delta E \propto \sqrt{l}$ as the cutoff is lowered according to the discussion in section 3.2. While this establishes that the periodic chain fixed point is unstable under this perturbation, we also know that a local perturbation should not affect the bulk behavior of the system. In particular, we expect that correlation functions of points which are far away from the impurity compared to their relative distance are not affected by the presence of the impurity and can still be calculated by the field theory as presented in chapters 2 and 3. A reasonable conclusion to draw from this scenario is that the system renormalizes to another, more stable conformal fixed point, which is characterized by a different boundary condition, but uses the same field theory description. This is in analogy with the ideas which were discussed in section 1.2 (see also figure 1.1).

In the case of one perturbed link, we can easily analyze where the periodic chain fixed point will renormalize to. Since we expect a slightly weakened link to become weaker

under renormalization, the obvious guess for the stable fixed point is the chain with open boundary conditions. A slightly strengthened link will grow as the cutoff is lowered, and the two strongly coupled spins will eventually lock into a singlet which decouples from the rest of the chain, so that we expect the stable fixed point again to be the open chain, but now with two sites removed.

To test this assumption, we analyze the scaling dimension of a weak link across the open ends. In the field theory, this is described by the product of two independent boundary operators at the weakly coupled ends

$$\begin{aligned} S_1^z S_l^z &\propto \frac{\partial \phi_L}{\partial x}(1)\frac{\partial \phi_L}{\partial x}(l) \\ S_1^+ S_l^- &\propto e^{4\pi i R\phi_L(1)} e^{-4\pi i R\phi_L(l)}, \end{aligned} \tag{4.58}$$

where we have used the boundary condition in equation (3.32). Since the scaling dimensions of independent operators simply add, we find that the $S_1^z S_l^z$ operator has a scaling dimension of $d = 2$ independent of J_z, while the $S_1^+ S_l^-$ part has a scaling dimension of $d = 4\pi R^2$ which is also irrelevant as a local perturbation for all positive values of J_z. Thus, a weak link across the open ends renormalizes to zero. The open chain fixed point is therefore indeed stable, and our assumptions above are consistent. At the Heisenberg point all operators from a perturbation of one weak link across the open ends of a chain have $d = 2$, and we expect that corrections to the open chain spectrum should flow to zero as $1/l$ according to the discussion in section 3.2.

We can generalize these findings since the operator in equation (4.54) is always the most relevant operator that can be produced by a local perturbation. A general perturbation in the chain will therefore produce this operator unless special symmetries (e.g. site parity) are present. Since relevant coupling constants will in general renormalize to zero or infinity, we conclude that the periodic chain fixed point flows to the more stable open chain fixed point as the temperature is lowered, if a local perturbation is present.

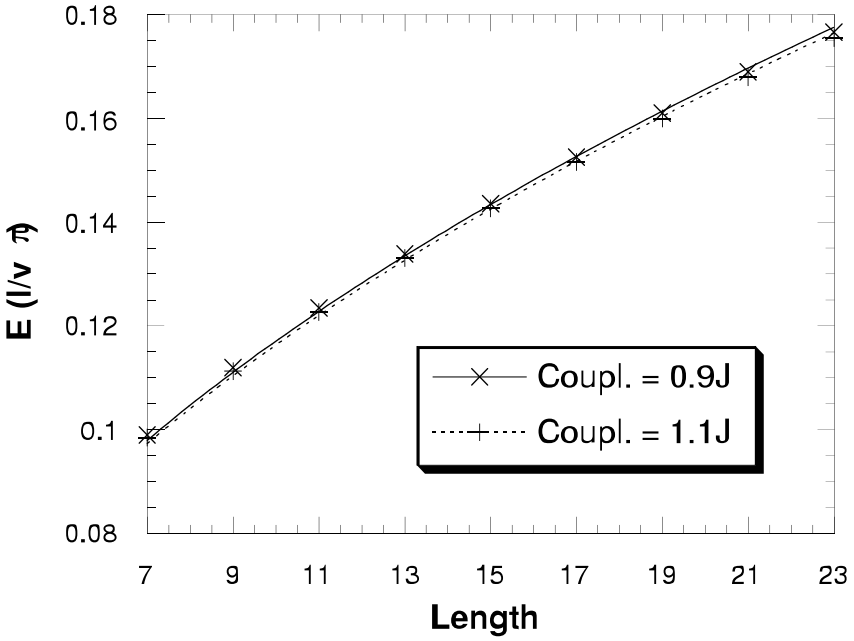

Figure 4.10: Flow away from the periodic chain fixed point due to one altered link for an odd length chain with $7 \leq l \leq 23$. The lowest excitation gap $\frac{1}{2}^+$, $\frac{1}{2}^-$ is fitted to $lE = a\ l^{1/2}$, which is the predicted scaling.

At the open chain fixed point, decoupled singlets may also be left over, and the effective length of the chain may be reduced by an even number of sites.

We can test the scaling analysis from above numerically by looking at the energy corrections $l\Delta E$ of the energy gaps if a small perturbation is present. Since we want to determine the scaling exponents accurately, all numerical simulations were done with a next nearest neighbor coupling $J_2 = 0.24J$ present, to avoid logarithmic corrections. Perturbations from the periodic point should correspond to a scaling with $l\Delta E \propto \sqrt{l}$ as mentioned above, which is indeed the case as shown in figure 4.10. A weak coupling across open ends of the chain should lead to corrections to the spectrum $l\Delta E \propto 1/l + \mathcal{O}(1/l^2)$, which is demonstrated nicely in figure 4.11.

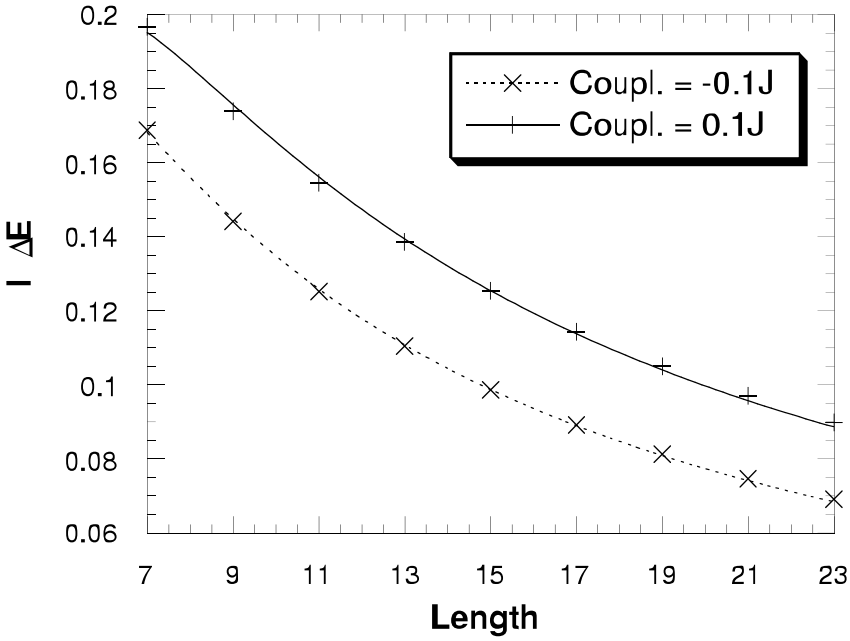

Figure 4.11: Renormalization group flow towards the open chain fixed point due to one weak link for an odd length chain with $7 \leq l \leq 23$. The corrections to the lowest excitation gap $\frac{1}{2}^+$, $\frac{1}{2}^-$ is fitted to $l\Delta E = a/l + b/l^2$, exhibiting the predicted $1/l$ scaling up to higher order.

4.2 Two Perturbed Links

Since the operator in equation (4.54) does not respect site parity, we expect fundamentally different behavior for site parity symmetric perturbations. As a generic case of a site parity symmetric perturbation, we will consider the equal perturbation of two neighboring links in the chain as shown in figure 4.12. Since the operator in equation (4.54) is alternating, we immediately find that the most relevant site parity invariant operator is the derivative

$$\frac{d}{dx} \sin \frac{\phi}{R}. \tag{4.59}$$

Because the derivative increases the scaling dimension by one, this operator has scaling dimension $d = 1 + 1/4\pi R^2$, corresponding to $d = 3/2$ at the Heisenberg point. It is

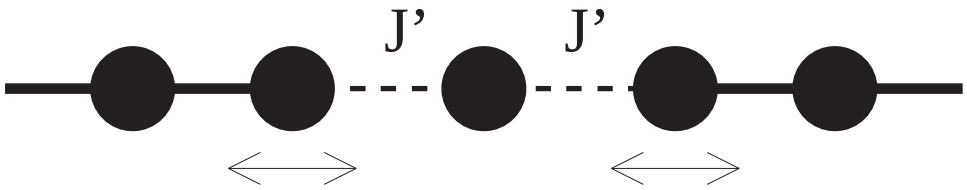

Figure 4.12: A quantum spin chain with two altered links.

therefore *irrelevant* as a local perturbation. The uniform parts of the interaction have dimension $d = 2$ as discussed before and are even more irrelevant.

The situation at the open chain fixed point is completely different, however, because the open ends are now coupled to an external spin-1/2. The corresponding boundary operators at l

$$\begin{aligned} S_l^z S_{\text{imp}}^z &\propto \frac{\partial \phi_L}{\partial x}(l) S_{\text{imp}}^z \\ S_l^- S_{\text{imp}}^+ &\propto e^{-4\pi i R \phi_L(l)} S_{\text{imp}}^+ \end{aligned} \tag{4.60}$$

now have scaling dimensions of $d = 1$ and $d = 2\pi R^2$, respectively, since the impurity spin is dimensionless. The boundary operators at $x = 0$ have corresponding expressions. The coupling of open ends to an external spin is therefore found to be marginally *relevant* at the Heisenberg point for anti-ferromagnetic coupling and marginally irrelevant for ferromagnetic sign. We therefore expect the open chain to renormalize to the more stable periodic chain if a site symmetric antiferromagnetic perturbation is present. The chain effectively "heals" in this scenario.

These predictions can be tested numerically as before. Figure 4.13 shows the predicted scaling with $1/\sqrt{l}$ for site symmetric perturbations from the periodic chain which correspond to the scaling dimension of $d = 3/2$ as discussed in section 3.2. Figure 4.14 establishes the marginally relevant scaling for two weak anti-ferromagnetic links of the open ends to an additional spin, while the marginally irrelevant case of two ferromagnetic

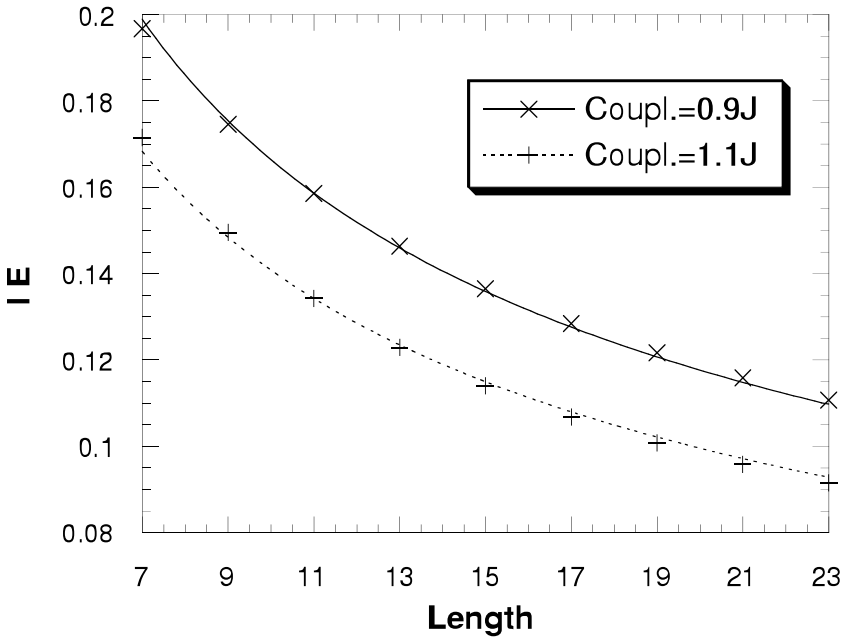

Figure 4.13: Flow towards the periodic chain fixed point for two altered antiferromagnetic links. The $\frac{1}{2}^+, \frac{1}{2}^-$ gap is fitted to $lE = a/l^{1/2}$, which is the predicted scaling.

links is shown in figure 4.15. We can see that the logarithmic corrections increase and decrease relative to the original coupling in the two cases. Since logarithmic scaling is slow we have to also consider the irrelevant $1/l$ contribution in the two figures to obtain a good fit. Although this three parameter fit is not entirely convincing, we can show that the logarithmic contribution is essential to achieve a good fit as presented in figures 4.14 and 4.15. Even other three parameter fits which we tested cannot reproduce an equally good fit without taking the logarithmic contribution into account.

4.3 Relation to Other Problems

Both link and site parity symmetric impurities that we have discussed above correspond to special cases of models studied in the context of defects in one-dimensional quantum wires[23, 24]. In these papers spinless fermions were considered, which are equivalent

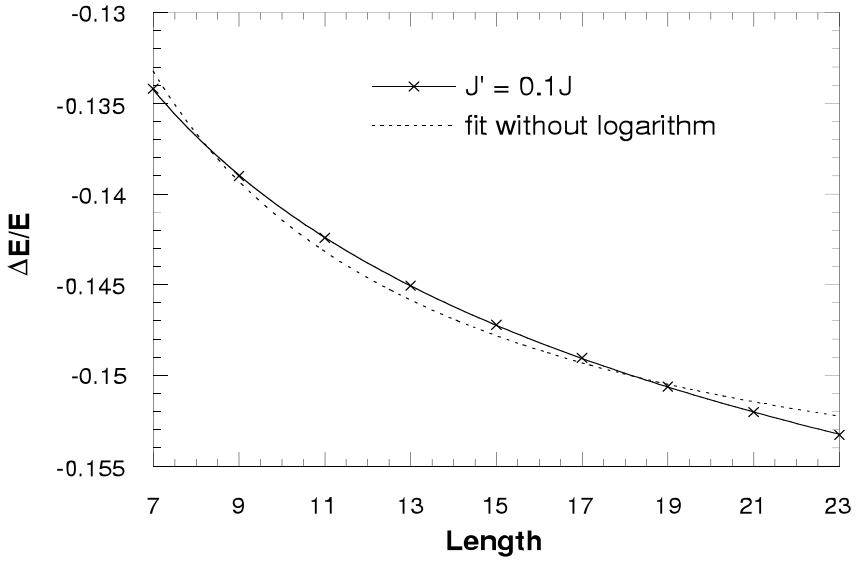

Figure 4.14: Flow away from the open chain fixed point for two weak antiferromagnetic links. Corrections to the $\frac{1}{2}^+, \frac{1}{2}^-$ gap are fitted to $\Delta E/E = (a+b/l+c\ln l)$, demonstrating relevant logarithmic scaling ($ac > 0$). The dotted line is the best fit for $c = 0$.

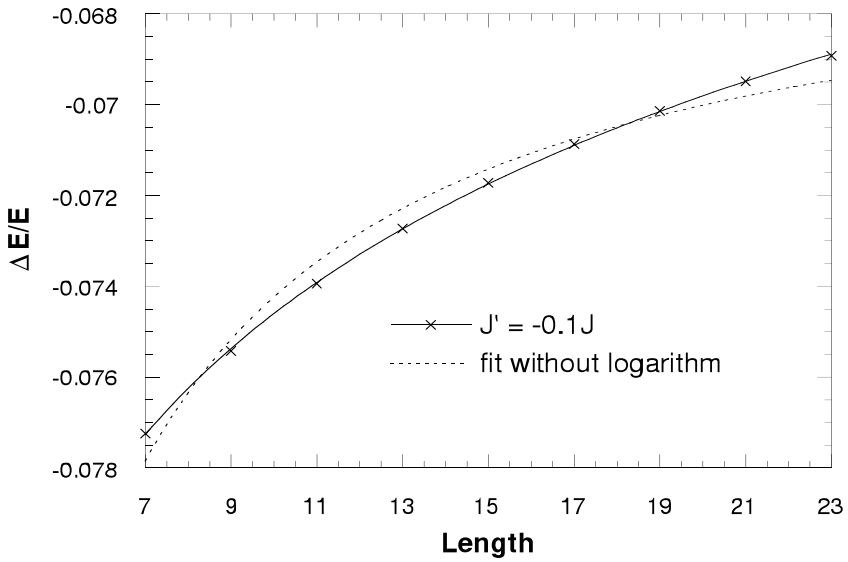

Figure 4.15: Flow towards the open chain fixed point for two weak ferromagnetic links. Corrections to the $\frac{1}{2}^+, \frac{3}{2}^-$ gap are fitted to $\Delta E/E = (a + b/l + c\ln l)$, demonstrating irrelevant logarithmic scaling ($ac < 0$). The dotted line is the best fit for $c = 0$.

to the xxz spin chain by the Jordan-Wigner transformation. The Heisenberg model corresponds to a particular value of the repulsive interaction. The flow of a single modified link to the open chain fixed point corresponds to the perfectly reflecting fixed point[23]. The "healing" discussed here corresponds to resonant tunneling[24]. In that work, it was necessary to adjust one parameter to achieve the resonance condition (even with exact site-Parity maintained). This parameter, a local chemical potential at the impurity site, corresponds to an external magnetic field term $h\ S_0^z$ at the impurity site. In the spin problem this is naturally set to zero by spin-rotation symmetry or time-reversal. Thus resonance (healing) occurs without fine-tuning in the spin chain.

The case of two equally perturbed links J' also has an interesting equivalent in the two-channel Kondo problem[9], which has been realized independently in reference [25]. The description in the field theory language is completely analogous in the spin sector of the Kondo problem if we identify the marginal coupling constants J' of the spins at the ends to the impurity spin in figure 4.12 with the Kondo coupling. The operators in equation (4.60) can be identified with the spin currents that couple to the impurity in the Kondo effect. The two ends of the spin chain are effectively independent of each other and can be regarded as being described by two independent fields which play the role of the two spin channels in the Kondo effect. The central spin in figure 4.12 represents the impurity spin in the Kondo case. The overscreened Kondo problem is known to renormalize to a non-trivial intermediate coupling fixed point[26], which corresponds to the healed chain. For higher impurity spin, we recover the normal underscreening of the Kondo problem in the spin chain model as well. It is, however, important to realize that the spins in the chain are not equivalent to the spins of the electrons in the Kondo problem, although the boson theory describing them is identical. The Kondo problem additionally has charge excitations which do not couple to the impurity and can therefore be neglected.

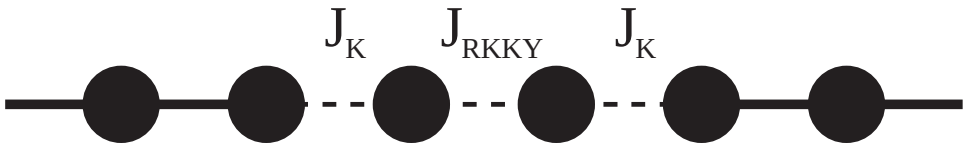

Figure 4.16: The equivalent spin chain model to the two impurity Kondo problem.

We can carry this analogy over to the single channel Kondo problem as well. In this case, we imagine a semi-infinite spin chain with the open end coupled to the impurity spin. As before, anti-ferromagnetic coupling J' is marginally relevant, and the stable fixed point is the open end with one extra site added (i.e. coupling $J' = J$). This corresponds to the strongly coupled fixed point in the Kondo effect. We see that we recover the famous $\pi/2$ phase shift of the fermions according to equation (2.4). As in the Kondo effect, the effect of the renormalization can be described by the so called fusion with a $s = 1/2$ primary field[8]. For higher impurity spin we obtain the correct size of the effective left-over spin $s - 1/2$ at the strong coupling fixed point $J' \to \infty$ as well, and the usual underscreening of the Kondo problem is recovered[26].

Recently, it has been discovered that the two-impurity Kondo problem has an analogy in a spin chain problem as well[8, 27]. In the equivalent spin chain model, two spin-1/2 impurities are coupled together with an RKKY coupling J_{RKKY}, and each of the spins is coupled separately to one of the open ends of the chain with a Kondo coupling J_K as shown in figure 4.16. In this case, both coupling constants are relevant in the weak coupling limit, but a healed chain *unstable* fixed point $J_{RKKY} = J_K = J$ separates the two strong coupling stable phases. The two open ends of the spin chain now play the role of the electron spin sectors at the two impurity sites in the Kondo problem. This scenario is just another case of a link symmetric perturbation as discussed in section 4.1. The two stable fixed points correspond to open chains with a possible decoupled singlet

and two sites removed if J_{RKKY} scales to infinity. From the analysis above, we conclude that the non-trivial fixed point should be unstable with scaling dimension $d = 1/2$.

These analogies are very useful since the spin chain Hamiltonians can be treated with a variety of numerical techniques, which might give some better insight in correlation functions and the size of the screening cloud in the Kondo effect. Moreover, it is easy to visualize non-trivial fixed points for spin chain problems, and additional fixed points may be found by simply adjusting the corresponding coupling constants.

Chapter 5

Susceptibilities

Now that a good theoretical understanding of the effect of impurities is established, it is necessary to make clear predictions on how this can be seen in an experiment. As indicated above, a μSR experiment on quasi one-dimensional magnetic compounds seems to be a good choice to observe the predicted effects. In this setup, we expect that the temperature dependence of the effective susceptibility at the muon site will be different from the results of a conventional susceptibility measurement due to the renormalization of the induced perturbation. In section 5.4 we will present the idea of the experimental setup in more detail. But before we can make any definite predictions for an experiment, it is necessary to take a closer look at the susceptibility of the spin chain and the effect of perturbations on this susceptibility in general. In this chapter we primarily discuss the field theory predictions for the susceptibility, while most of the Monte Carlo results are presented in chapter 6.

The local susceptibility χ_i in the z-direction at site i is given by

$$\chi_i(T) \equiv \frac{\partial}{\partial h}\langle S_i^z\rangle|_{h=0} = \int_0^\beta d\tau \sum_j \langle S_j^z(\tau) S_i^z(0)\rangle = \frac{1}{T}\sum_j \langle S_j^z S_i^z\rangle, \tag{5.61}$$

where h is the uniform magnetic field on the chain. We can drop the time dependence of the expectation value, because the total spin-z $\mathcal{S}_z$ commutes with the Hamiltonian. We also have set the Bohr magneton times the gyromagnetic ratio $g\mu_B$ and the Boltzmann constant k_B to one. The susceptibility is then measured in units of $1/J$. This local susceptibility will be different in the bulk and near a boundary since it is directly related

to the correlation function. In some cases we will refer to the total susceptibility χ_{total} of the chain, which is simply the sum of all local susceptibilities

$$\chi_{\text{total}} \equiv \sum_i \chi_i \tag{5.62}$$

The following calculations assume that we are in the scaling limit $T \ll J$, $l \gg 1$, so that the field theory analysis is valid. A "thermal length" is naturally defined by v/T, and the width of the boundary layer is given by v/T_K, where T_K has been mentioned in section 1.2. The meaning of the thermal length will become clearer shortly in equation (5.64). For our analysis, we require that the system size l is very large compared to all other scales in the system, in particular compared to v/T, i.e. $Tl/v \gg 1$. The ultraviolet cutoff can then always be reduced down to the temperature T.

5.1 Periodic Chain Susceptibility

Because the periodic chain is translationally invariant, the local susceptibility will be independent of the site index i. All spins in the chain therefore have the same susceptibility χ, which defines the bulk susceptibility per site. Using equation (2.24) we find that the sum over the S^z correlation function in equation (5.61) is given by

$$\sum_j \langle S_j^z S_i^z \rangle = \frac{-1}{16\pi^3 R^2} \int_{-l/2}^{l/2} dx \left(\frac{1}{(x+vt)^2} + \frac{1}{(x-vt)^2} \right). \tag{5.63}$$

This expression is useful for calculating the susceptibility of the free boson model, i.e. ignoring all irrelevant operators of the theory. Note, that the alternating part in equation (2.24) does not contribute when summed over and can therefore be neglected. To get a finite temperature result, we first make a Wick rotation to imaginary time τ, which we associate with the inverse temperature β. A conformal transformation of the space time continuum onto a cylinder with circumference β and length $l \to \infty$ then yields the finite

temperature correlation functions according to equation (A.107)

$$x \pm vt \to x \pm iv\tau \to \frac{-iv\beta}{\pi} \sin\left[\frac{(ix \mp v\tau)\pi}{v\beta}\right]. \tag{5.64}$$

The bulk susceptibility for the free boson model is thus given by

$$\chi = \frac{\beta}{16\pi^3 R^2} \int_{-\infty}^{\infty} dx \left\{ \left[\frac{v\beta}{\pi} \sin\left(\frac{(v\tau - ix)\pi}{v\beta}\right)\right]^{-2} + \left[\frac{v\beta}{\pi} \sin\left(\frac{(v\tau + ix)\pi}{v\beta}\right)\right]^{-2} \right\}. \tag{5.65}$$

The integral can be done by the change of variables: $u = \tan\frac{\tau\pi}{\beta}$ and $w = -i\tan\frac{ix\pi}{v\beta}$[28], giving

$$I = \int_{-\infty}^{\infty} dx \left(\frac{v\beta}{\pi} \sin\frac{(ix + v\tau)\pi}{v\beta}\right)^{-2} = \int_{-1}^{1} dw \frac{\pi(1+u^2)}{v\beta(u+iw)} = \frac{2\pi}{v\beta}, \tag{5.66}$$

which is independent of τ or u as it should be since the total spin-z $\mathcal{S}^z$ is conserved. The final result for the bulk susceptibility per site of the free boson model is therefore[29]

$$\chi = \frac{1}{v(2\pi R)^2}, \tag{5.67}$$

which is *independent* of temperature. This expression agrees with the zero temperature expressions from the analytical Bethe ansatz[12]. We can improve this formula for the spin chain in the field theory treatment by using perturbation theory in the irrelevant operators, which will give us temperature dependent corrections to this expression. We know from conformal invariance that finite size scaling should be analogous to finite temperature scaling upon identifying $l = v/T$, so that we can use the same analysis as in section 3.2.

5.1.1 Contributions from the leading irrelevant operator

The first order contribution to the bulk susceptibility from the leading irrelevant operator $\cos(2\phi/R)$ vanishes. The second order contribution is determined by our scaling

arguments in section 3.2 and the scaling dimension $d = 1/\pi R^2$, giving:

$$\chi(T) \to \frac{1}{v(2\pi R)^2} \; + \; \text{const. } T^{2(1/\pi R^2 - 2)}. \tag{5.68}$$

For $1/\pi R^2 > 3, \;\; J_z < J/2$ the exponent will get replaced by 2, because in this case $T_L T_R$ from equation (2.16) is the leading irrelevant operator. For $J_z > J\cos^{-1}(\pi/5) \approx .809J$ we notice that the correction leads to an infinite slope at zero temperature.

At the Heisenberg point $J_z = J, \;\; R = 1/\sqrt{2\pi}$, we expect a logarithmic correction according to section 3.2, because the leading irrelevant operator is marginal. These corrections have been calculated by using the non-abelian bosonization of the spin chain[10], in which the low energy effective field theory description is given by the $k = 1$ Wess-Zumino-Witten (WZW) non-linear σ-model. The uniform part of the spin density is given by the conserved current operators, $\vec{J}_L$, $\vec{J}_R$ for left and right-movers:

$$\vec{S}_x \approx \vec{J}_L(x) + \vec{J}_R(x). \tag{5.69}$$

In the WZW model $\vec{J}_L$ and $\vec{J}_R$ are uncorrelated and their self-correlations are given by

$$\begin{aligned} \langle J_L^a(\tau, x) J_L^b(0,0)\rangle &= \frac{\delta^{ab}}{8\pi^2(v\tau - ix)^2} \\ \langle J_R^a(\tau, x) J_R^b(0,0)\rangle &= \frac{\delta^{ab}}{8\pi^2(v\tau + ix)^2}. \end{aligned} \tag{5.70}$$

The leading irrelevant operator is marginal and is now given by

$$\frac{-8\pi^2 v}{\sqrt{3}} g \vec{J}_L \cdot \vec{J}_R. \tag{5.71}$$

Using first order perturbation theory gives a correction to χ that involves four current operators

$$\chi = \frac{1}{2\pi v} + v\beta^2 \frac{8\pi^2 g}{\sqrt{3}} \int_{-l/2}^{l/2} dx \int_{-l/2}^{l/2} dy \langle [J_L^z + J_R^z](0)[J_L^z + J_R^z](x) \vec{J}_L \cdot \vec{J}_R(y)\rangle. \tag{5.72}$$

Due to the fact that the left and right currents are uncorrelated, this expression factorizes into a product of two two-point Green's functions, one for left-movers and one for right-movers according to equation (5.70). Using translational invariance, the spatial integrals factorize into two independent integrals of the form of equation (5.66), giving

$$\begin{aligned}\chi &= \frac{1}{2\pi v} + v\beta^2 \frac{8\pi^2 g}{\sqrt{3}} \int_{-l/2}^{l/2} dx \int_{-l/2}^{l/2} dy \, (\langle J_L^z(0) J_L^z(y)\rangle \langle J_R^z(x) J_R^z(y)\rangle \\ &\quad + \langle J_R^z(0) J_R^z(y)\rangle \langle J_L^z(x) J_L^z(y)\rangle) \\ &= \frac{1}{2\pi v} + v\beta^2 \frac{8\pi^2 g}{\sqrt{3}} \left[\left(\frac{1}{8\pi^2} \frac{2\pi}{v\beta} \right)^2 + \left(\frac{1}{8\pi^2} \frac{2\pi}{v\beta} \right)^2 \right] \\ &= \frac{1}{2\pi v} + \frac{g}{v\sqrt{3}}. \end{aligned} \tag{5.73}$$

Again, the correction is naively temperature-independent, since g is dimensionless. However, this formula can be improved by replacing g with $g(T)$, the effective renormalized coupling at temperature T. By integrating the lowest order β -function, $g(T)$ is given by[19]

$$g(T) \approx \frac{g_1}{1 + 4\pi g_1 \ln(T_1/T)/\sqrt{3}}. \tag{5.74}$$

Here g_1 is the value of the effective coupling at some temperature T_1. Both g_1 and $g(T)$ must be small for this formula to be valid. We may write this more compactly, as

$$g(T) \approx \frac{\sqrt{3}}{4\pi \ln(T_0/T)}, \tag{5.75}$$

for some temperature T_0. Thus we obtain the leading T-dependence of χ

$$\chi(T) = \frac{1}{2\pi v} + \frac{1}{4\pi v \ln(T_0/T)}. \tag{5.76}$$

As mentioned before, we can adjust g_1 and T_0 by introducing a next nearest neighbor coupling J_2, and at $J_2 \approx 0.24J$ we expect $T_0 \to \infty$. However, for the model in equation (1.1), $J_z = J, \;\; J_2 = 0$, we expect a finite T_0 and a logarithmic divergence of the slope at $T = 0$.

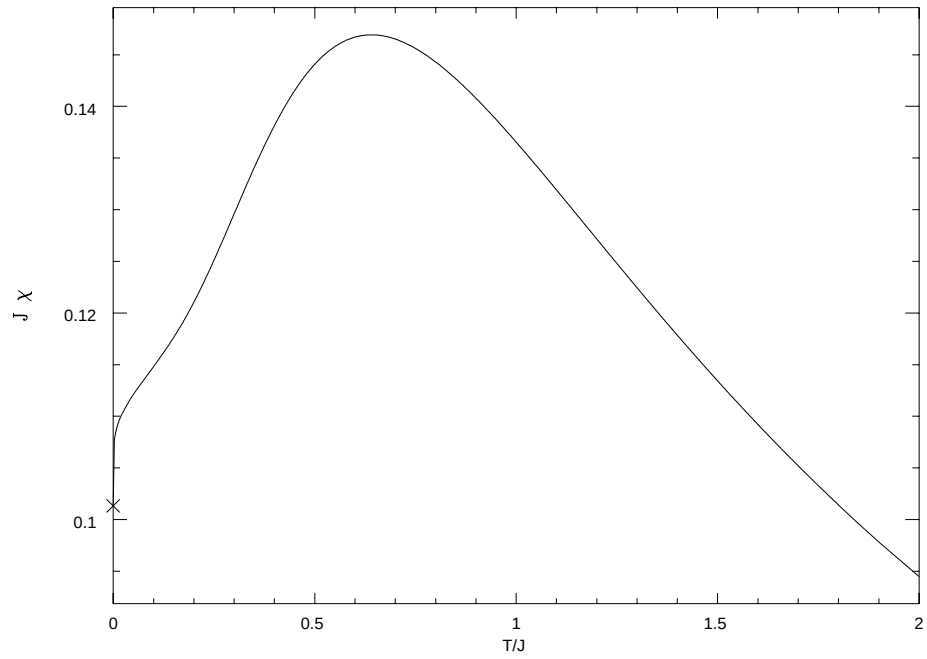

Figure 5.17: $\chi(T)$ from the Bethe ansatz. $\chi(0) = 1/J\pi^2$ is taken from equation (5.67).

As shown in figure 5.17, we have calculated the complete bulk susceptibility curve for this case by use of the numerical Bethe ansatz of Takahashi[3, 30]. The bulk susceptibility obeys Curie's law for large temperatures and goes through a maximum at $T \approx 0.640824J$, $\chi \approx 0.147/J$ before the slope starts to increase again below an inflection point at $T \approx 0.087J$. We will use this curve as the unperturbed reference point for our Monte Carlo simulations, which of course give identical results for this case, but with larger error-bars. The existence of the maximum has been known for a long time[31] and is used in experiments to establish the one-dimensional characteristics and determine the coupling strength J[4, 5]. Our calculations give an additional prediction of an inflection point at $T \approx 0.087J$, which might be observable in some very highly one-dimensional materials.

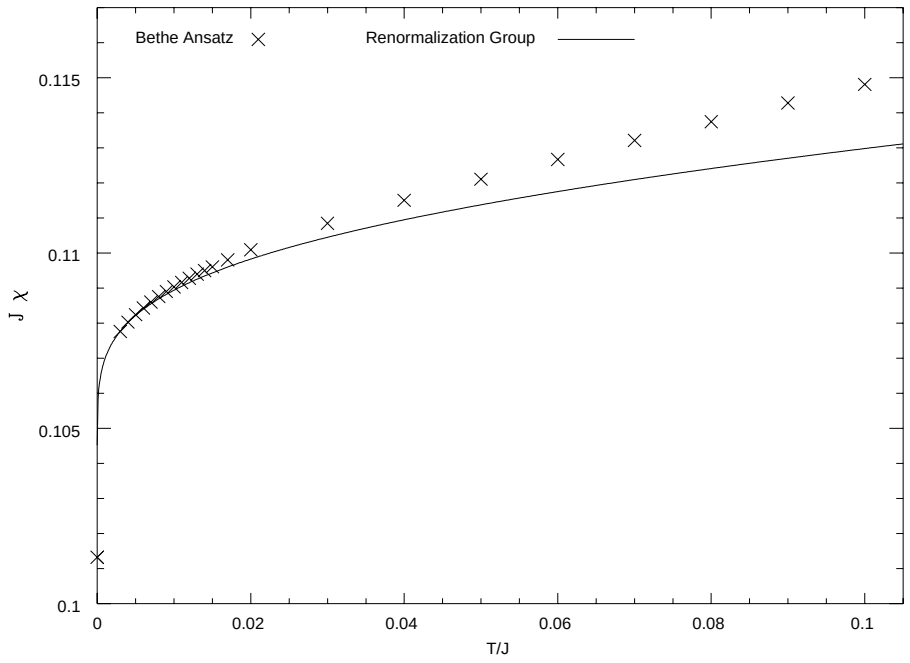

Figure 5.18: Field theory [equation (5.76), $T_0 \approx 7.7J$] versus Bethe ansatz results for $\chi(T)$ at low temperature.

According to figure 5.18 our field theory predictions agree reasonably well with the low temperature susceptibility behavior for a value of $T_0 \approx 7.7J$. The curve starts to deviate from our first order calculation as corrections of order $(1/\ln T)^3$ and T^2 become important. The magnitude of these corrections are not known, but $\ln T_0/T \gg 1$ should be a sufficient condition for the validity of equation (5.76) which is consistent with figure 5.18. The divergent slope is not accessible by experiments, because of a finite ordering temperature in quasi one-dimensional spin compounds, but the onset of this behavior may have been observed in some cases[5].

The logarithmic scaling behavior has been observed before in numerical Bethe ansatz calculations for finite size systems[19]. We can compare the result in the finite length

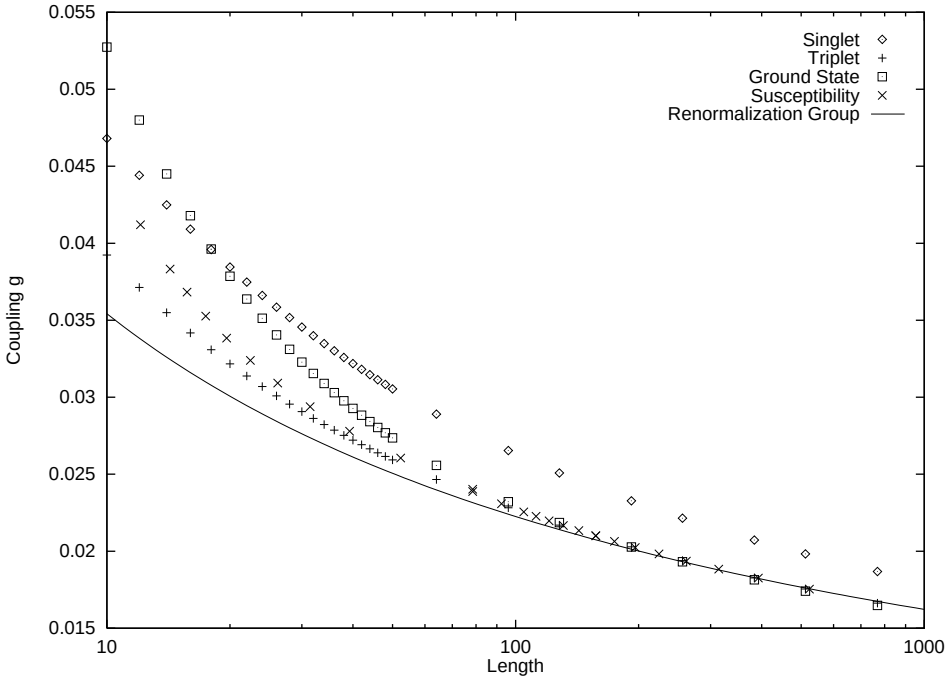

Figure 5.19: Estimates for the effective coupling g from lowest order perturbation theory correction to the finite-size energy of ground-state, first excited triplet state, first excited singlet state[19] and to the susceptibility, using $l \leftrightarrow v/T$. The renormalization group prediction of equation (5.75) is also shown.

limit $lT/v \to 0$ from reference [19] directly with our calculation in the finite temperature limit $lT/v \to \infty$ upon identifying $l = v/T$, which appears to be the appropriate relation (see figure 5.19).

It is possible to continue the expansion in the irrelevant operators to higher orders in perturbation theory which will give higher order corrections in T. In the limit $lT/v \gg 1$ the system size is always much larger than the finite temperature correlation length, and we expect that finite length corrections to the periodic chain susceptibility are exponentially small in lT/v. Because we have translational invariance we can therefore write the total susceptibility of the periodic chain as $\chi_{\text{total}} = l\chi(T)$, where χ is independent of the system size l up to exponentially small corrections.

5.2 Open Chain Susceptibility

The situation is somewhat different for the open chain since translational invariance is broken. In this case it is possible to have an additional impurity contribution to the total susceptibility which is independent of length

$$\chi_{imp} \equiv \lim_{l\to\infty} \left(\sum_i \chi_i - l\chi \right), \tag{5.77}$$

where χ_i is now the local susceptibilities at site i of the open chain and χ is the bulk susceptibility per site from the previous section. This impurity susceptibility comes from *local* irrelevant operators as in equation (3.39) in the field theory, which will be discussed in section 5.2.2. The boundary condition condition itself does *not* contribute to the uniform part of the susceptibility and therefore does not affect the impurity susceptibility as will be explained at the end of section 5.2.1. An impurity susceptibility is also present for any local perturbation on the periodic chain, and if no local operators were present, neither fixed point in the field theory would have an impurity susceptibility contribution. (Note, that the open chain in the lattice model corresponds to the open field theory

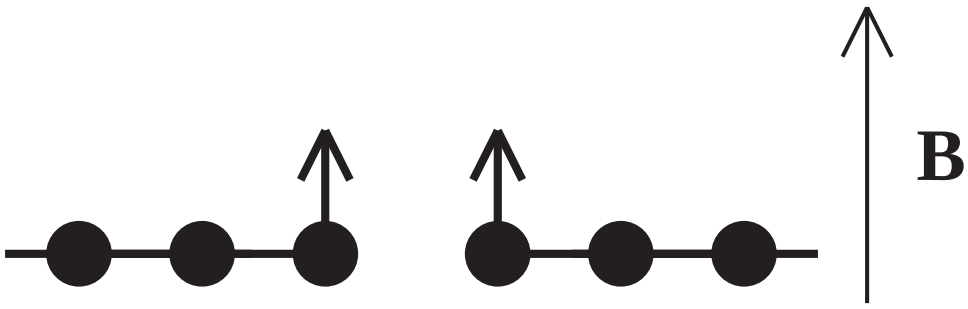

Figure 5.20: The open ends of the broken chain are expected to be more susceptible.

fixed point from section 3.3.2 only up to irrelevant operators and therefore always has an impurity susceptibility).

It seems intuitively clear that the open chain will be more susceptible at the ends than bulk spins in the periodic chain as indicated in figure 5.20. To calculate this effect, we have to take into account that the correlation functions will be different near the boundary as described in section 3.1.2 and that there will be a correction due to the leading irrelevant operator in equation (3.39).

5.2.1 Contributions from the boundary condition

Let us first consider the effect of the boundary condition itself. Although the boundary condition is *not* responsible for the impurity susceptibility as mentioned above, we do expect that the correlation functions and therefore the local susceptibility will be affected. According to equation (5.61) one index j in the expectation value $\langle S_i^z S_j^z \rangle$ is always summed over, so that the alternating part of the second operator S_j^z does not contribute to the local susceptibility. Because the boundary condition relates left and right movers according to equation (3.32), there is now however a possibility for a non-zero cross term of the uniform part of S_j^z and the alternating part of S_i^z, which gives an alternating contribution to the local susceptibility as a function of the site index i relative to the

boundary. We therefore choose to separate the local susceptibility into a sum of an alternating and a uniform part, corresponding to the alternating and uniform parts of $S^z(x)$ in equation (2.17):

$$\begin{aligned}\chi_x &= \frac{1}{T}\int dy \langle S^z(x) S^z(y)\rangle \\ &= \frac{1}{T}\langle \{S^z_{\rm uni}(x) + (-1)^x S^z_{\rm alt}(x)\}\int dy S^z_{\rm uni}(y)\rangle \\ &= \chi_x^{\rm uni} + (-1)^x \chi_x^{\rm alt} \end{aligned} \tag{5.78}$$

This separation should be valid in the scaling limit, but at short distances it is of course somewhat ambiguous (e.g. within a few lattice spacings of the boundary).

The corresponding expression for $\chi_x^{\rm alt}$ can be non-vanishing, because it is now expressed in terms of a three point Green's function (without the boundary condition, it is a vanishing two point function). After expressing the cosine in equation (2.17) in terms of exponentials and using equation (3.32) we find

$$\begin{aligned}\chi_x^{\rm alt} &\propto \beta\int_{-\infty}^{\infty} dy \left\langle e^{-i\sqrt{2\pi}\phi_L(x,t')} e^{i\sqrt{2\pi}\phi_L(-x,t')} \frac{\partial \phi_L}{\partial x}(y,t)\right\rangle \\ &\propto \beta\int_{-\infty}^{\infty} dy \frac{\sqrt{2x}}{(y+vt-x-vt')(y+vt+x-vt')}, \end{aligned} \tag{5.79}$$

according to equation (A.108) with scaling dimensions $d_1 = d_2 = 1/4$ and $d_3 = 1$ at the Heisenberg point. Here, the index x measures the distance from the boundary in units of the lattice spacing. We can evaluate this expression for finite T by using equation (5.64)

$$\begin{aligned}\chi_x^{\rm alt} &\propto \int_{-\infty}^{\infty} dy \frac{\sqrt{v\beta \sinh\frac{2\pi x}{v\beta}}}{\beta \sinh\frac{\pi}{v\beta}(y+x+iv\tau)\sinh\frac{\pi}{v\beta}(y-x+iv\tau)} \\ &\propto \int_{-\infty}^{\infty} dy \frac{\sqrt{v\beta \sinh\frac{2\pi x}{v\beta}}}{\beta(\cosh^2\frac{\pi}{v\beta}(y+iv\tau) + \sinh^2\frac{\pi}{v\beta}(y+iv\tau) - \cosh\frac{2\pi x}{v\beta})}. \end{aligned} \tag{5.80}$$

This integral can be done if we set $u = \coth\frac{\pi}{v\beta}(y+iv\tau), \quad du = -\frac{\pi}{v\beta}\frac{dy}{\sinh^2\frac{\pi}{v\beta}(y+iv\tau)}$. The final result is

$$\chi_x^{\rm alt} \propto \int_{-1}^{1} du \frac{\sqrt{v\beta \sinh\frac{2\pi x}{v\beta}}}{u^2+1-(u^2-1)\cosh\frac{2\pi x}{v\beta}}$$

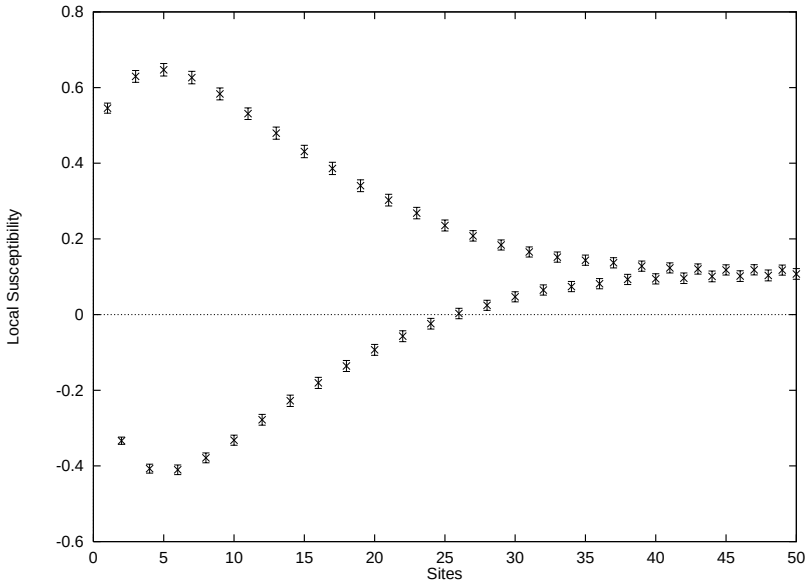

Figure 5.21: The local susceptibility near open ends from Monte Carlo simulations for $\beta = 15/J$.

$$\propto \frac{x}{\sqrt{v\beta \sinh \frac{2\pi x}{v\beta}}}. \tag{5.81}$$

Note, that the alternating part may *increase* as we increase the distance x from the boundary if we are at low temperatures. In particular at $T = 0$ we expect the alternating part to increase exactly with $\sqrt{x}$, which seems very counter-intuitive. (Note, however, that experimental systems always contain the exponential drop-off from finite temperatures.) This surprising effect has been checked by Monte Carlo simulations using the algorithm in appendix C. The local susceptibility as a function of distance from the open ends is shown in figure 5.21 for $\beta = 15/J$.

Using this Monte Carlo data, we can extract the uniform and alternating parts as shown in figure 5.22 (as mentioned before this is somewhat ambiguous very close to the boundary). The alternating part fits the predicted form $0.52(x+2)/\sqrt{\beta \sinh 2\pi(x+2)/v\beta}$ up to a constant $\alpha = 0.52$ and a shift of two sites. This functional dependence holds

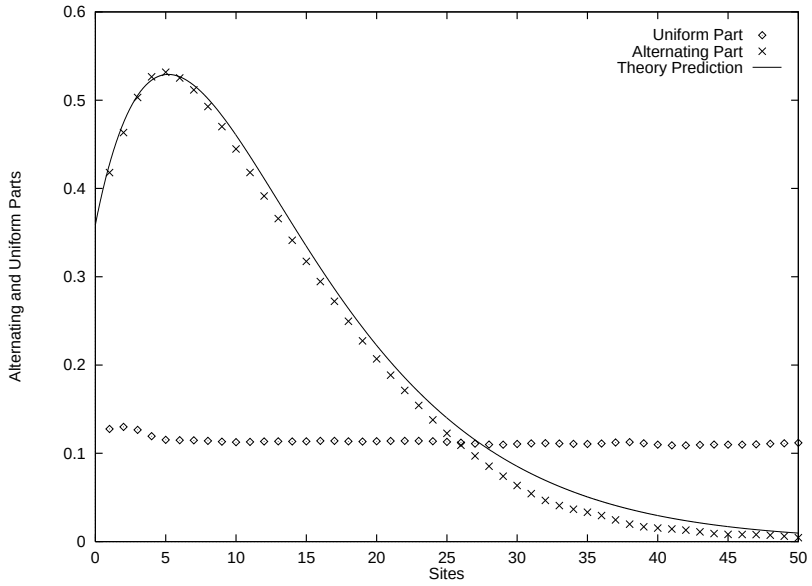

Figure 5.22: The uniform and alternating parts of the local susceptibility near open ends from Monte Carlo simulations for $\beta = 15/J$. We compare this data to the theoretical prediction for the alternating part $0.52(x+2)/\sqrt{\beta \sinh 2\pi(x+2)/v\beta}$.

rather well for all temperatures that were sampled.

It is important to notice that the uniform part of the susceptibility does not acquire any change from the boundary condition in equation (3.32) because the uniform part of S_i^z is a sum of left and right movers and not a product. In particular we can rewrite the integral over the correlation function of the uniform part with the use of equation (3.32)

$$\begin{aligned}
\chi_{\text{total}} &= \frac{1}{4\pi^2 R^2}\int_0^\infty dx \int_0^\infty dy \left\langle \frac{\partial\phi}{\partial x}(x)\frac{\partial\phi}{\partial x}(y)\right\rangle \\
&= \frac{1}{4\pi^2 R^2}\int_0^\infty dx \int_0^\infty dy \left\langle \left(\frac{\partial\phi_L}{\partial x}(x)+\frac{\partial\phi_L}{\partial x}(-x)\right)\left(\frac{\partial\phi_L}{\partial x}(y)+\frac{\partial\phi_L}{\partial x}(-y)\right)\right\rangle \\
&= \frac{1}{2\pi^2 R^2}\int_{-\infty}^\infty dx \int_{-\infty}^\infty dy \left\langle \frac{\partial\phi_L}{\partial x}(x)\frac{\partial\phi_L}{\partial x}(y)\right\rangle
\end{aligned} \tag{5.82}$$

which gives the same result as the periodic case in equations (5.63-5.67).

5.2.2 Contributions from the leading irrelevant boundary operator

Although the local corrections due to the boundary condition are large, there will be no impurity contribution to the total susceptibility since the alternating part does not contribute under the integral and the uniform part does not change. This is in complete agreement with the statement that the impurity susceptibility comes entirely from the irrelevant boundary operators. In this section we will consider the contribution from the leading irrelevant boundary operator in equation (3.39) with some unknown coupling constant c. This boundary operator is present at each end, $T_L(0)$ and $T_L(l)$, but the two operators are independent at the open chain fixed point and we may consider only the operator at the origin and then generalize our findings for both ends.

The impurity correction in equation (5.77) to the susceptibility from $T_L(0)$ can be calculated to first order with a simple trick, which has been used before in the context of the Kondo problem[32]. The operator in equation (3.39) is proportional to the local energy density, so that its effect to first order in perturbation theory is simply a length dependent renormalization of the velocity v for any bulk quantity. In particular for the bulk susceptibility to first order we can write

$$\begin{aligned} & cv \int_{-l}^{l} dx \int_{-l}^{l} dy \int_{-l}^{l} dz \ \left\langle \delta(z) T_L(z) \frac{\partial \phi_L}{\partial x}(x) \frac{\partial \phi_L}{\partial x}(y) \right\rangle \\ \rightarrow \ & \frac{c}{l} v \int_{-l}^{l} dx \int_{-l}^{l} dy \int_{-l}^{l} dz \ \left\langle T_L(z) \frac{\partial \phi_L}{\partial x}(x) \frac{\partial \phi_L}{\partial x}(y) \right\rangle \end{aligned} \tag{5.83}$$

The integral over dz can now be reabsorbed to first order in the free Hamiltonian by rescaling $v \rightarrow v(1 + c/l)$. In the thermodynamic limit, the effect for all translational invariant quantities is then simply a rescaling of the temperature $T \rightarrow T/(1 + c/l)$ in the partition function. In particular, the susceptibility per site can be calculated as a function of the coupling constant c

$$\chi(c, T) \ = \ \frac{1}{T} \int dx \, \langle S_x^z S_0^z \rangle_{c,T}$$

$$\begin{aligned} &= \frac{1}{T}\int dx\, \langle S_x^z S_0^z\rangle_{c=0,T/(1-c/l)} \\ &= \chi\left(c=0, \frac{T}{1-c/l}\right)\frac{1}{1-c/l} \\ &\approx \chi + \frac{\chi_{\rm imp}}{l}. \end{aligned} \tag{5.84}$$

At $T=0$ the correction corresponds to a shift $c\chi/l$ in the susceptibility per site. The sum over all sites gives us the impurity correction to the susceptibility $\chi_{\rm imp} \approx c\chi$, which is independent of length as it should be in the limit $l \to \infty$ in equation (5.77).

Although this argument can give us the impurity correction to the total susceptibility, it is not sufficient to predict the local corrections $\delta\chi_x$ due to the irrelevant operator in equation (3.39). These can be calculated by doing first order perturbation theory in the coupling constant c of the operator in equation (3.39)

$$\delta\chi_x \;\propto\; c\beta^2 \int_{-\infty}^{\infty} dy\; \left\langle : \left[\frac{\partial\phi_L}{\partial x}(0)\right]^2 : \frac{\partial\phi_L}{\partial x}(x)\frac{\partial\phi_L}{\partial x}(y)\right\rangle, \tag{5.85}$$

where we again only consider the boundary operator at 0 for simplicity. After replacing β with an integral over $d\tau$ to take the proper time-correlations into account we can calculate this expression by using the usual boson Green's functions and Wick ordering:

$$\begin{aligned} &\left\langle \frac{\partial\phi_L}{\partial x}(x+iv\tau'')\frac{\partial\phi_L}{\partial x}(iv\tau)\right\rangle \left\langle \frac{\partial\phi_L}{\partial x}(y+iv\tau')\frac{\partial\phi_L}{\partial x}(iv\tau)\right\rangle \\ \propto\;& (x-iv\tau+iv\tau'')^{-2}(y+iv\tau'-iv\tau)^{-2}. \end{aligned} \tag{5.86}$$

The finite temperature result for the local susceptibility correction can now be derived from equation (5.64)

$$\begin{aligned} \delta\chi_x \;&\propto\; c\beta\int_0^\beta d\tau \left(\frac{v\beta}{\pi}\sin\frac{i\pi(x-iv\tau+iv\tau'')}{v\beta}\right)^{-2}\int_{-\infty}^{\infty} dy \left(\frac{v\beta}{\pi}\sin\frac{\pi(iy-v\tau'+v\tau)}{v\beta}\right)^{-2} \\ &\propto\; c\int_0^\beta d\tau \left(\frac{v\beta}{\pi}\sin\frac{\pi(v\tau-v\tau''+ix)}{v\beta}\right)^{-2}, \end{aligned} \tag{5.87}$$

where we also used equation (5.66). The integral over $d\tau$ gives $-\pi\cot[\pi(v\tau - v\tau'' + ix)/\beta v]/v^2\beta$, which cancels for the given limits of integration and any finite x. For $x=0$,

however, we can get a non-zero value, which can be determined by doing the integral over all x using equation (5.66). Therefore, the local correction to the uniform part of the susceptibility is given by

$$\delta\chi_x \;=\; c\delta(x)\chi. \tag{5.88}$$

This result simply says that the impurity susceptibility $\chi_{\rm imp} = c\chi$ from equation (5.84) is only added directly at the open ends, but we have to keep in mind that our field theory analysis is valid only in the scaling limit so that we have to allow some finite width of a few lattice spacings for the delta-function. In addition we still have the alternating part from equation (5.81), which does not contribute when summed over x, but gives a large local contribution. This picture agrees with the numerical findings in figure 5.22, although the separation into the alternating and uniform part is somewhat ambiguous right at the origin.

In chapter 4 we discussed some cases in which the boundary conditions did not only correspond to the usual field theory fixed points, but also had sites removed or additional decoupled impurity spins. In particular, the periodic chain with one strengthened link renormalizes to the open chain with two sites removed. The impurity correction to the susceptibility is now $2(c-1)\chi$, which may be positive or negative. Likewise, the unstable fixed point in section 4.2 represents an open chain with a decoupled impurity spin. In this case the impurity susceptibility has an additional Curie contribution proportional to $1/T$ from the decoupled spin.

5.3 Susceptibility Contributions from Perturbations

To study the effect of perturbations on the lattice Hamiltonian, it is useful to review the renormalization group arguments which have been successfully applied in the Kondo problems[32, 33]. These renormalization group arguments are directly related to the

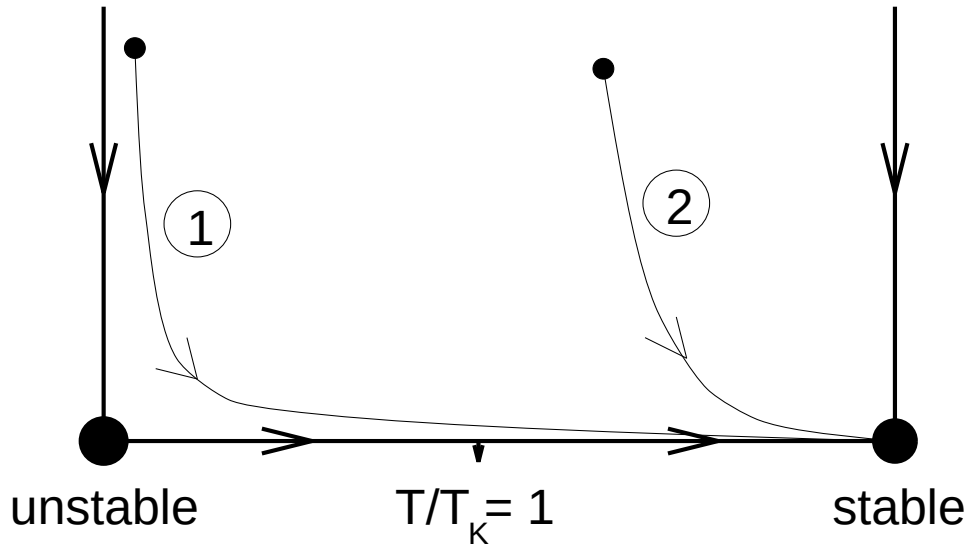

Figure 5.23: Renormalization group analysis of the cross-over from an unstable to a stable fixed point as the temperature is lowered.

discussion in section 1.2, which might be helpful in understanding the general ideas. At the fixed points the system is completely scale invariant, but as soon as we introduce a perturbation we expect that an energy scale T_K is introduced, which simply corresponds to the temperature where we expect the breakdown of perturbation theory. For stable (unstable) fixed points the description of the free Hamiltonian is then approximately valid for temperatures below (above) T_K. If there is a renormalization from an unstable to a stable fixed point, we expect the energy scales at the two fixed points to be related, so that there is really only one energy scale T_K that governs the cross-over.

In the case where a small perturbation creates all local operators near the fixed point, we usually only have to consider the leading operator with the smallest scaling dimension d, since all corrections due to the more irrelevant local operators vanish under renormalization. We can then determine the relation between T_K and the bare coupling constant λ by a simple renormalization argument. According to the discussion in section

3.2 we expect the breakdown of perturbation theory when λT^{d-1} becomes of order one for a local perturbation, so that

$$T_K^{1-d} \propto \lambda. \tag{5.89}$$

For marginally relevant perturbations (i.e. $b\lambda < 0$) with $d = 1$ this formula is replaced by $T_K \propto e^{1/b\lambda}$ due to equation (3.37). The cross-over from an unstable to a stable fixed point is universal since it is only governed by one energy scale, and impurity corrections should be functions only of the dimensionless ratio T/T_K. This idea is illustrated in figure 5.23, assuming that there is one relevant operator at the unstable fixed point and one leading irrelevant operator at the stable fixed point. If we ignore all other higher irrelevant terms the cross-over is described by one universal trajectory, which represents the x-axis in figure 5.23. Each point on the x-axis is labeled by only one parameter T/T_K which is decreasing along the x-axis and all impurity corrections are functions only of this parameter. In the limit $T \ll J$ we can write the impurity susceptibility as

$$\chi_{\text{imp}} = \frac{1}{T_K}\, f\left(\frac{T}{T_K}\right), \tag{5.90}$$

where the factor of $1/T_K$ has to be inserted for dimensional reasons. The other higher order irrelevant operators are represented by the y-axis in figure 5.23 and can be neglected for most purposes. Consider for example if we start close to the unstable fixed point, i.e. with only a small relevant coupling constant as well as other arbitrary irrelevant coupling constants as indicated by the trajectory (1) in figure 5.23. The irrelevant coupling constants become small very quickly and the actual renormalization trajectory (1) follows the x-axis very closely for several orders of magnitude in the parameter T/T_K. In this sense the cross-over function in equation (5.90) is universal. This equation is also useful for an arbitrary perturbation which may start closer to the stable fixed point as indicated by trajectory (2), corresponding to a larger value of T_K. The trajectory still approaches the universal cross-over function represented by the x-axis, but equation (5.90) is now

valid only in an asymptotic region $T/T_K \to 0$.

This analysis fails if there is more than one leading irrelevant (or relevant) coupling constant, since each coupling constant may set an independent cross-over energy scale. In the case of two coupling constants c and λ with a leading scaling dimension d equation (5.90) must be replaced by

$$\chi_{\text{imp}} = \frac{1}{T}\, g\left(cT^{d-1}, \lambda T^{d-1}\right), \tag{5.91}$$

This expression becomes equivalent to equation (5.90) if one of the coupling constants is set to zero, which can be seen by using equation (5.89).

For the two-channel spin-1/2 Kondo problem the asymptotic behavior has been determined to be[34, 35]

$$\chi_{\text{imp}} \propto \ln(T_K/T)/T_K, \tag{5.92}$$

for $T \ll T_K$. Curie's law has to be recovered for $T \gg T_K$, so that $\chi_{\text{imp}} \propto 1/T$ in that regime. If the initial Kondo coupling J' is weak, equation (5.92) reduces to $\chi_{\text{imp}} \propto \ln(J/T)e^{v\pi/J'}/J$ at low temperatures, which is less divergent than the unperturbed Curie law behavior for any finite J'. The scaling of T_K with J' follows from the discussion that lead to equation (5.89) and the fact that the corresponding operator is marginally irrelevant ($b = 1/v\pi$).

5.3.1 Two perturbed links

The case of two weak links of the spin chain is very closely related to the two-channel spin-1/2 Kondo effect as discussed in section 4.3, and we therefore expect the same logarithmic divergence as in equation (5.92) of the impurity susceptibility at low temperatures. Starting from the weak coupling limit $J' \to 0$ equation (5.92) is valid for $T \ll T_K$. In this limit we can keep only the most divergent part of the impurity contribution (i.e.

drop any constant terms) which results in the relation

$$\chi_{\text{imp}} \propto \ln\left(\frac{J}{T}\right)\frac{e^{v\pi/J'}}{J}, \tag{5.93}$$

since the marginal coupling constant of the "Kondo interaction" in equation (4.60) is given by J' to first order. The complete analytic form of the cross-over function is difficult to determine, but we can easily see that we have to recover Curie law behavior $\chi_{\text{imp}} \propto 1/T$ in the opposite limit $T \gg T_K$, corresponding to a nearly free impurity spin. The divergent part of the impurity susceptibility is expected to come mostly from the central "impurity spin" in figure 4.12, which is clear from the analogy to the two-channel Kondo effect and the analysis when J' is small (i.e. when the "impurity spin" produces a divergent Curie law susceptibility).

A small perturbation of two links from the periodic chain fixed point of $\delta J \equiv J - J'$ is the more interesting scenario for a μSR experiment. In this case there is no local operator in the Hamiltonian at the unperturbed fixed point, and all local field theory operators will have coupling constants of order δJ or higher. In this case we only have to consider the leading irrelevant operator which is given in equation (4.59) with scaling dimension of $d = 3/2$ at the Heisenberg point. We can use equation (5.89) to predict the low temperature behavior of the impurity susceptibility for small perturbations δJ on the lattice model. Since δJ produces the leading irrelevant operator to first order $\lambda \propto \delta J/J^{3/2} + \mathcal{O}(\delta J^2)$ according to the analysis in section 4.2 we can write

$$\chi_{\text{imp}} \propto -\frac{\delta J^2}{J^3}\ln\left(\frac{T}{J}\right), \tag{5.94}$$

where the powers of J were inserted by dimensional analysis. This expression follows directly from equations (5.89) and (5.92). Note, that we have inserted powers of J only to relate coupling constants in the lattice models to coupling constants in the field theory description with the correct units. However, J does not appear as an energy scale in the

field theory description, because we lowered the ultraviolet cutoff all the way to the temperature and J has been absorbed in the definition of the spin-wave velocity v.

In summary, the impurity susceptibility χ_{imp} increases monotonically with decreasing temperature or increasing perturbation δJ.

5.3.2 One perturbed link

A similar analysis can be applied for the perturbation of one link from the periodic chain δJ with the leading operator in equation (4.54) of dimension $d = 1/2$. By using perturbation theory in the leading relevant operator with coupling constant of order $\lambda \propto \delta J/\sqrt{J}$ we see that the leading order correction to the susceptibility is proportional to $\delta J^2/J$. This is because the first order contribution to the susceptibility $\langle \partial_x \phi \partial_x \phi \sin \phi/R \rangle$ has a vanishing expectation value, which can be seen by equation (A.105). Since $T_K \propto \delta J^2/J$ according to equation (5.89), we conclude that the cross-over function in equation (5.90) has an asymptotic behavior of $f(r) \to \text{const}/r^2$ as $r \to \infty$. The simplest assumption for small temperatures is $f(0) = \text{const}$.

There is one complication, however, which causes a problem near the open chain fixed point, because there are now *two* dimension $d = 2$ leading irrelevant boundary operators. The effect of the operator from equation (3.39) with coupling constant c has been discussed above, but the operator from equation (4.58) must also be taken into account, which has a coupling constant $\lambda \propto J'/J^2$ for a weak link. The relative magnitude of the two leading operators changes with J'. For bare coupling constants $J' \to 0$, which correspond to the open chain fixed point, the energy scale is therefore determined by two independent parameters c and J'. Therefore, we have to consider the more general case of equation (5.91). We can expand g to first order by using the notion that both first order corrections are independent of temperature according to equation

(5.84) and the fact that $f(0) = \text{const}$. The resulting relation is

$$\chi_{\text{imp}} = \frac{1}{T} g(cT, \lambda T) \to c\chi + \text{const. } J'/J^2 \tag{5.95}$$

where χ is the bulk susceptibility per site and c is the coupling constant of the local operator T_L in equation (3.39). We have also used $\lambda \propto J'/J^2$ and equation (5.84). Equation (5.95) reduces to equation (5.90) as $\lambda \to 0$ or $c \to 0$.

These findings can be directly carried over to the case of a very large link $J' \to \infty$, which also corresponds to the open chain fixed point but with two sites removed. In this case there is an effective virtual coupling of order J^2/J' across the open ends, which now determines the leading order of λ and the same analysis as above can be applied. However, it is not clear if the impurity susceptibility is positive or negative for large J' as discussed at the end of section 5.2.2, and therefore we cannot make any reliable scaling arguments in this limit.

For a bare coupling constant $\delta J \to 0$, which corresponds to the periodic chain fixed point, there is only one leading relevant operator with $d = 1/2$. Now, the energy scale is determined by only one parameter $\lambda \propto \delta J/\sqrt{J}$ According to equation (5.89) this energy scale becomes smaller as we approach the periodic chain $T_K \propto \delta J^2/J$, which just represents an expected small cross-over temperature near the unstable fixed point. This has a very interesting consequence for the zero temperature impurity susceptibility, because equation (5.90) predicts $\chi_{\text{imp}} \propto 1/T_K \propto J/\delta J^2$, which means a large impurity susceptibility close to the periodic chain. The sign of the overall constant of proportionality cannot be determined, because we are in the open chain fixed point regime $T < T_K$ and the two leading irrelevant operators may partially cancel. This large $T = 0$ impurity susceptibility is of little experimental relevance, however, because as soon as the temperature is increased beyond $\delta J^2/J$ we find ourselves in the periodic fixed point regime, and $\chi_{\text{imp}} \propto T_K/T^2 \propto \delta J^2/T^2$ which gives a small impurity susceptibility as expected.

5.4 A Muon Spin Resonance Experiment

Now that we have a good understanding of the local and impurity susceptibilities, it would be nice to find experimental evidence for the predicted effects. As we mentioned in the introduction one possible experiment to consider is a Muon Spin Resonance experiment on quasi one-dimensional spin-1/2 compounds, in which the muon would perturb the system and also probe the system locally at the impurity site[36]. The following discussion will focus on this particular experiment, but it would of course be possible to use the Monte Carlo results in chapter 6 for other kinds of experiments.

5.4.1 Experimental Setup

Positive muons are relatively long living particles ($\tau \approx 2.2 \times 10^{-6}$ sec) which carry a positive charge and a spin-1/2 and have about 200 times the mass of the electron. In a μSR experiment, a low energy beam of muons is sent into the magnetic material to be sampled. The beam is polarized, i.e. all muon spins are pointing in the same direction perpendicular to a small applied magnetic field (see figure 5.24). The muons enter the setup one at a time, and a timer is started for each muon. Once in the sample, the muons quickly find chemically preferred sites, and the magnetic moment of the spin precesses in the local magnetic field. Because weak interactions violate parity, the muon then decays into a positron and two neutrinos in a way that the positron is most likely ejected in the direction of the muon spin. The location where the positron hits one of the detectors gives some information about the direction of the muon spin before the decay. Given this direction and the time spent inside the sample, we can infer the strength of the local magnetic field in which the muon precessed. Typically about 10,000-100,000 such events per second can yield sufficient data within one or two hours. If a small external magnetic field H is applied, this setup effectively measures the local susceptibility of the sample,

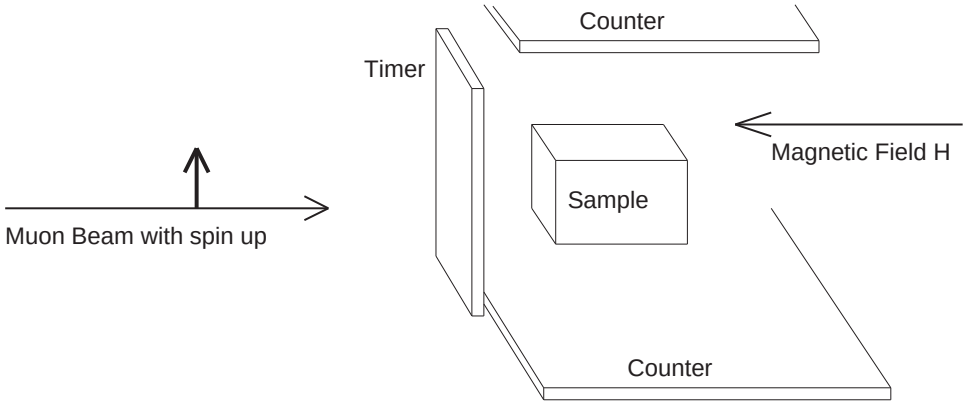

Figure 5.24: Schematic Muon Spin Resonance setup: One Muon at a time enters through the thin timer and stops inside the sample where its spin precesses. Decay positrons are detected in the two counters.

weighted with a dipole interaction at the chemically preferred site of the muon.

Unfortunately, the impurity susceptibility is not necessarily directly related to the μSR signal since the muon measures the local magnetic field $\vec{B}$, which is the sum of the dipole fields from all spin sites and the applied field $\vec{H}$. The dipole moment at each site j is proportional to the local susceptibility χ_j, so that an applied magnetic field in the z-direction H^z results in a magnetic field $\vec{B}$ at the muon site

$$\vec{B} = H^z \left(\hat{z} + \sum_j \frac{3\hat{r}_j(\hat{r}_j \cdot \hat{z}\chi_j) - \hat{z}\chi_j}{|\vec{r}_j|^3} \right), \tag{5.96}$$

where $\vec{r}_j$ is the location of site j relative to the muon. The second term in equation (5.96) is proportional to the so called Knight shift. The measured signal depends crucially on the perpendicular distance $d_\perp$ of the muon from the chain as shown in figure 5.25 as well as on the direction of the applied field H_z relative to the chain. Although we determined the z-component of the local susceptibility, this coordinate is not related to the orientation of the chain. The field H^z can therefore be applied in any direction relative to the chain, in particular parallel, perpendicular, or on a powdered sample. In general, it is useful to

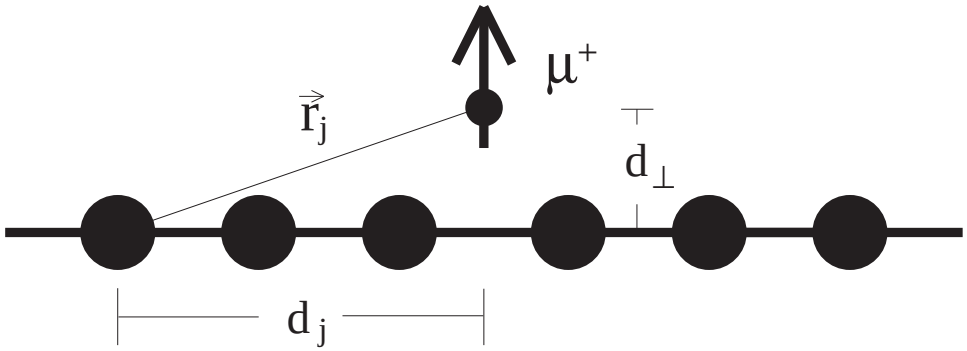

Figure 5.25: The location of the muon relative to the chain for the link parity symmetric case.

define an "effective" susceptibility at the muon site which is given by the second term in equation (5.96) divided by the applied magnetic field

$$\chi_{\text{eff}} \equiv \sum_j \chi_j \frac{3(\hat{z}\cdot\hat{r}_j)^2 - 1}{|\vec{r}_j|^3} \tag{5.97}$$

The different cases for the various field directions will be discussed in chapter 6, but for simplicity in this section we consider only the effective susceptibility χ_{eff} at the muon site for a powdered sample as an rough indication of the muon signal

$$\chi_{\text{eff}} = \sum_j \frac{\chi_j}{|\vec{r}_j|^3}, \tag{5.98}$$

where we performed an integration over the solid angle in equation (5.97).

So far we have discussed how the muon is used as a magnetic probe in the system, but a very important effect of the muon is of course the fact that it acts as an impurity as well. Although we use the dipole interaction to probe the system, we do not expect that this will produce a significant perturbation on the chain, since it is small compared to the exchange interaction, the coulomb interaction, and even the interchain coupling. The main effect of the muon therefore is a lattice distortion from inserting a positive

charge in the system as shown in figure 5.25 for a link symmetric site. It is reasonable to assume that the lattice distortion will drop off at least as fast as the derivative of the coulomb force i.e. as $1/r^3$ and belongs to the same universality class as a short range distortion. In cases where the muon binds directly to ions in the lattice or an electron the distortion may be even more localized. The effect on the exchange interaction J can only be roughly estimated by a previous experiment that observed a 20% shift in the hyperfine levels under the influence of the muon[37], which indicates a distortion of the orbitals and therefore a change of J of the same order of magnitude. Lattice distortions due to the muon may be in excess of 30%[38]. But even small distortions are bound to create large changes in J, since it is known from studies on MnO[39] that $\delta J/J$ can be more than one order of magnitude larger than the lattice distortion $\delta a/a$, where a is the lattice spacing.

The magnitude and range of the perturbation will vary from material to material. It is therefore most appropriate to use a generic model for link and site parity symmetric perturbations, corresponding to one or two equally perturbed links of various magnitude. Although it seems unlikely that the effect of the muon will exactly correspond to one of those two perturbations, it is reasonable to expect that it creates a symmetric perturbation. All preceding calculations do not require the knowledge of the actual form of the perturbation, but only refer to the leading operator, which is directly related to the symmetry properties of the perturbation. The renormalization group arguments should therefore be valid for any generic site or link parity symmetric perturbation of the muon.

Unfortunately, the muon will primarily probe the "non-universal" boundary region, which is not accessible by the field theory analysis and *does* depend on the specific form of the perturbation. As a first attempt to calculate the effective susceptibility quantitatively, we consider the cases of either two equally or one perturbed isotropic couplings. Depending on the results of the proposed experiment[36], further simulations

may be appropriate. The Monte Carlo data for the μSR experiment in section 6.2 should therefore be taken as a rough estimate of the predicted effects. The detailed signal of an experiment may look different, but we expect that the size of the corrections to the local susceptibility will be determined by the renormalization effects and the alternating operator, both of which are large.

5.4.2 Field Theory Analysis

Let us first consider the site parity symmetric case, which is modeled by two adjacent, equally perturbed links. We concluded that in this case the logarithmically divergent part of the impurity susceptibility comes primarily from the local susceptibility of the central "impurity" spin in figure 4.12. This followed from the analogy to the two channel Kondo effect and should be true for small J' or for $T > T_K$. Since this central spin is also the closest to the muon we expect that the μSR signal is directly related to the impurity susceptibility. The induced alternating susceptibility in the chain for small J' will be secondary because the affected sites are further away and the magnitude of $\delta\chi_i$ will be smaller. Nevertheless, this alternating part is interesting from a theoretical point of view and we expect interesting behavior in the local susceptibility from the Monte Carlo simulations. For small coupling J' and temperatures $T > T_K$ we expect open chain behavior with an induced alternating part from the boundary condition, which is positive at the ends. The interesting effect occurs when we lower the temperature or increase the coupling J' so that we approach the periodic chain fixed point. The central impurity spin is then considered part of the chain, but still has a large local susceptibility (i.e. a large $\langle S^z \rangle$ expectation value when a small magnetic field is applied). But since the spin is now considered part of a periodic chain equation (2.24) is valid and this large $< S^z \rangle$ expectation value propagates into the chain. In particular it induces a large alternating part which is of opposite sign of that from the boundary condition, so that

we should be able to observe a cross-over from a regime where the boundary alternating part dominates to a regime where the induced alternating part from the impurity spin dominates. This behavior is discussed again with the Monte Carlo data in section 6.1.3 and figures 6.35 - 6.38.

A similar analysis can be applied for the case corresponding to one weak link in the chain. We now expect that the two sites connected by the weak link dominate the Knight shift. Those two sites have a large contribution to the uniform part of the local susceptibility which is directly related to the impurity susceptibility according to equation (5.88). However, we now also have to consider the effect of the large alternating part from equation (5.81), which is of similar magnitude at the two sites. We are somewhat saved by the fact that there is no cancellation of the two parts in this case and the alternating part adds to the uniform contribution, so that the muon signal is roughly related to the impurity susceptibility. If the link is strengthened the effective susceptibility in equation (5.98) is always decreased because the two closest sites in figure 4.9 lock into a singlet at low temperatures. Their local susceptibility will therefore be lower and this behavior will dominate the effective susceptibility at the muon site. In this case it is not even clear if the impurity susceptibility (which involves a sum over the complete chain) should be positive or negative as indicated at the end of section 5.2.2. The effect of the perturbation on the effective susceptibility should be large in all scenarios.

Note, that only the uniform part of the local susceptibility is dependent on the bare coupling constant J' while the alternating part is produced by the boundary condition itself. The uniform part of the local susceptibility of the first few sites near the impurity therefore should depend on the coupling constant J' while the alternating part far away should be independent at a fixed temperature (provided that J' is small enough that the open fixed point description is valid).

Chapter 6

Monte Carlo Results

The field theory treatment of the spin chain is very useful in predicting impurity effects in quasi one-dimensional spin systems, but unfortunately this analysis cannot give us any quantitative results for the experiments other than the scaling behavior in certain limits. To tie the theoretical predictions to experiments it is therefore useful to have an independent method of determining the quantitative effects of impurities. With the help of the standard quantum Monte Carlo algorithm as described in appendix C we are able to present these quantitative results, which can provide experimentalists with an initial estimate of the magnitude of the effects and should also be helpful in separating out the impurity contribution from other effects in the analysis of the experimental data.

6.1 Impurity Susceptibility Effects

Monte Carlo simulations always have an inherent statistical error associated with them. In our case there is also a critical slowing down at low temperatures, so that the simulations do not produce useful data for $T < J/15$ (see also appendix C). Although the local susceptibilities and the μSR signal have been determined with reasonable accuracy, the error bars of the impurity susceptibility are rather large. Since we have to sum all local susceptibilities to calculate the overall impurity susceptibility, its error bars are larger by a factor of the square root of the system size (i.e. one order of magnitude for $l \approx 48 - 128$). As an example, the temperature dependence of the open chain impurity susceptibility and the local susceptibility correction $(\chi_1 - \chi)$ of the site closest to the

impurity have been plotted in figure 6.26. The error bars of the local susceptibility are much smaller, but unfortunately we can normally not extract the impurity susceptibility directly from this quantity, because it also contains an unspecified alternating contribution, which is apparently large. As predicted, the impurity susceptibility seems to approach a constant positive value as $T \to 0$. The local susceptibility at the first site seems to be roughly related to this impurity susceptibility, but with smaller error bars. The alternating contribution adds so that the signal at the first site is larger than the uniform impurity susceptibility. However, the accurate determination of the zero temperature impurity susceptibility is difficult, and the computer simulations for this quantity can only give a trend and a consistency check of our analysis in sections 5.3.1 and 5.3.2. Figure 6.26 gives a good estimate for the approximate error bars in general for the local and impurity susceptibilities, respectively. To make the presentation of the Monte Carlo data less confusing, the error bars of figures 6.27 - 6.38 in this section have been omitted and should simply be taken from figure 6.26.

6.1.1 One weak link

Figure 6.27 shows the impurity susceptibility of an open chain which has been slightly perturbed with a coupling J' across the open ends. The large error bars as given in figure 6.26 make this Monte Carlo data not unambiguous, but the findings seem to be consistent with equation (5.95) which predicts a change in the impurity susceptibility proportional to J'. We believe that the apparent crossing for some parameters J' is only produced by the large uncertainties.

The more interesting case is a small weakening by δJ of one link from the periodic chain. At intermediate temperatures $T_K < T < J$ the impurity susceptibility should be proportional to δJ^2 according to section 5.3.2. Figure 6.28 confirms an increase of the impurity susceptibility in this temperature regime, but higher order irrelevant operators

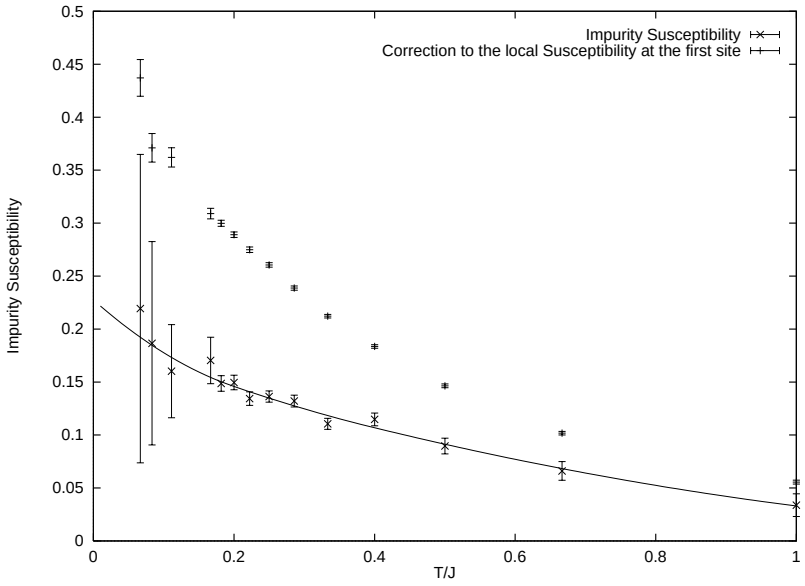

Figure 6.26: The open chain impurity susceptibility as a function of temperature. The solid line is only drawn for visual guidance and does not necessarily reflect an accurate estimate.

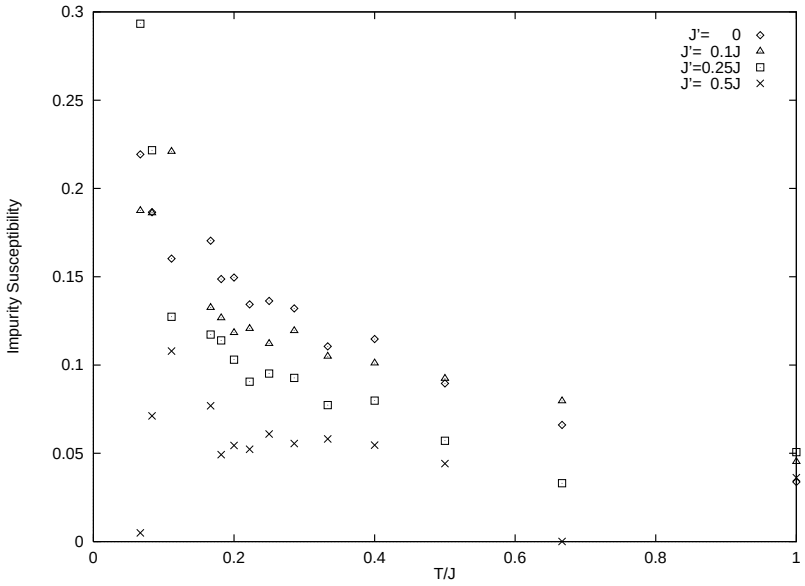

Figure 6.27: The impurity susceptibility for a small coupling J' across the open ends as a function of temperature.

seem to alter the scaling dependence, which appears to be linear with δJ. Perturbation theory in the lattice model actually does predict a linear dependence on δJ. The scaling prediction with δJ^2 comes from perturbation theory in the field theory Hamiltonian with the leading relevant operator only, which does not seem to be valid at the intermediate temperatures $0.3J < T < J$. Other irrelevant operators [e.g. $T_L(0)$ from equation (3.39)] become important in this regime, which do contribute to first order in perturbation theory and also have coupling constants of order δJ. Hence, the linear change with δJ in the impurity susceptibility is consistent with the field theory analysis.

For temperatures below the small cross-over scale $T_K \propto \delta J^2/J$ we expect that the impurity susceptibility should go as $J/\delta J^2$. If a negative proportionality constant is assumed, the numerical findings are consistent with this prediction. However, our Monte Carlo data is not good enough to give a reliable confirmation of the sharp cross-over at

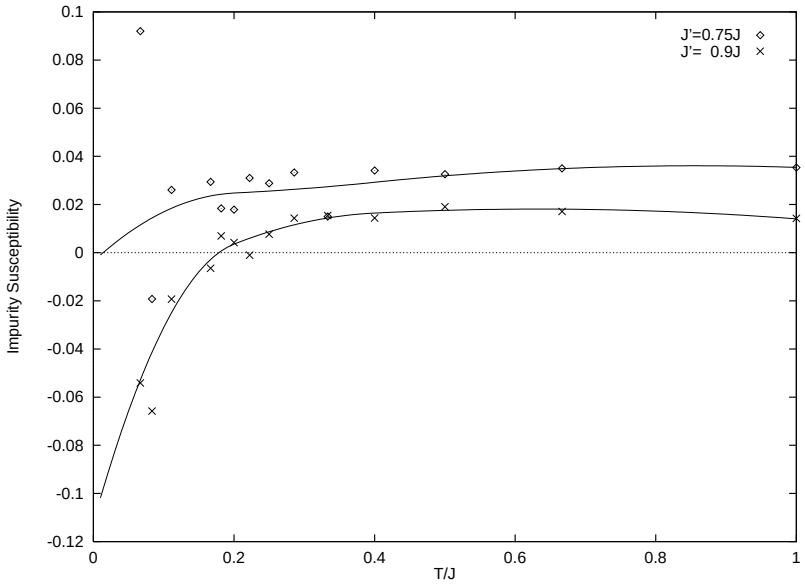

Figure 6.28: The impurity susceptibility for a small perturbation δJ of one link in the chain as a function of temperature. The solid lines are only drawn for visual guidance and do not necessarily reflect an accurate estimate.

very low temperatures as we approach the periodic chain.

6.1.2 Two weak links

As discussed in section 5.3.1 we expect a divergent impurity susceptibility as $T \to 0$ for any finite weakening of two adjacent links. For small perturbations δJ, equation (5.94) predicts a scaling of the impurity susceptibility with δJ^2, which is consistent with figure 6.29. However, the large error bars in figure 6.26 also make this Monte Carlo data somewhat ambiguous. It is therefore instructive to look at the correction to the local susceptibility of the central spin closest to the impurity in figure 4.12, because of the smaller error bars associated with local susceptibilities. This central spin is equivalent to the "impurity spin" in the Kondo problem and presumably carries the divergent part of the impurity susceptibility. Figure 6.30 seems to indicate a saturation of the impurity

susceptibility at $T_K \approx 0.3J$, $\delta J = 0.1J$, which might be interpreted as cross-over from a Curie-law behavior to a weaker logarithmic scaling. This would imply that the cross-over temperatures for all other coupling constants considered are too small to observe, because $T_K \propto J/\delta J^2$. This would indicate that the "healing" process as described in section 4.2 is very slow, as might be expected from the dimensionalities of the leading operators, which are only marginal relevant and only weakly irrelevant at the two fixed points. Figure 6.30 also seems consistent with equation (5.94).

Figure 6.31 shows the impurity susceptibility for small bare coupling constants J' to the impurity spin. It is again instructive to look at the local susceptibility of the "impurity spin", which can be compared with the Curie-law behavior of a completely decoupled spin as shown in figure 6.32. Since the cross-over temperature is much lower than the lowest accessible temperature, we cannot observe the predicted behavior with $-e^{v\pi/J'} \ln T$, but the Monte Carlo data certainly is consistent with this scaling function.

6.1.3 Alternating Parts

Predictions for the alternating part of the impurity susceptibility can be tested much more easily, because it only involves local susceptibilities with much smaller uncertainties. The functional dependence of the alternating part has already been confirmed in figure 5.22, but it is interesting to note that the strong staggered behavior persists even for small perturbations of one link in the periodic chain as shown in figure 6.33. In fact, we expect the staggered part to be asymptotically independent of the bare coupling constant in the limit $T \ll T_K$ and $x > v/T_K$, which is confirmed in figure 6.34. At $T = J/15$, the staggered part is only very weakly dependent on J' as long as J' is small (which also means v/T_K is small). For perturbations of the order of $J' \approx 0.5J$ we find a different amplitude at short distances from the boundary, but far away from the boundary all

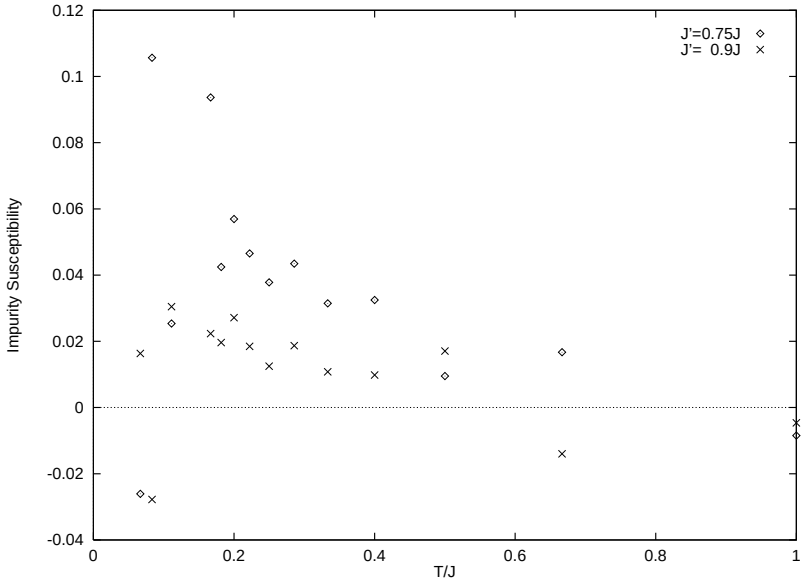

Figure 6.29: The impurity susceptibility for a small perturbation δJ of two links in the chain as a function of temperature.

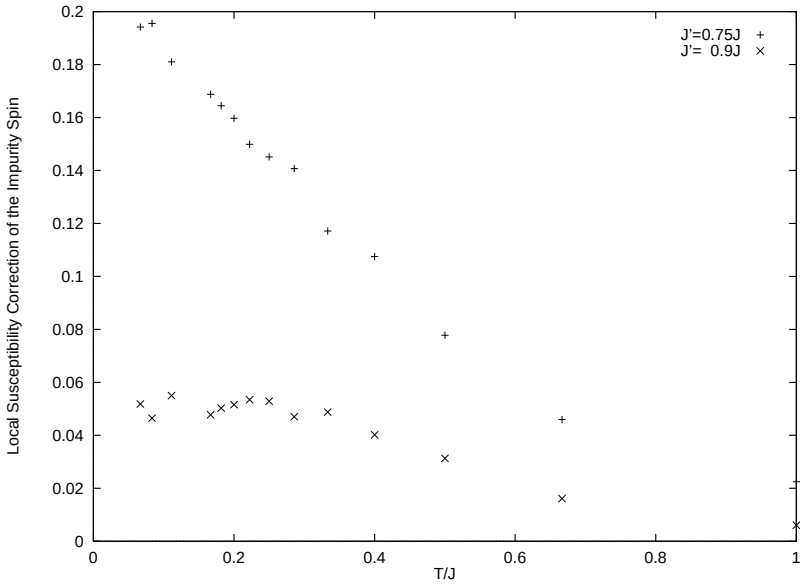

Figure 6.30: The local susceptibility correction of the central spin closest to the impurity for a small perturbation δJ on two links in the chain as a function of temperature.

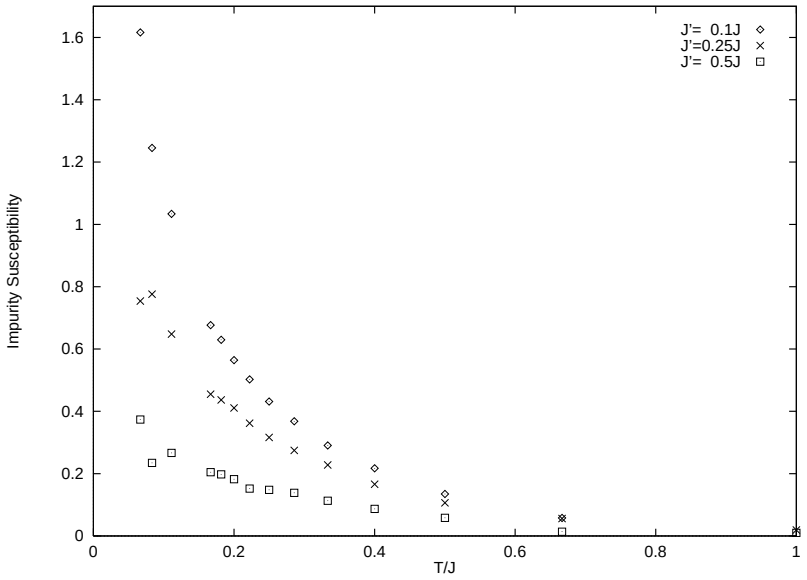

Figure 6.31: The impurity susceptibility for a small coupling J' of the open ends to an impurity spin as a function of temperature.

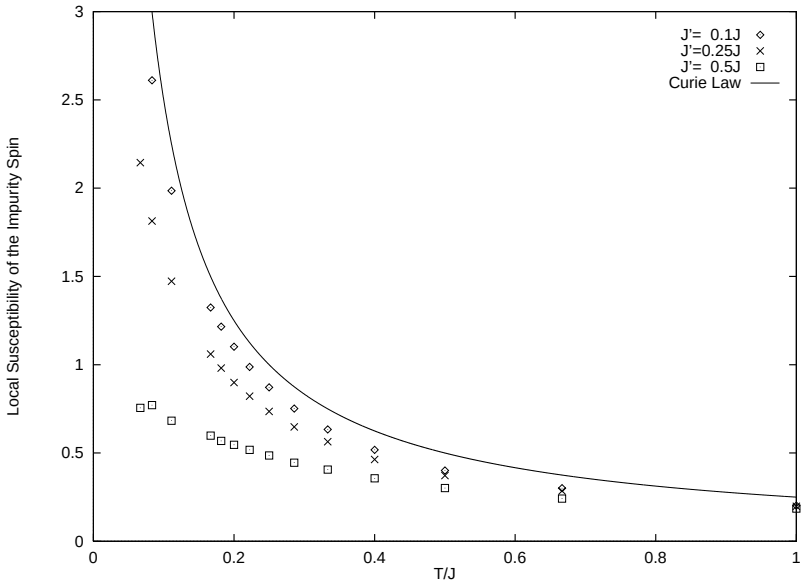

Figure 6.32: The local susceptibility of an impurity spin coupled with a small perturbation J' to the open ends of the chain as a function of temperature.

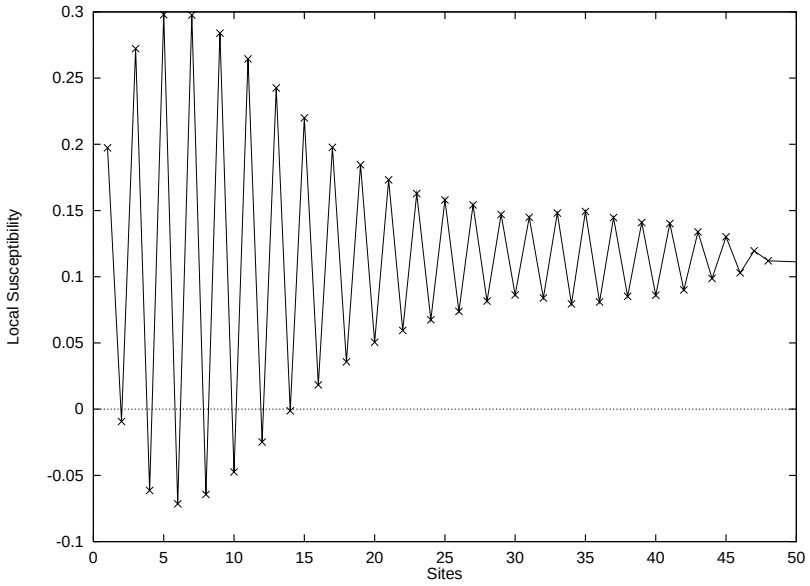

Figure 6.33: The local susceptibility as a function of distance from a weakened link $J' = 0.75J$ at $T = J/15$.

curves seem to follow a universal shape within the error bars (see figure 6.26 for an estimate of the error bars of the local susceptibility).

For site parity symmetric perturbations, on the other hand, we expect the opposite behavior in the limit $T \ll T_K$ and $x > v/T_K$, corresponding to no alternating part due to the boundary condition. Unfortunately, we cannot test this behavior because of the low cross-over temperatures, but we can observe a competition between the alternating part due to the boundary condition (the "boundary contribution") according to equation (5.81) and the alternating part which has been induced by the impurity spin according to equation (2.24) as discussed in section 5.4. The boundary contribution is positive at the first site away from the impurity, while the induced alternating part from the central spin is negative. The induced alternating part becomes stronger as the temperature is lowered, but drops off fast with $1/x$ where x is the distance from the impurity. The

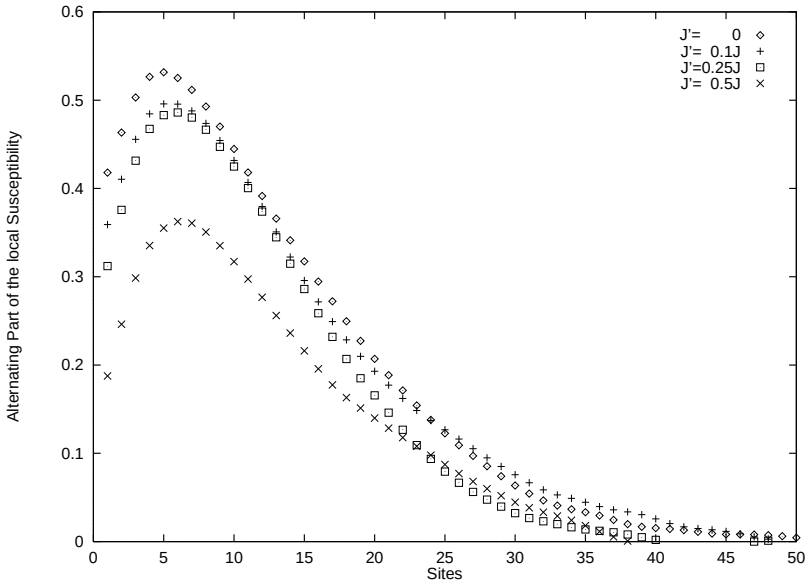

Figure 6.34: The alternating part of the local susceptibility as a function of distance from the weakly coupled link J' across the open ends at $T = J/15$.

boundary contribution decreases as $J' \to J$, but always dominates for larger distances from the impurity (unless $T \ll T_K$). This behavior is demonstrated in figures 6.35 - 6.38. For bare coupling constants close to the open chain $J' \to 0$ the boundary alternating part completely dominates, but as we get closer to the periodic chain $J' \to J$ we only see a small boundary alternating part far away from the impurity while the induced alternating part dominates near the impurity site.

6.2 Muon Knight Shift

Since the measured Knight shift depends strongly on the direction of the applied magnetic field we want to distinguish three cases of interest: field direction perpendicular or parallel to the chain or a powdered sample. The signal also depends on the perpendicular offset (distance) $d_\perp$ of the muon from the chain as shown in figure 5.25, but generally it is

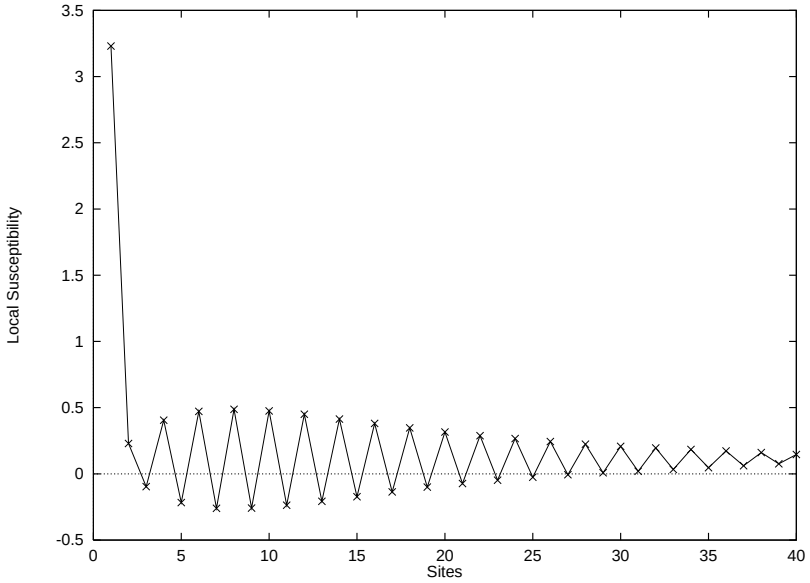

Figure 6.35: The local susceptibility as a function of distance with the open ends coupled with $J' = 0.1J$ to an impurity spin at the first site at $T = J/15$.

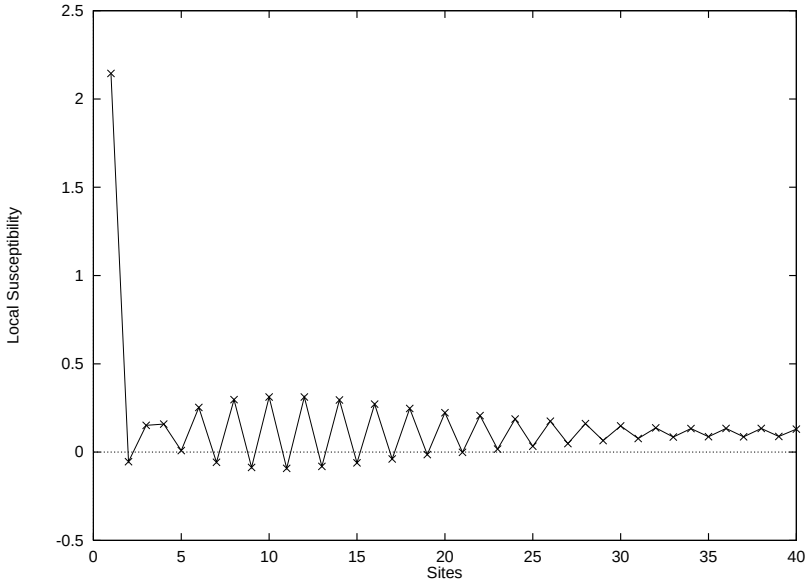

Figure 6.36: The local susceptibility as a function of distance with the open ends coupled with $J' = 0.25J$ to an impurity spin at the first site at $T = J/15$.

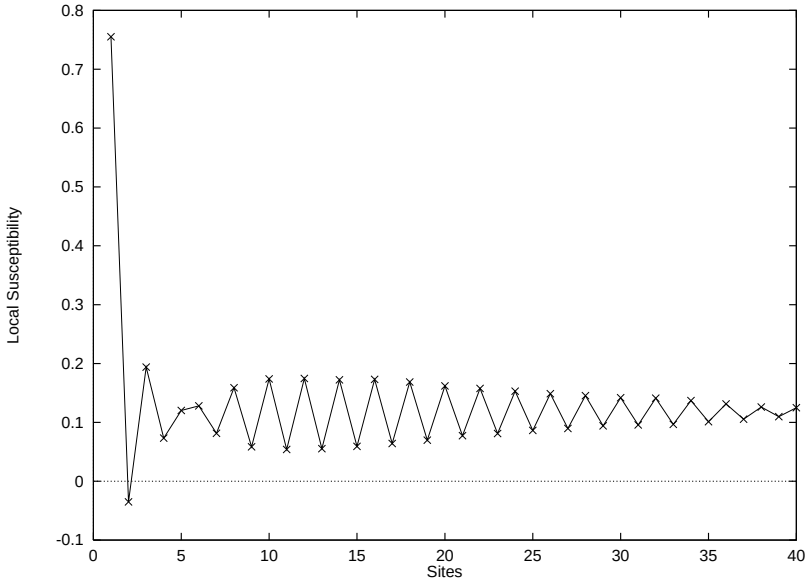

Figure 6.37: The local susceptibility as a function of distance with the open ends coupled with $J' = 0.5J$ to an impurity spin at the first site $T = J/15$.

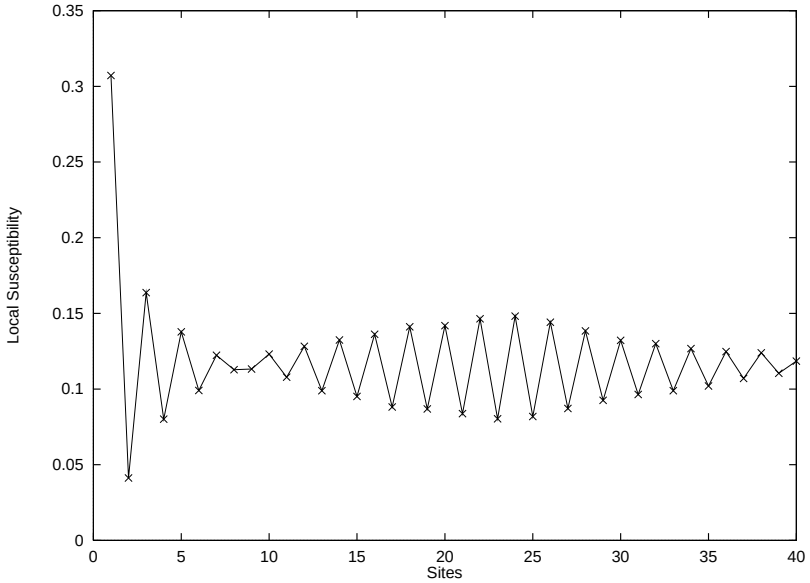

Figure 6.38: The local susceptibility as a function of distance from two slightly weakened links $J' = 0.75J$ at $T = J/15$.

sufficient to choose only two different values for $d_\perp$ corresponding to one-half or one units of lattice spacing in order to get a good impression on the impurity effects. The distance of the individual sites from the muon along the chain d_j is always taken to be either half-odd-integer or integer values for link or site parity symmetric locations, respectively. Figure 5.25 shows the geometrical arrangement with the example of a link parity symmetric location. We can simply use the effective susceptibility in equation (5.97) to derive the expected muon signal from the local susceptibilities in the Monte Carlo simulations. Since this effective susceptibility is to be compared with the unperturbed bulk susceptibility in figure 5.17, we always consider χ_{eff} normalized by a geometrical factor γ, which is simply obtained by setting all $\chi_j = 1$ in equation (5.97)

$$\gamma \equiv \sum_j \frac{3(\hat{z} \cdot \hat{r}_j)^2 - 1}{|\vec{r}_j|^3} \tag{6.99}$$

The case of the powdered sample has been discussed in section 5.4 where angular averaging yielded equation (5.98). Using equation (5.97) we can immediately compute the effective susceptibility at the muon site for the other two cases. If the field is applied parallel to the chain, we find:

$$\chi_{\text{eff}} = \sum_j \left(3d_j^2/|\vec{r}_j|^2 - 1\right) \frac{\chi_j}{|\vec{r}_j|^3}. \tag{6.100}$$

where $\vec{r}_j$ is the location of the spin at site j relative to the muon and d_j is the horizontal offset along the chain of site j from the impurity (i.e. $|\vec{r}_j| = \sqrt{d_\perp^2 + d_j^2}$). The analogous expression for an applied field perpendicular to the chain is

$$\chi_{\text{eff}} = \sum_j \left(3d_\perp^2/|\vec{r}_j|^2 - 1\right) \frac{\chi_j}{|\vec{r}_j|^3}. \tag{6.101}$$

Note, that the arithmetic mean of the expressions for the two field directions reduces to the effective susceptibility of a powdered sample. We should mention that there is a possible fourth case when the applied field is perpendicular to both the chain orientation

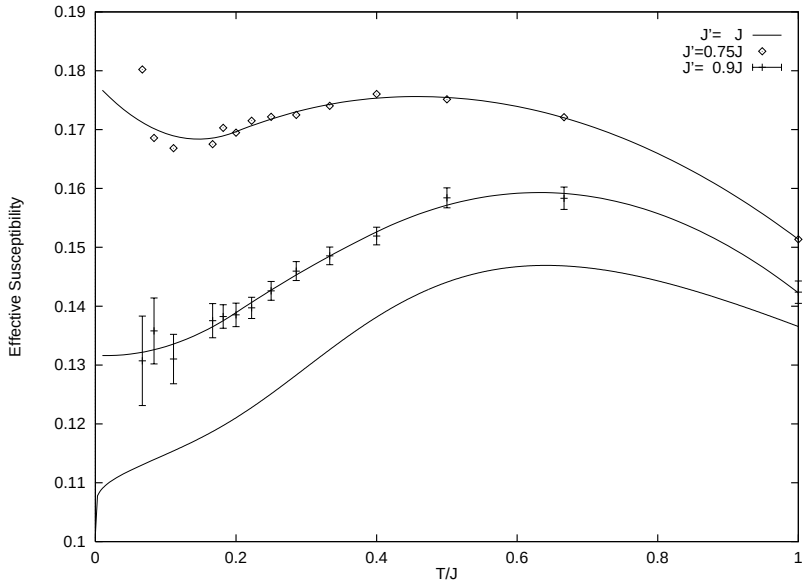

Figure 6.39: The effective normalized susceptibility in a powdered sample for small perturbations on one link and $d_\perp = 0.5$ as a function of temperature.

and the vertical offset $d_\perp$. In this case the normalized effective susceptibility reduces to the effective susceptibility of the powdered sample in equation (5.98), so that we do not need to discuss it separately.

6.2.1 One perturbed link

Figures 6.39 and 6.40 show the effective susceptibility at the muon site with a vertical offset of $d_\perp = 1/2$ and $d_\perp = 1$ in units of lattice spacing, respectively, in a powdered sample for a small perturbation on one link of the periodic chain. The error bars in figure 6.39 will serve us as an estimate for the relative error of the predicted muon signal in figures 6.39- 6.73.

The maximum seems to be shifted to lower temperatures with increasing perturbation, and the overall amplitude of the signal is increased. Apparently, the predicted

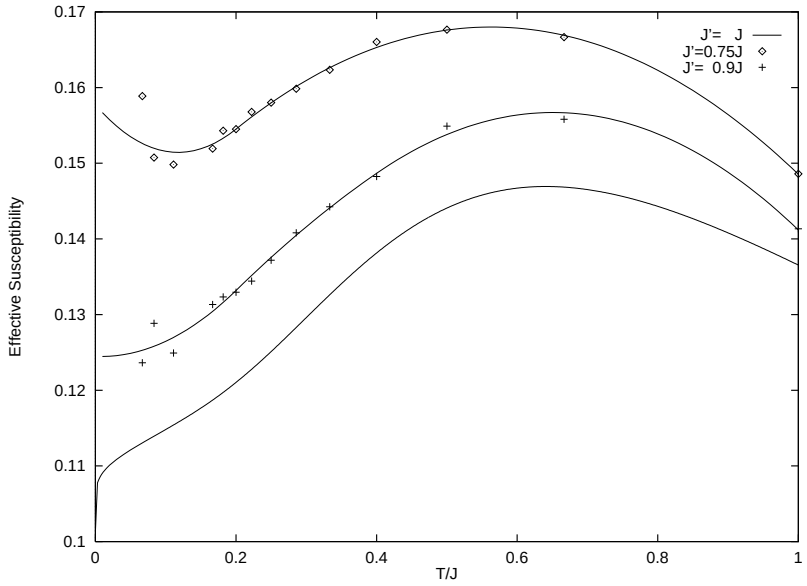

Figure 6.40: The effective normalized susceptibility in a powdered sample for small perturbations on one link and $d_\perp = 1$ as a function of temperature.

renormalization of the weakened link is responsible for the observed effects. In particular, we expect the contributions of both the impurity susceptibility and the alternating part to increase as we lower the temperature as shown in figure 6.26. In addition the renormalization of the weak link across the open ends enhances this effect. These increased susceptibility contributions at low temperatures are responsible for the shifted maximum and the larger overall signal. In a μSR experiment, the location of the maximum as well as the ratio of the maximum susceptibility to the low temperature susceptibility will give an indication of the strength of the perturbation.

The opposite effect is observed when one link is strengthened as shown in figures 6.41 and 6.42. The maximum seems to be shifted to lower values and the overall amplitude is reduced. This effect has to be attributed to the formation of a singlet by the two strongly coupled spins. The observed upturn of the signal at low temperatures on the

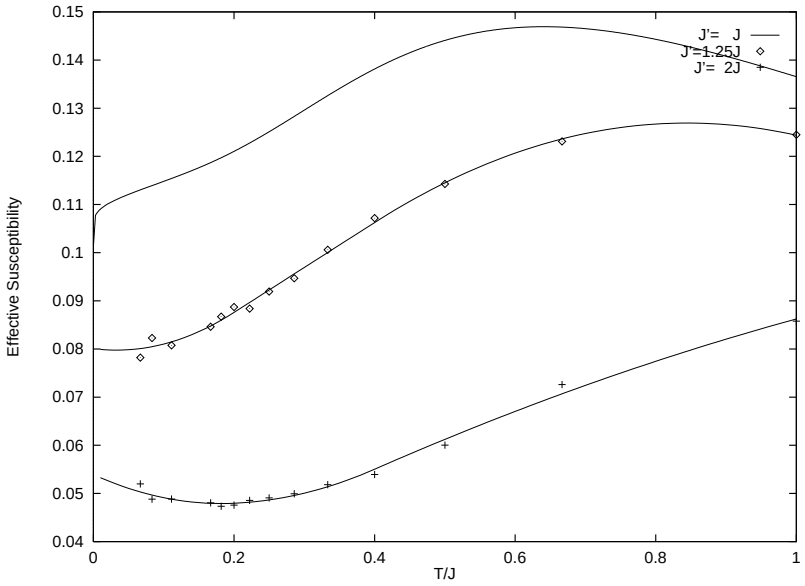

Figure 6.41: The effective normalized susceptibility in a powdered sample for one strengthened link and $d_\perp = 0.5$ as a function of temperature.

other hand might be a renormalization effect of the small virtual coupling across the open ends. When the perturbation is strong enough to produce bare coupling constants that correspond to the open chain (i.e. J' small) a complete vanishing of the maximum is observed as shown in figures 6.43 and 6.44. In this case the renormalization effects dominate even at intermediate temperatures. All observed effects become weaker as the distance $d_\perp$ of the muon is increased, because bulk spins will influence the signal more for larger distances $d_\perp$.

If a magnetic field is applied perpendicular to the orientation of the chain the same qualitative picture can be observed, as shown in figures 6.45 - 6.50. Equation (6.101) indicates that the spins closest to the impurity are sampled much more, because the first term drops off with $1/|\vec{r}_j|^5$. Therefore, the effects which we observed for a powdered sample are much more pronounced. However, the upturn of the signal for a strengthened

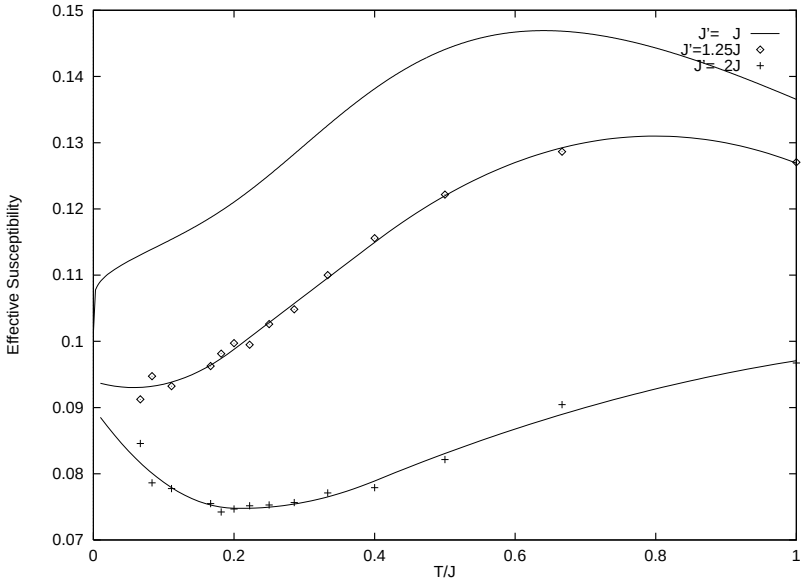

Figure 6.42: The effective normalized susceptibility in a powdered sample for one strengthened link and $d_\perp = 1$ as a function of temperature.

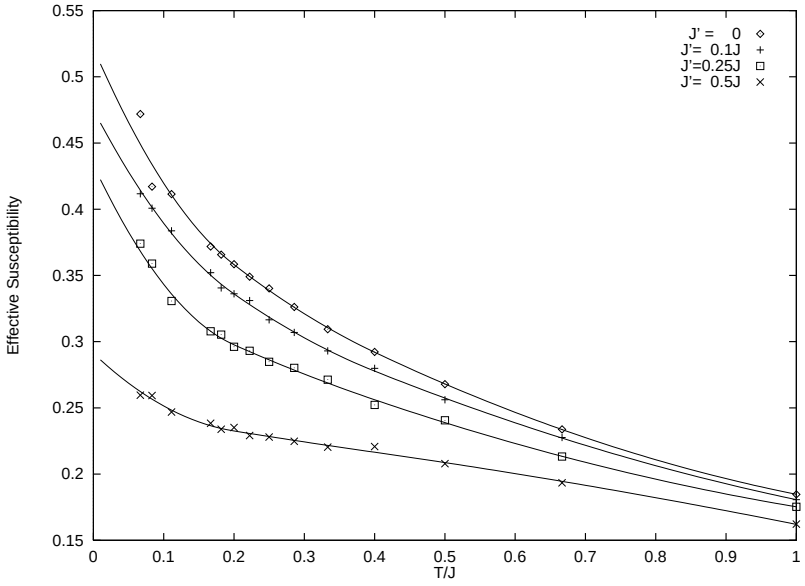

Figure 6.43: The effective normalized susceptibility in a powdered sample for strong perturbations on one link and $d_\perp = 0.5$ as a function of temperature.

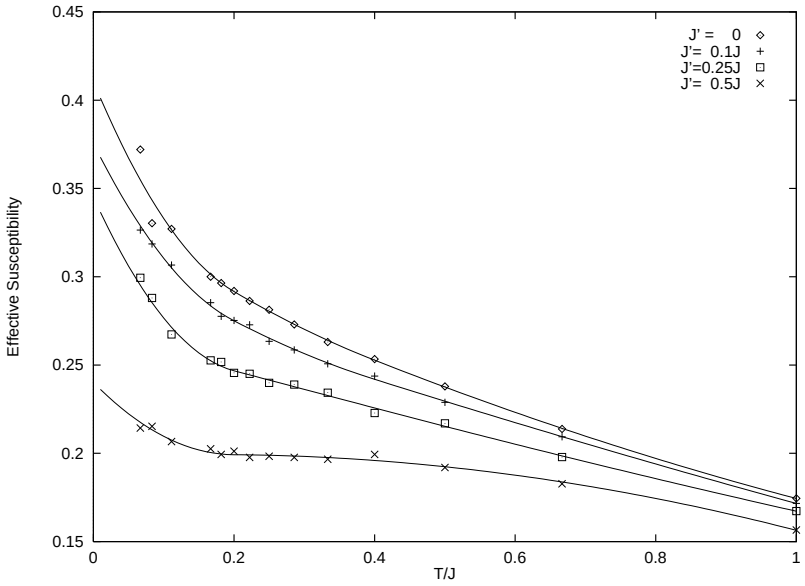

Figure 6.44: The effective normalized susceptibility in a powdered sample for strong perturbations on one link and $d_\perp = 1$ as a function of temperature.

link at low temperatures is not observed in figures 6.47 and 6.48 since this effect comes from the second sites in the chain.

Figures 6.51 - 6.53 show the analogous effects for an applied field parallel to the chain. The same features can be observed, but again with different magnitude (this anisotropy effect might help to determine the actual location of the muon in the sample). If, however, $d_\perp$ is chosen so that the geometrical normalization factor γ for equation (6.100) or (6.101) becomes very small, we can see very pronounced impurity effects. Since the absolute signal of the unperturbed susceptibility is very small in this case, small perturbation can produce big relative changes of arbitrary sign. As an example, we simulated a vertical offset of $d_\perp = 1$ which reduces the geometrical factor γ for a field parallel to the chain by a factor of 200 compared to $d_\perp = 0.5$. The resulting signal is shown in figures 6.54 - 6.56 which shows completely different behavior than the previous

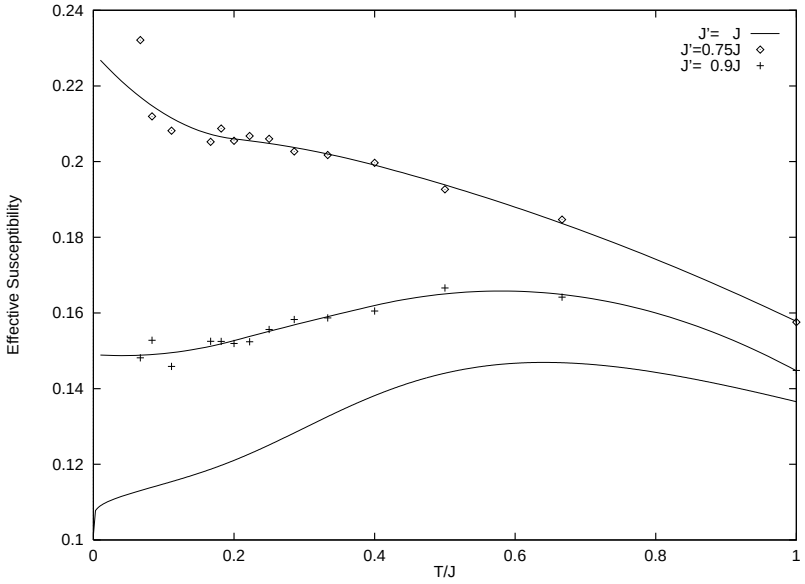

Figure 6.45: The effective normalized susceptibility for an applied field perpendicular to the chain, small perturbations on one link and $d_\perp = 0.5$ as a function of temperature.

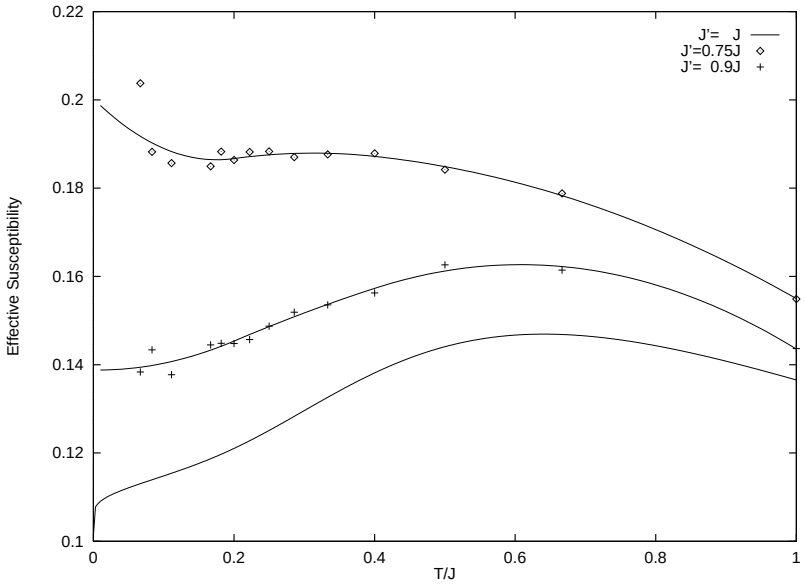

Figure 6.46: The effective normalized susceptibility for an applied field perpendicular to the chain, small perturbations on one link and $d_\perp = 1$ as a function of temperature.

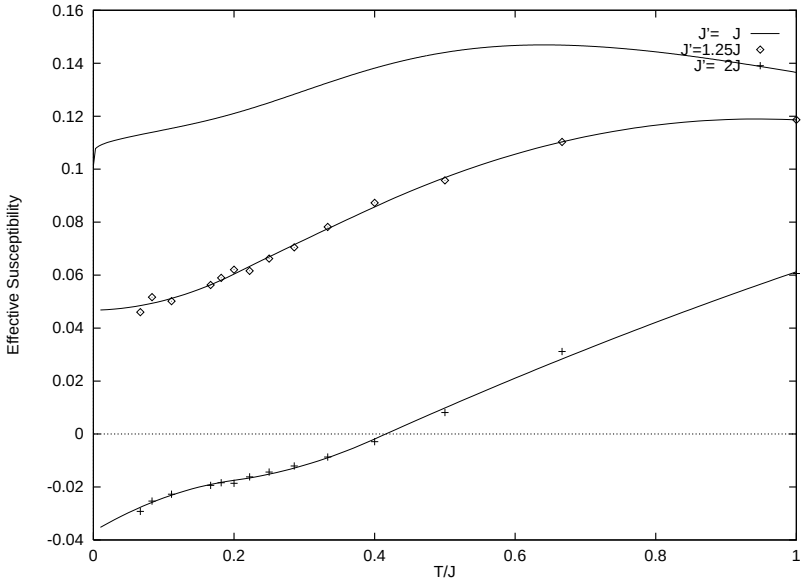

Figure 6.47: The effective normalized susceptibility for an applied field perpendicular to the chain, one strengthened link and $d_\perp = 0.5$ as a function of temperature.

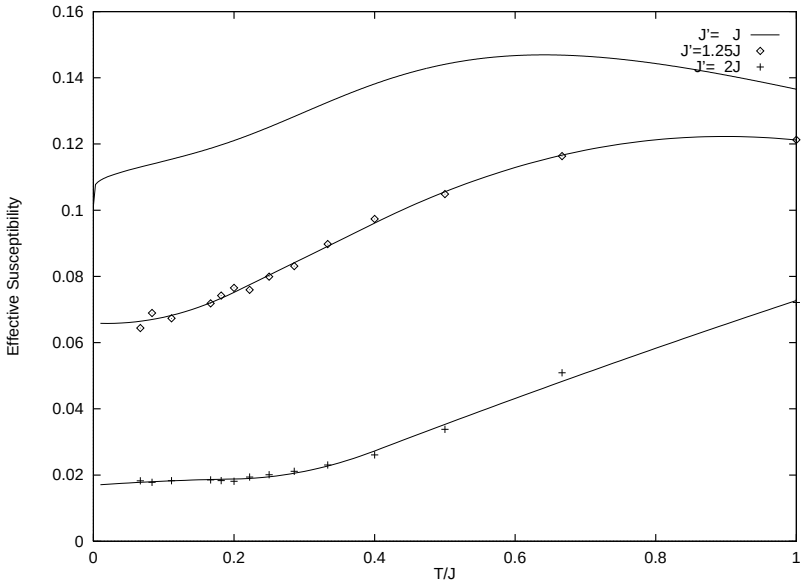

Figure 6.48: The effective normalized susceptibility for an applied field perpendicular to the chain, one strengthened link and $d_\perp = 1$ as a function of temperature.

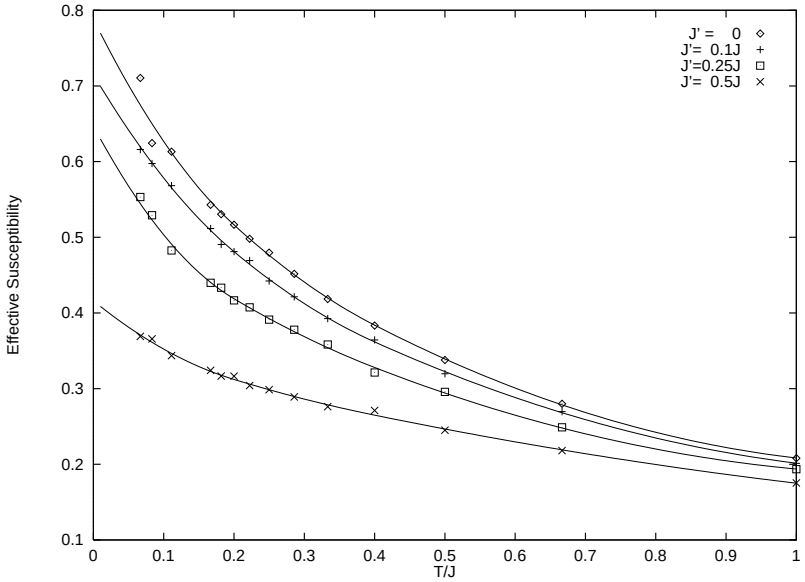

Figure 6.49: The effective normalized susceptibility for an applied field perpendicular to the chain, strong perturbations on one link and $d_\perp = 0.5$ as a function of temperature.

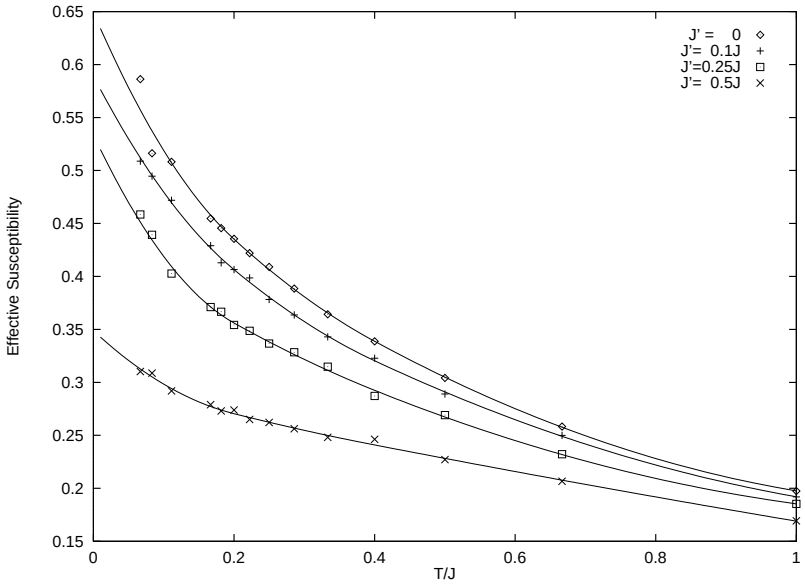

Figure 6.50: The effective normalized susceptibility for an applied field perpendicular to the chain, strong perturbations on one link and $d_\perp = 1$ as a function of temperature.

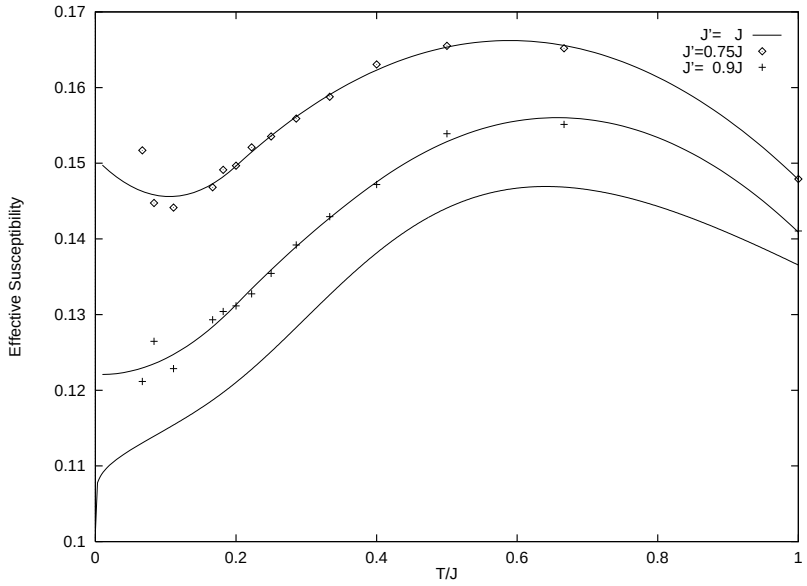

Figure 6.51: The effective normalized susceptibility for an applied field parallel to the chain, small perturbations on one link and $d_\perp = 0.5$ as a function of temperature.

figures.

6.2.2 Two perturbed links

Let us now consider the analogous cases for a site symmetric perturbation on two adjacent links in the chain. The muon signal will be dominated by the strong local susceptibility of the impurity spin for any weakened coupling $0 < J' < J$. Monte Carlo simulations confirm this picture for a powdered sample in figures 6.57 - 6.60 (see also figures 6.30 and 6.32). The measured effect again decreases with distance $d_\perp$. The maximum can only be observed for small perturbations and is shifted by large amounts even for $J' = 0.9J$ since the strong logarithmic impurity susceptibility dominates the behavior for any larger perturbation. This behavior is much stronger than the corresponding cases for one weak link, which may be somewhat surprising, since we expect *healing* of the chain in this

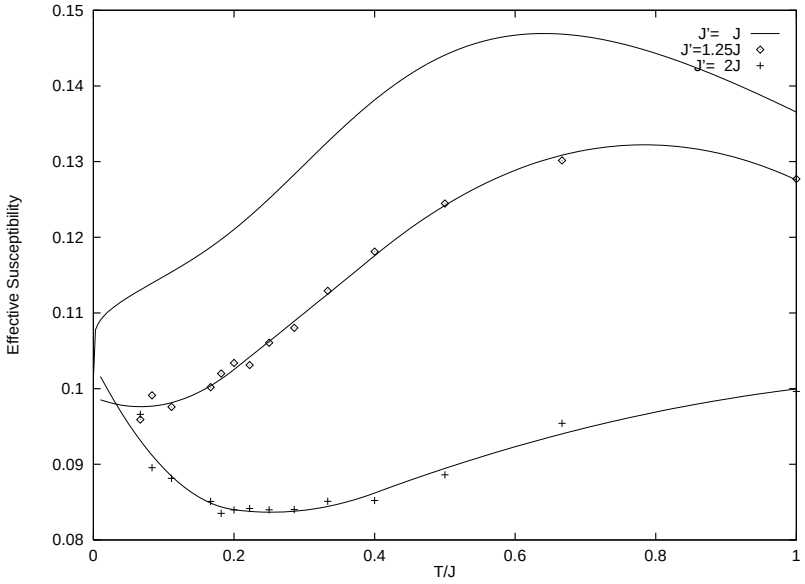

Figure 6.52: The effective normalized susceptibility for an applied field parallel to the chain, one strengthened link and $d_\perp = 0.5$ as a function of temperature.

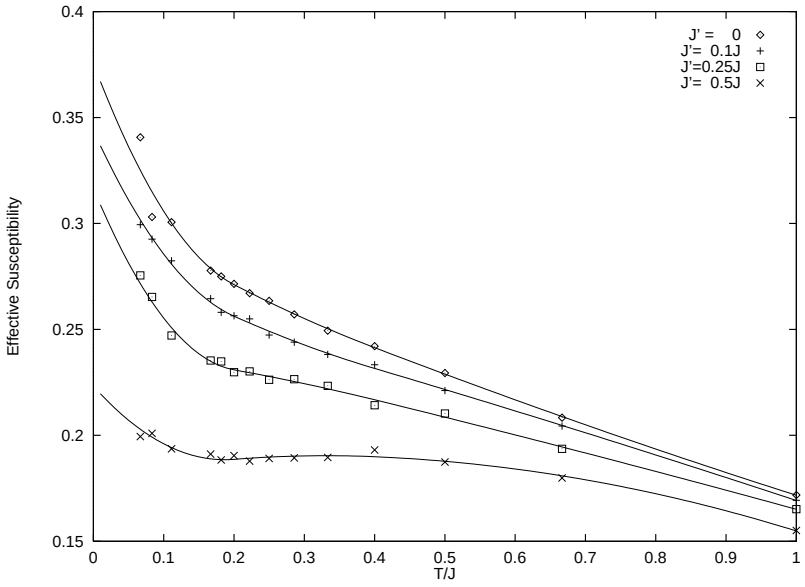

Figure 6.53: The effective normalized susceptibility for an applied field parallel to the chain, strong perturbations on one link and $d_\perp = 0.5$ as a function of temperature.

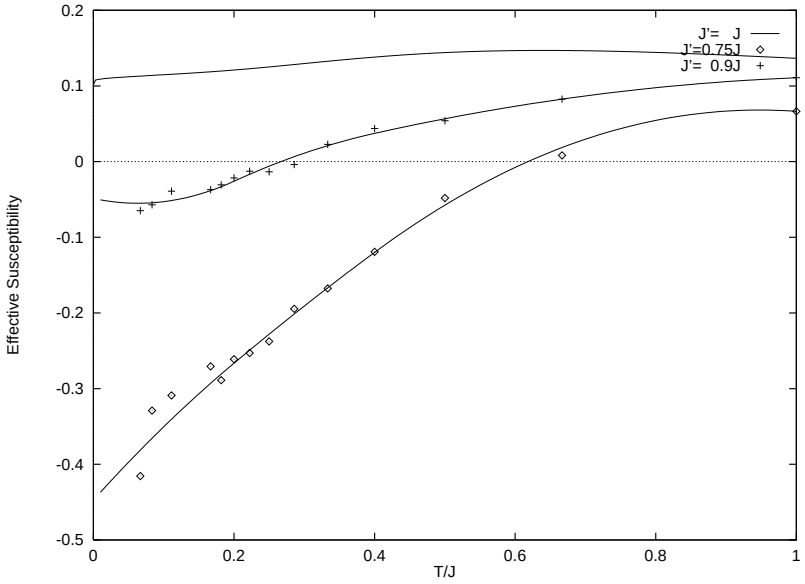

Figure 6.54: The effective normalized susceptibility for an applied field parallel to the chain, small perturbations on one link and $d_\perp = 1$ as a function of temperature.

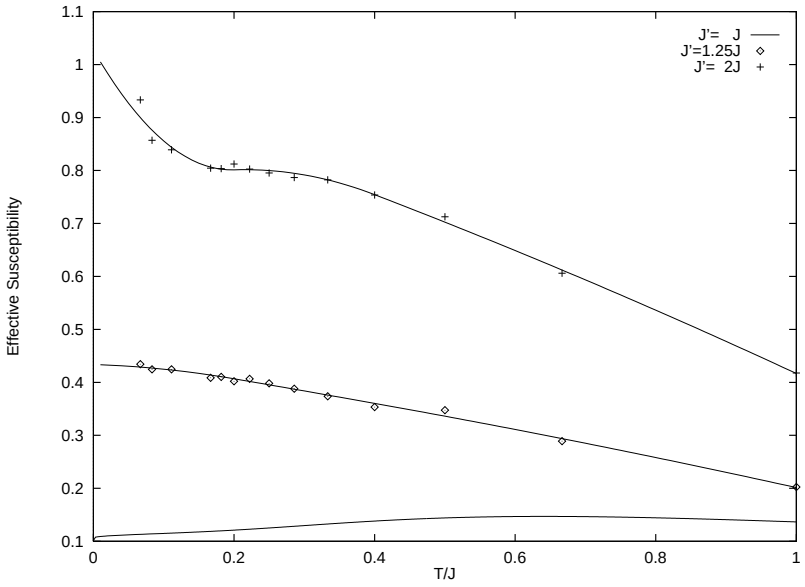

Figure 6.55: The effective normalized susceptibility for an applied field parallel to the chain, one strengthened link and $d_\perp = 1$ as a function of temperature.

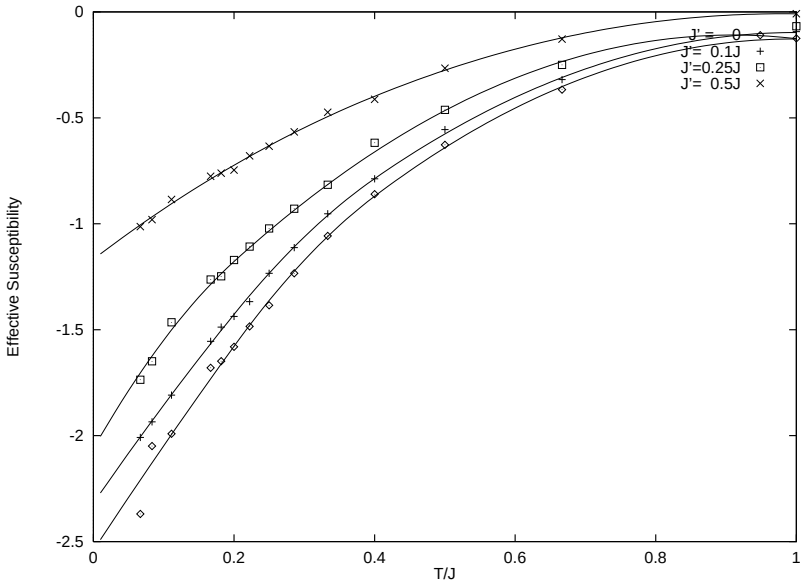

Figure 6.56: The effective normalized susceptibility for an applied field parallel to the chain, strong perturbations on one link and $d_\perp = 1$ as a function of temperature.

scenario. However, as we saw in section 6.1.2 the healing process is very slow so that the impurity susceptibility is initially Curie like and apparently becomes very large before the renormalization effects contribute. Even after complete renormalization to a healed chain the remaining impurity susceptibility is still logarithmic divergent.

A strengthening of two links also produces a significant change in the signal, corresponding to a shifted maximum to higher temperatures, an overall lowered signal, and a curious downturn at low temperatures as shown in figures 6.61 and 6.62. Although we do not have any reliable renormalization arguments for this case, the Monte Carlo data provides an interesting estimate for the μSR signal.

The Monte Carlo data for the two field directions perpendicular and parallel to the chain in figures 6.63 - 6.73 give virtually identical results because it is always the impurity spin that dominates the behavior. For a special choice of $d_\perp = 1$ and a field parallel to

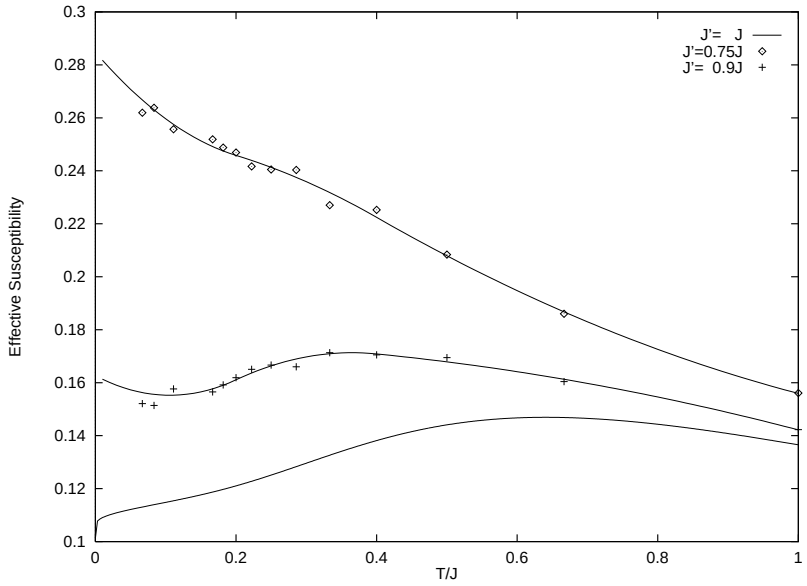

Figure 6.57: The effective normalized susceptibility in a powdered sample for small perturbations on two links and $d_\perp = 0.5$ as a function of temperature.

the chain, the geometrical factor γ is again very small. The effect of perturbations is therefore artificially inflated as shown in figures 6.71 - 6.73. The effect is only large relative to the unperturbed signal, but small in absolute terms.

6.3 Conclusions

In summary we have managed to analyze the interesting renormalization behavior of impurities in quantum spin-1/2 chains and their effects on the susceptibility (which turned out to be quite exotic in some cases). Numerical simulations are always consistent with our analysis and support the validity of the methods of boundary critical phenomena.

We were able to propose a μSR experiment on quasi one-dimensional spin-1/2 compounds, which might be able to show some of the predicted effects. Since the impurity effect of the muon will be strongly dependent on the particular material, we do not expect

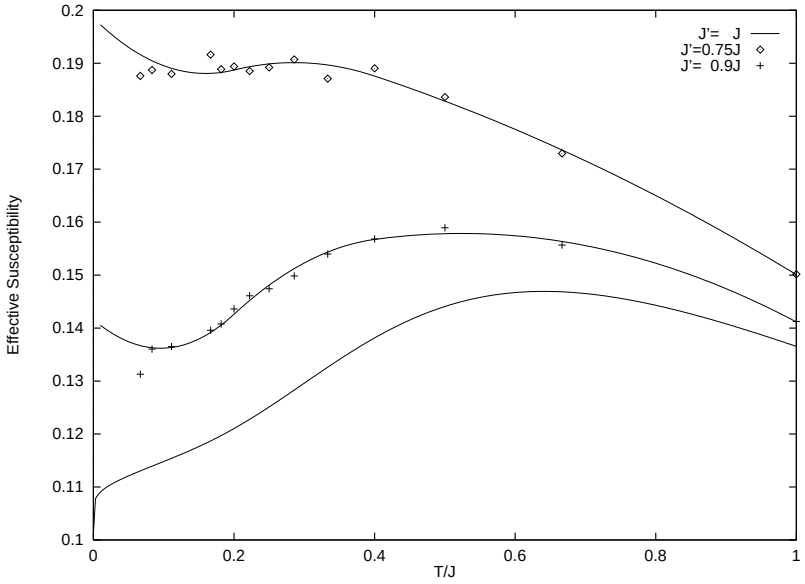

Figure 6.58: The effective normalized susceptibility in a powdered sample for small perturbations on two links and $d_\perp = 1$ as a function of temperature.

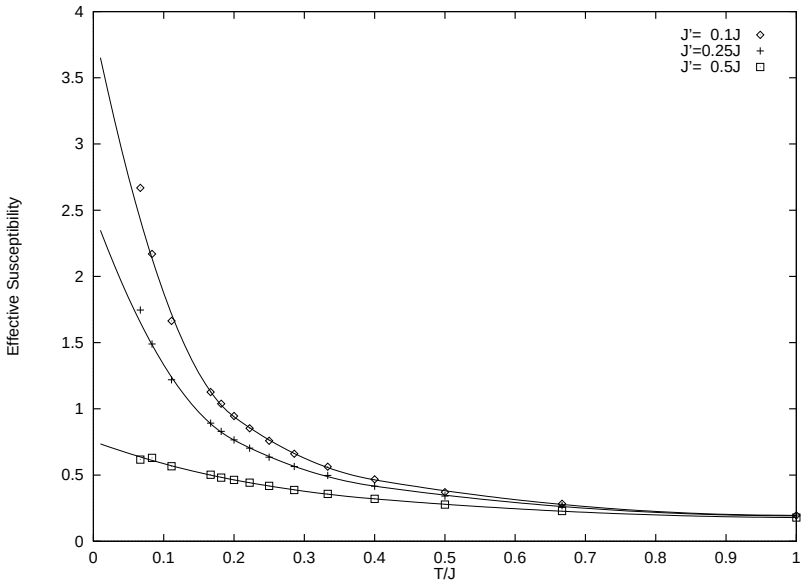

Figure 6.59: The effective normalized susceptibility in a powdered sample for strong perturbations on two links and $d_\perp = 0.5$ as a function of temperature.

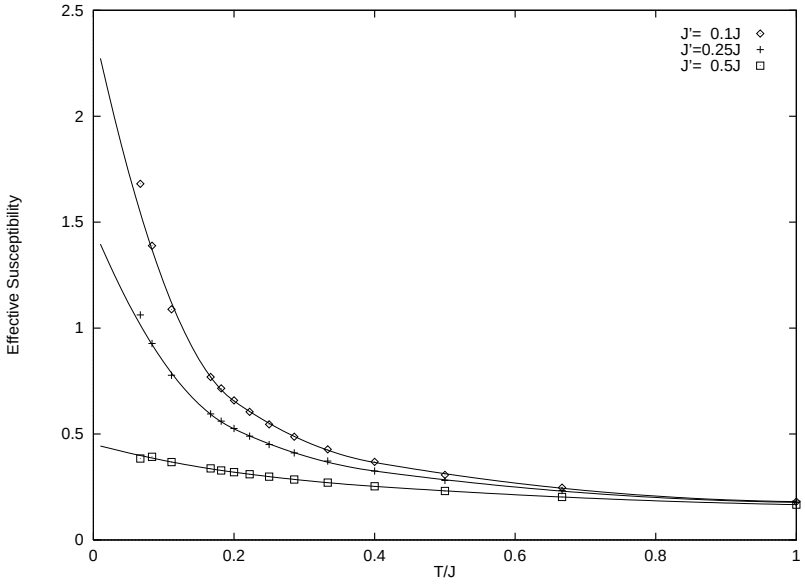

Figure 6.60: The effective normalized susceptibility in a powdered sample for strong perturbations on two links and $d_\perp = 1$ as a function of temperature.

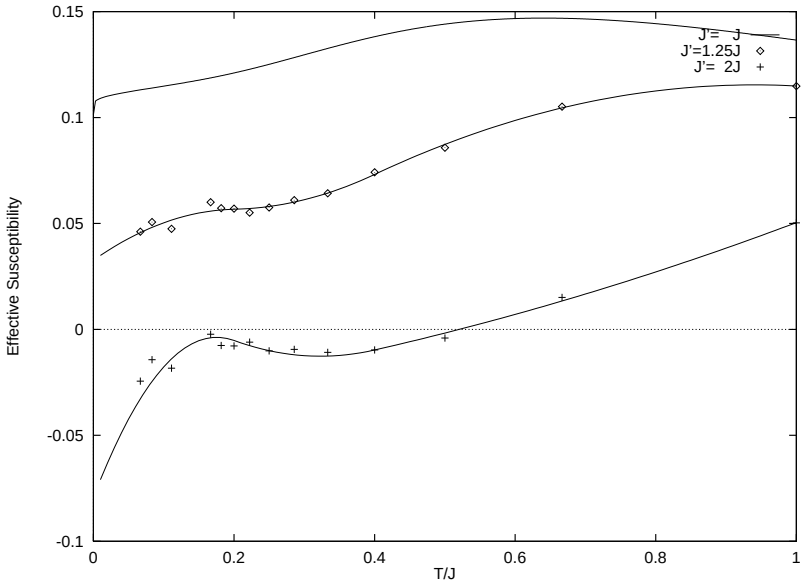

Figure 6.61: The effective normalized susceptibility in a powdered sample for two strengthened links and $d_\perp = 0.5$ as a function of temperature.

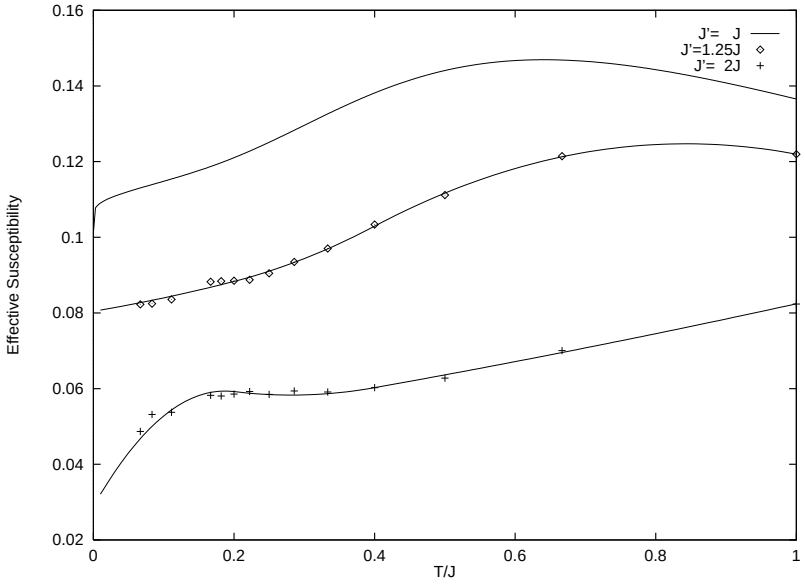

Figure 6.62: The effective normalized susceptibility in a powdered sample for two strengthened links and $d_\perp = 1$ as a function of temperature.

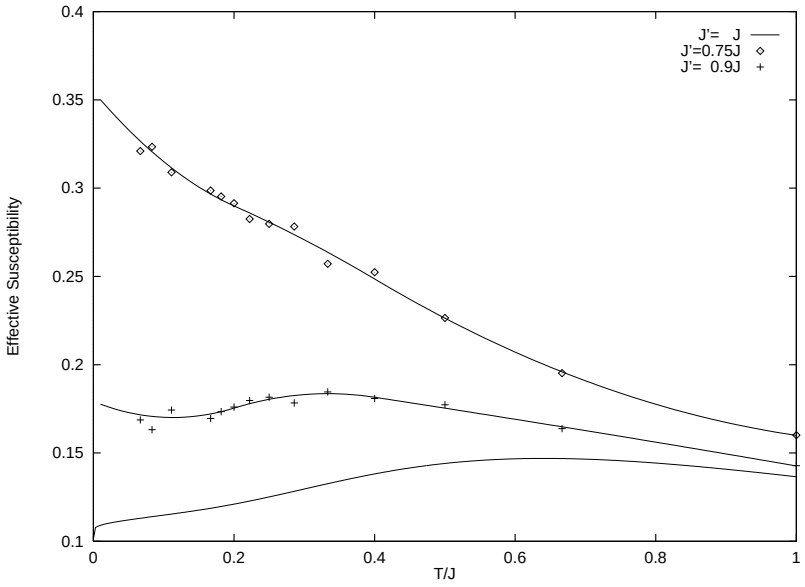

Figure 6.63: The effective normalized susceptibility for an applied field perpendicular to the chain, small perturbations on two links and $d_\perp = 0.5$ as a function of temperature.

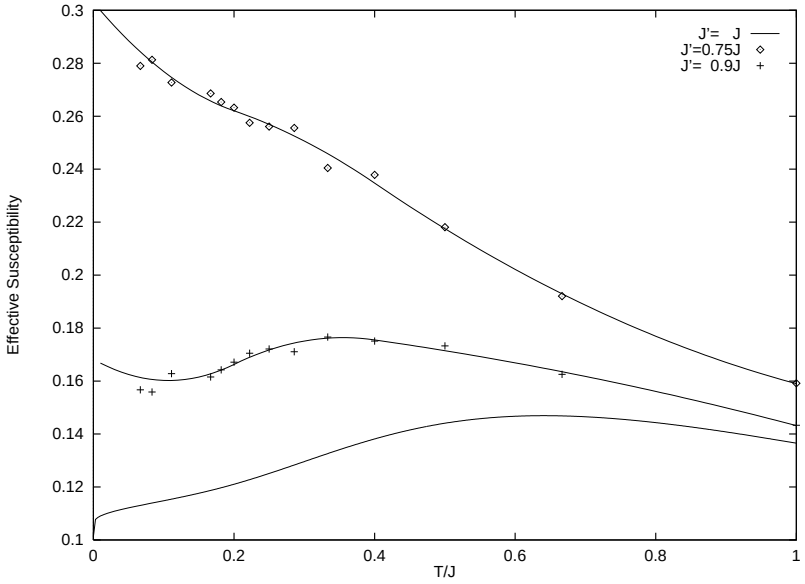

Figure 6.64: The effective normalized susceptibility for an applied field perpendicular to the chain, small perturbations on two links and $d_\perp = 1$ as a function of temperature.

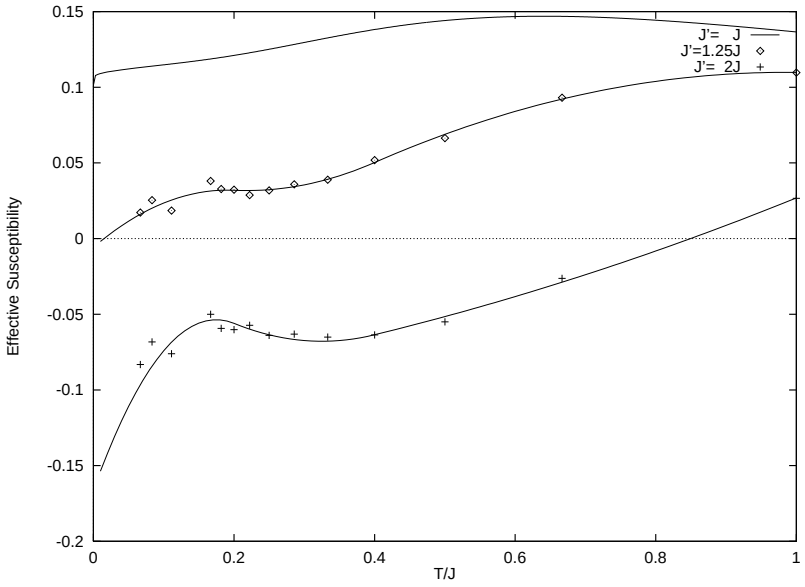

Figure 6.65: The effective normalized susceptibility for an applied field perpendicular to the chain, two strengthened links and $d_\perp = 0.5$ as a function of temperature.

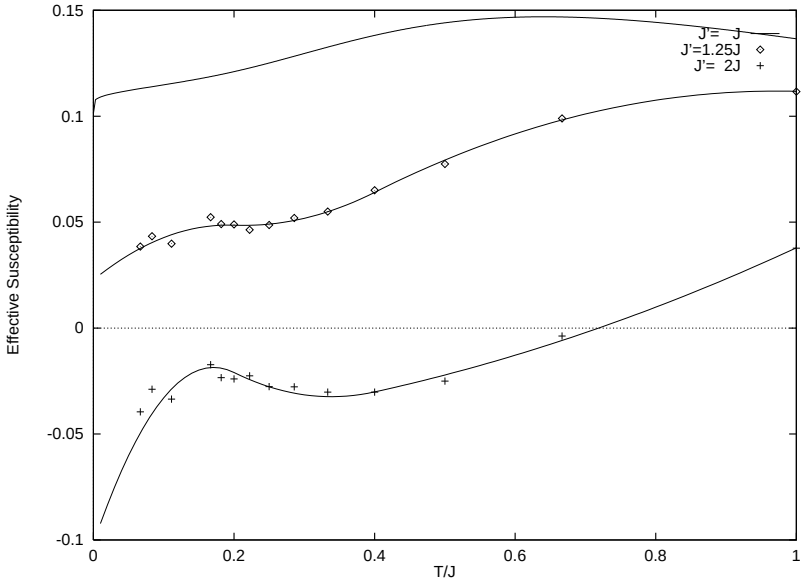

Figure 6.66: The effective normalized susceptibility for an applied field perpendicular to the chain, two strengthened links and $d_\perp = 1$ as a function of temperature.

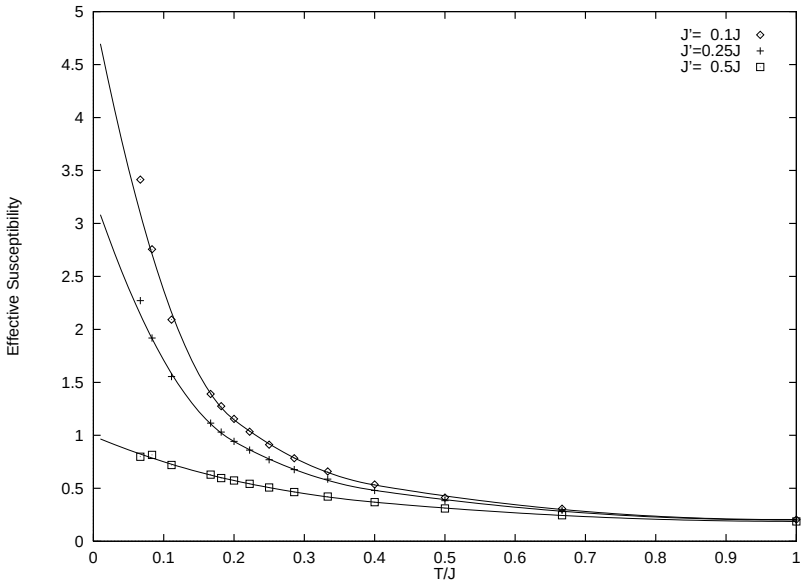

Figure 6.67: The effective normalized susceptibility for an applied field perpendicular to the chain, strong perturbations on two links and $d_\perp = 0.5$ as a function of temperature.

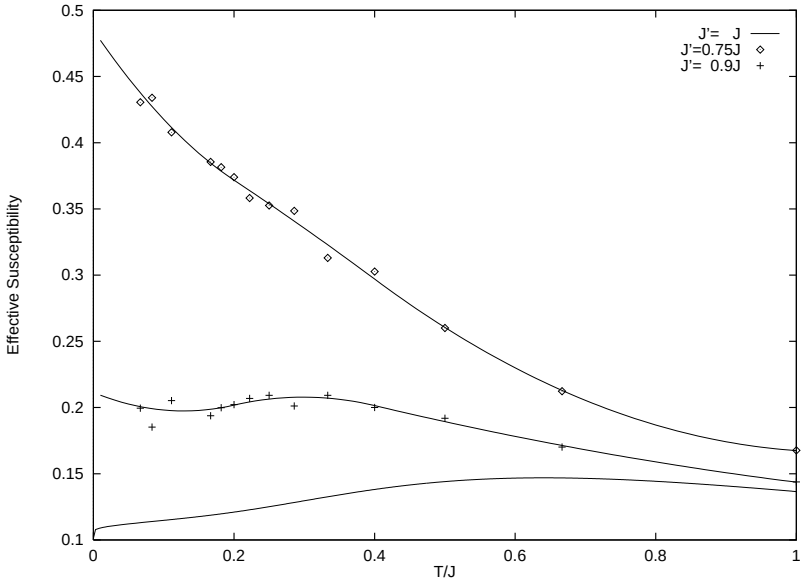

Figure 6.68: The effective normalized susceptibility for an applied field parallel to the chain, small perturbations on two links and $d_\perp = 0.5$ as a function of temperature.

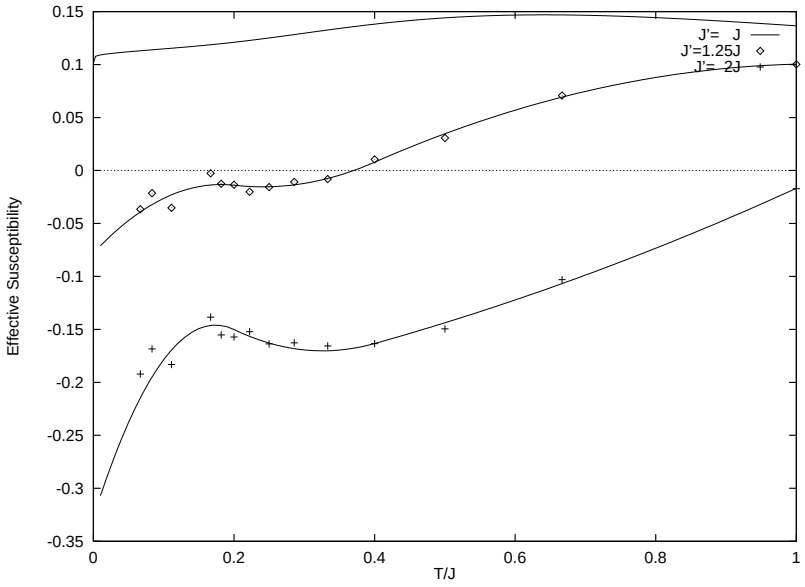

Figure 6.69: The effective normalized susceptibility for an applied field parallel to the chain, two strengthened links and $d_\perp = 0.5$ as a function of temperature.

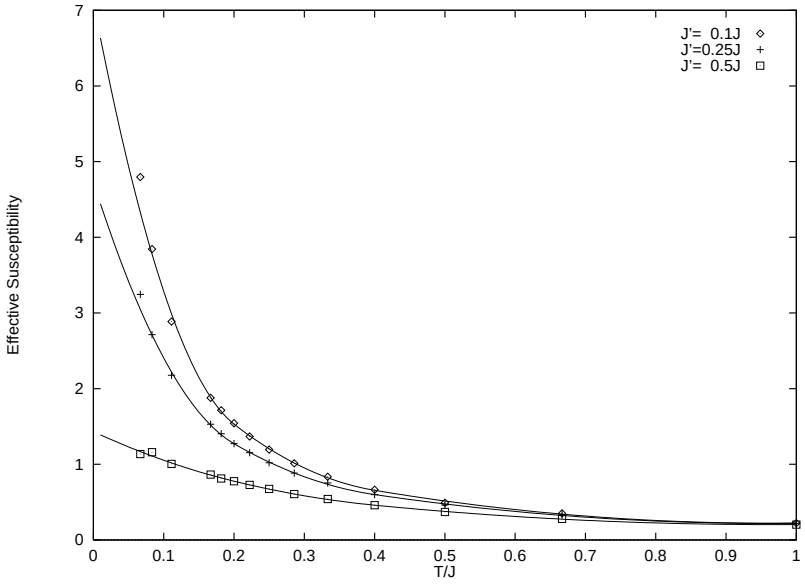

Figure 6.70: The effective normalized susceptibility for an applied field parallel to the chain, strong perturbations on two links and $d_\perp = 0.5$ as a function of temperature.

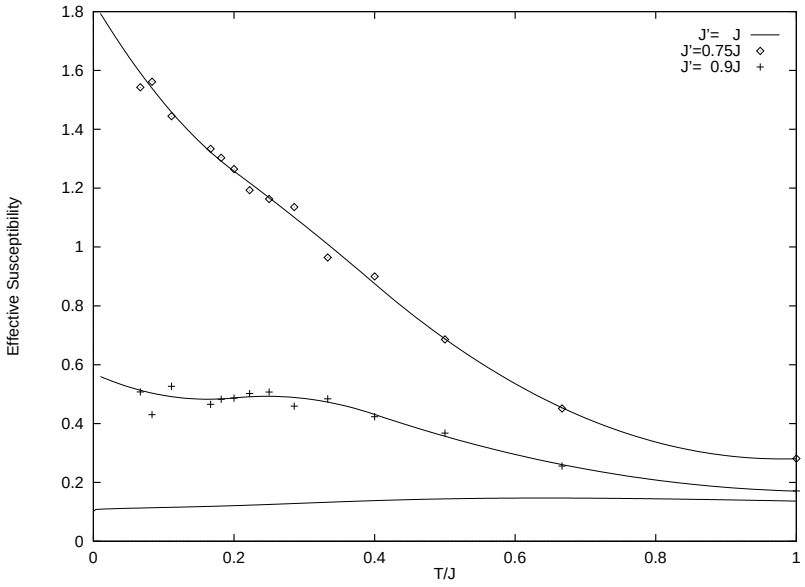

Figure 6.71: The effective normalized susceptibility for an applied field parallel to the chain, small perturbations on two links and $d_\perp = 1$ as a function of temperature.

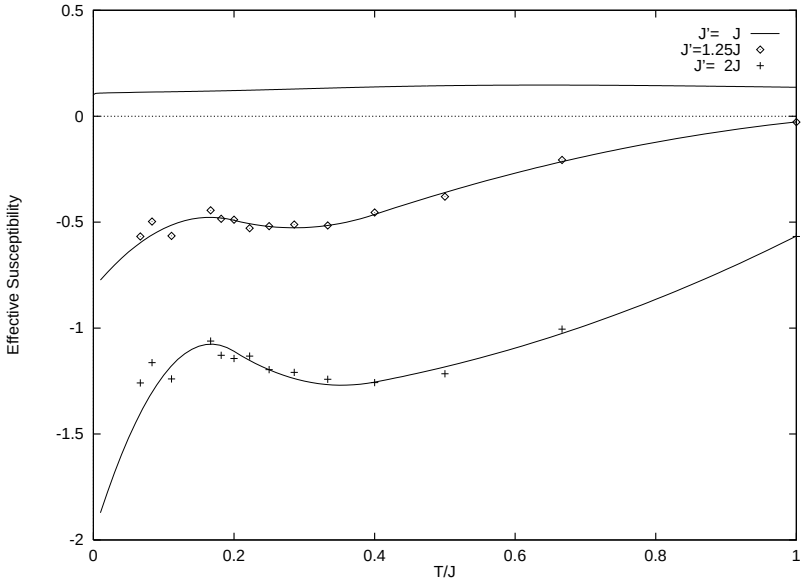

Figure 6.72: The effective normalized susceptibility for an applied field parallel to the chain, two strengthened links and $d_\perp = 1$ as a function of temperature.

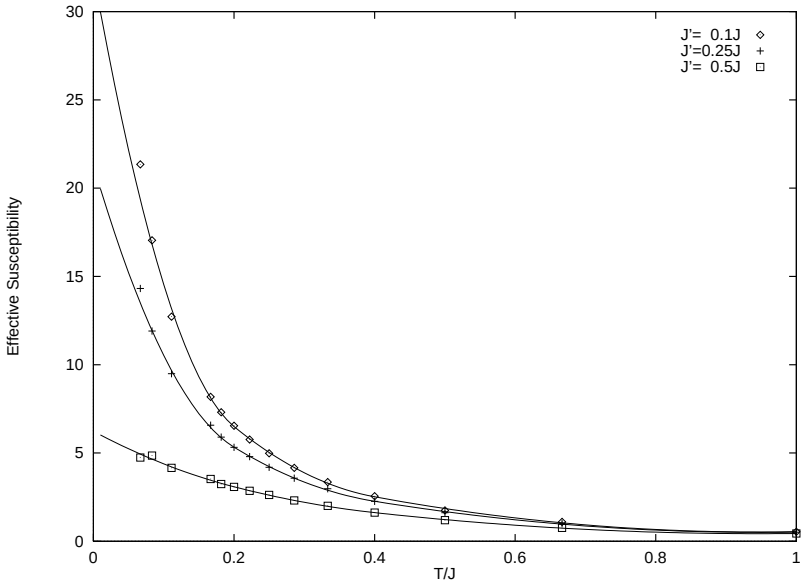

Figure 6.73: The effective normalized susceptibility for an applied field parallel to the chain, small perturbations on two links and $d_\perp = 1$ as a function of temperature.

that the numerical simulations of our generic models will be able to describe the expected signal in full detail. However, we are confident that our Monte Carlo data provides a rough quantitative estimate of the effects and describes the generic renormalization behavior, which seems to depend only on the symmetry properties of the perturbation (e.g. the shift of the maximum and the increase of the signal can most likely be observed for most any link symmetric weakening of links in the chain.) The Monte Carlo simulations can be extended for any material once the location of the muon and its effect on the chain have been estimated.

The main conclusion which can be drawn from the field theory analysis as well as from the numerical simulations is the fact that impurities have a surprisingly large effect on the susceptibility in these one-dimensional systems. The impurity effects on the measured Knight shift for a muon in the chain are of the same order of magnitude as the unperturbed susceptibility and may even dominate the signal. On the other hand, in μSR experiments on higher dimensional magnetic compounds the impurity effect of the muon is neglected in most cases.

Appendix A

Field Theory Formulas

In this appendix we would like to give a short summary of the central (1+1) dimensional field theory formulas, which have been used in this thesis. These formulas are explained and derived in references [18] and [40] in a pedagogical way. Reference [10] may also be of some use. We will *not* attempt to reproduce the derivation in a compressed form, since it is not possible without assuming a common background.

Green's functions of left- and right-movers always separate into a product, unless they are related by a boundary condition. We can therefore look at the expressions for left- and right-movers separately and simply add the scaling dimensions $d = d_L + d_R$. The two-point boson Green's function can be calculated directly from the infinite length mode expansion:

$$\begin{aligned} \langle \phi_L(x,t)\phi_L(0,0)\rangle &= -\frac{1}{4\pi}\ln i(x+vt) + \text{const.} \\ \langle \phi_R(x,t)\phi_R(0,0)\rangle &= -\frac{1}{4\pi}\ln i(x-vt) + \text{const.}, \end{aligned} \tag{A.102}$$

where the constant is cutoff dependent. The Green's function for the boson derivative is given by the second derivative of equation (A.102)

$$\begin{aligned} \left\langle \frac{\partial\phi_L}{\partial x}(x,t)\frac{\partial\phi_L}{\partial x}(0,0)\right\rangle &= -\frac{1}{4\pi(x+vt)^2} \\ \left\langle \frac{\partial\phi_R}{\partial x}(x,t)\frac{\partial\phi_R}{\partial x}(0,0)\right\rangle &= -\frac{1}{4\pi(x-vt)^2} \end{aligned} \tag{A.103}$$

so that the usual fermion current scaling dimension $d = 1$ is recovered. Equation (A.102)

also implies a scaling dimension of $d_L = \gamma^2/8\pi$ for $e^{i\gamma\phi_L}$, since

$$\begin{aligned}\left\langle e^{i\gamma\phi_L(x,t)}e^{-i\gamma\phi_L(0,0)}\right\rangle &\propto \left\langle :e^{i\gamma[\phi_L(x,t)-\phi_L(0,0)]}:\right\rangle e^{\gamma^2\langle\phi_L(x,t)\phi_L(0,0)\rangle} \\ &\propto e^{-\ln i(x+vt)\gamma^2/4\pi} = \left(\frac{-i}{x+vt}\right)^{\gamma^2/4\pi} \end{aligned} \tag{A.104}$$

which is in complete agreement with bosonization in equation (2.9) and fermionic Green's functions. This equation can be generalized to

$$\langle e^{i\sum_j \gamma_j\phi_L(z_i)}\rangle \propto \prod_{j\neq k}\left(\frac{-i}{z_j - z_k}\right)^{\gamma_j\gamma_k/8\pi}, \tag{A.105}$$

where $z_i = x_i + vt_i$. This relation is useful for equation (3.35). We also see that single powers of $e^{i\gamma\phi_L}$ have a vanishing expectation value.

From equation (2.10) it is clear that the commutator of the left- and right-moving bosons is $i/4$ which is essential for the bosonization formulas (2.9) to work. For fixed boundary conditions the commutation relation is modified at the origin because left- and right-movers are related there. It takes some careful analysis of the finite length mode expansion in equation (3.48) to obtain the correct value of the commutator at the boundary. This calculation has been done by Eugene Wong (unpublished), and the results are

$$\begin{aligned}[\phi_L,\phi_R] = \;& 0, && x = y = 0 \\ & \tfrac{i}{2}, && x = y = l \\ & \tfrac{i}{4}, && \text{else}\end{aligned} \tag{A.106}$$

Conformal transformations are represented by analytic functions in the complex plane $\omega(z)$, and chiral primary operators $\mathcal{O}_L$ are defined as operators which transform as

$$\mathcal{O}_L(z) \to \left(\frac{d\omega}{dz}\right)^{d_L}\mathcal{O}_L(\omega), \tag{A.107}$$

where d_L is the scaling dimension of $\mathcal{O}_L$. In this sense conformal transformations generalize scale transformations, Lorentz transformations and translations all of which can be represented by an analytic function $\omega(z)$ in the complex plane for (1+1) dimensions. One application of equation (A.107) is the the transformation $\omega(z) = e^{2\pi z/v\beta}$ which gives the well known result in equation (5.64) for finite temperature correlation functions. Note, that ω is periodic in imaginary time with radius β.

Conformal invariance dictates a unique form for three-point Green's functions of primary operators

$$\left\langle \mathcal{O}_1^L(z_1)\mathcal{O}_2^L(z_3)\mathcal{O}_3^L(z_3)\right\rangle \;\propto\; (z_1-z_2)^{-(d_1+d_2-d_3)}(z_1-z_3)^{-(d_1+d_3-d_2)}(z_2-z_3)^{-(d_2+d_3-d_1)} \tag{A.108}$$

where d_i, $i = 1, 2, 3$ are the scaling dimensions of the three primary operators $\mathcal{O}_i^L$ and $z_i = x_i + vt_i$.

Appendix B

Exact Diagonalization Algorithm

The algorithm we used starts from a normalized initial trial vector Ψ_1 and successively minimizes the energy expectation value in each iteration step by forming the linear combination $\tilde{\Psi}_2 = b\Psi_1 + H\Psi_1$. The explicit formulae are

$$b = \frac{1}{2\Delta_2}(\Delta_3 - \sqrt{\Delta_3^2 + 4\Delta_2\Delta_4}), \tag{B.109}$$

so that the normalized improved ground state is given by

$$\Psi_2 = \frac{b\Psi_1 + H\Psi_1}{(b^2 + 2b\langle H\rangle + \langle H^2\rangle)^{\frac{1}{2}}}. \tag{B.110}$$

where

$$\begin{aligned} \Delta_2 &= \langle H^2\rangle - \langle H\rangle^2 \\ \Delta_3 &= \langle H\rangle\langle H^2\rangle - \langle H^3\rangle \\ \Delta_4 &= \langle H^2\rangle^2 - \langle H\rangle\langle H^3\rangle \end{aligned} \tag{B.111}$$

Here, we used the notation $\langle H^n\rangle = \langle \Psi_1 | H^n | \Psi_1\rangle$. The new energy expectation value is given by

$$\langle \Psi_2 | H | \Psi_2\rangle = \langle H\rangle - \frac{\sqrt{\Delta_3^2 + 4\Delta_2\Delta_4}}{b^2 + 2b\langle H\rangle + \langle H^2\rangle} \tag{B.112}$$

The algorithm terminates when we are close enough to the ground state so that the energy cannot be lowered much further. Clearly, all symmetries of Ψ_1 are preserved in each step, so the algorithm can be used to find ground states in different sectors of H, which are characterized by convenient quantum numbers.

We decided to work in the orthonormal S_z-basis because the next nearest neighbor coupling requires excessive computations in the valence bond basis[41], which keeps track of the total spin. The basis states can be represented by integer bit strings, and the Hamiltonian was implemented as a procedure that manipulates and then stores the bit strings and their coefficients as they are created. For numerical convenience we used the Exchange Hamiltonian, which differs by a factor of two and a constant from the Heisenberg Hamiltonian in equation (1.1) with $J = J_z$. The various tricks to optimize the algorithm include a hashing technique[15], extrapolation to the exact ground state, and reusing previously created information on how to update basis states. The resulting ground state can be used as an initial starting state for a similar Hamiltonian with only slightly modified parameters. The extrapolation is based on the fact that the actual ground state energy is approached exponentially and simply uses the last three iteration values to find an improved result. This can give reliably at least two more digits accuracy.

In all problems the translational invariance is broken by the impurity. Taking into account the limited remaining available symmetries of our problem, we can handle only about 22 sites on a SUN workstation (about 8 sites less than what can be done for a periodic chain in the valence bond basis). Some calculations were done on a NEC SX3/44 supercomputer because supercomputers generally allow for about four more sites. Working in the valence bond basis with $s = 0$ and using translational and parity invariance we can find the exact ground state to 8 digits accuracy of a periodic chain of 24 sites in only 15 seconds CPU time on a NEC SX3/44 supercomputer. This needs to be compared to 20 min CPU time on a SPARCstation2 when working in the S_z-basis on the same problem.

Appendix C

Monte Carlo Algorithm

The goal is to make predictions of measurements of physical quantities expressed in terms of quantum mechanical operators at finite temperatures. The expectation value of any operator A is given in terms of the partition function $Z = \sum_k \langle k|e^{-\beta H}|k\rangle$:

$$\langle A\rangle \;=\; \frac{\sum_k \langle k|Ae^{-\beta H}|k\rangle}{Z} \tag{C.113}$$

where the sum is over all basis states $|k\rangle$ of the system and $\beta = 1/T$. For example, the local susceptibility at site i would be given by:

$$\chi_i \;=\; \beta\frac{\sum_k \langle k|\sum_j S_j^z S_i^z e^{-\beta H}|k\rangle}{Z} \;=\; \beta\langle\sum_j S_j^z S_i^z\rangle \tag{C.114}$$

To calculate these sums exactly, we would first need to diagonalize H in the Hilbert space to express $\exp(-\beta H)$ and then sum over all eigenstates. Since the dimension of the Hilbert space grows exponentially with the system size l, the exact diagonalization of H cannot be done for more than $N \approx 30$ spins as indicated in appendix B. In addition we would have to sum over all eigenvalues to get a finite temperature expression.

To get around this problem of large Hilbert spaces we use the quantum Monte Carlo method. We first transform the expression in equation (C.113) so that the exponential of the Hamiltonian can be evaluated approximately by use of the Trotter formula. We can split the Hamiltonian (1.1) into two parts $H = H_e + H_o$, where the two parts involve only the links $\vec{S}_i \cdot \vec{S}_{i+1}$ with i even or odd, respectively. The two parts are easily diagonalized separately, but they do not commute. Although $\exp(-\beta H) \neq \exp(-\beta H_e)\exp(-\beta H_o)$,

we can write an approximate (Trotter) formula for the expression in (C.113):

$$\langle k|Ae^{-\beta H}|k\rangle \approx \tag{C.115}$$
$$\sum_{l_i}\langle k|Ae^{-2\beta H_e/m}|l_1\rangle\langle l_1|e^{-2\beta H_o/m}|l_2\rangle\langle l_2| \ldots\ldots |l_{m-1}\rangle\langle l_{m-1}|e^{-2\beta H_o/m}|k\rangle$$

This approximation becomes exact in the limit $m \to \infty$. We have inserted $m-1$ complete set of states $|l_i\rangle$ between each of the exponentials and we have to sum over all possible combinations. While it is now relatively easy to compute the exponentials, we now have the formidable task of summing over $(2^N)^m$ possible configurations. Here we make use of the principle of Monte Carlo integration: we statistically evaluate the sum by randomly summing expression (C.115) over a lot of different configurations $|l_i\rangle$ and assume that the average value will give us a good estimate of the complete sum.

This method is assisted by the fact that most configurations give a zero contribution because the expectation values $\langle l_i|e^{-\beta H}|l_{i+1}\rangle$ are only non-zero for states that obey certain selection rules. In fact we can evaluate the sums by going between allowed configurations by using "moves" in configuration space which explicitly obey the selection rules. By just using two different "moves" we can reach any allowed configuration, which is sufficient to assure a complete sampling.

Furthermore, by assigning each "move" from an *old* configuration to a *new* one a probability which is proportional to the change in the exponential

$$\frac{\langle \text{new}_i|e^{-\beta H}|\text{new}_{i+1}\rangle}{\langle \text{old}_i|e^{-\beta H}|\text{old}_{i+1}\rangle}$$

we automatically take care of evaluating the expression (C.115) without having to weigh each contribution separately. This method is called importance sampling. The physical idea is that the system spends most time in configurations for which the partition function Z is large. After a certain number of moves we can make a "measurement" of a quantity by applying the corresponding operator A on the given configuration. Successive

measurements may not be completely independent of each other unless a large number of moves have been made. Just like in a physical system, the measurement of a quantity A has a statistical distribution, and the mean would correspond to the expectation value $\langle A \rangle$ in equation (C.113).

The only approximation we have made corresponds to equation (C.115), where a larger m will yield better results. Fortunately, it is known[42] that the measurements of $\langle A \rangle$ will have a leading correction of order $1/m^2$, so that we can extrapolate analytically to the infinite m limit. This result follows directly from the accuracy of the Trotter formula itself.

On the computer this method is implemented in a very straightforward way. As indicated in equation (C.115) a complete configuration consists of m states, each of which has N spins which can point up or down. A complete configuration is therefore simply represented by an $N \times m$ array of boolean variables ("spins"). We select two possible moves: local and global. The local move may flip 4 adjacent spins depending on their configuration, and the global move may flip all spins at a given site, but for all m states simultaneously. The probabilities of these moves are known for a given temperature $T = 1/\beta$, and a good random number generator determines if a possible move will be executed. To derive the detailed nature of the moves and probabilities it takes some straightforward, but lengthy analysis of the physical system. This is omitted here because it is rather technical and not important for the understanding of the method. For more details see for example reference [42].

The update of the array is done in "sweeps" which consist of offering moves at all possible locations in the array. The actual measurements of χ_i from equation (C.114) take less time and are done after each sweep. Good results at lower temperatures require larger arrays (generally $2m \approx N > 10J/T$ is a good estimate). Typically the array has dimensions of $N = 48 - 128$ by $m = 24 - 64$. Both m and N are even numbers, because

periodic boundary conditions in the m direction are required. The number of offered moves per sweep is roughly given by $m \times N$.

Starting from any allowed configuration, a few thousand sweeps are done to bring the system into equilibrium. To get one good average value we then did 2,000,000 sweeps and measurements for a given array. For a choice of coupling and temperature, 3-5 of those average values have to be taken at different values for m, so that a reasonable extrapolation $m \rightarrow \infty$ can be done. For one measurement point a total of roughly 3×10^{10} moves have to be checked and will be offered if possible. How many of these possible moves will actually be executed strongly depends on the temperature. At higher temperatures moves are more likely to be performed, which results in a faster update and lower statistical errors.

It is obvious that the largest possible number of sweeps is desired, so that statistical errors can be kept to a minimum. For this reason, I ported my program to the vector supercomputer Fujitsu VPX240 of the HPC Centre, Calgary. The sweeps to update the array take most of the computer time, and it is highly desirable to offer and perform the moves in a vectorized way. This is not straight forward, because each move alters the array and this may affect the outcome of a successive move. It took some extensive analysis of the detailed nature of the moves to identify the dependencies, but finally it was possible to separate the array into sublattices, so that all moves can be offered and performed in vectorized loops.

Bibliography

[1] H. Bethe, Z. Physik, 71, 205 (1931)

[2] C.N. Yang, C.P. Yang, Phys. Rev. 50, 327 (1966).

[3] M. Takahashi, Prog. Theor. Phys. 46, 401 (1971); M. Takahashi, Phys. Rev. B43, 5788 (1990).

[4] K. Hirikawa, Y. Kurogi, Prog. Theor. Phys. 46, 147 (1970).

[5] CPC refers to "dichloro*bis*(pyridine)copper(II)" which has been studied by W. Duffy, Jr., J.E. Venneman, D.L. Strandburg, P.M. Richards, Phys. Rev. B9, 2220 (1974).

[6] Y. Imry, P. Pincus, D. Scalapino, Phys. Rev. B11, 1978 (1975).

[7] C.A. Doty, D. Fisher, Phys. Rev. B45, 2167 (1992); D. Fisher, unpublished notes.

[8] For a summary of various applications of boundary critical phenomena and earlier references see I. Affleck, "Conformal Field Theory Approach to Quantum Impurity Problems" preprint (1993), (Sissa preprint server number: cond-mat 9311054).

[9] S. Eggert, I. Affleck, Phys. Rev. B 46, 10866, (1992).

[10] For a review of the conformal field theory treatment of the spin-1/2 chain and earlier references see I. Affleck, *Fields, Strings and Critical Phenomena* (ed. E. Brézin and J. Zinn-Justin North-Holland, Amsterdam, 1990), p.563.

[11] E. Lieb, T. Schultz, D. Mattis, Ann. Phys. (N.Y.) 16, 407 (1961).

[12] J. des Cloiseaux, M. Gaudin J. Math. Phys. 7, 1384 (1966); R.J. Baxter, Ann. Phys. (N.Y.) 70, 193 (1972).

[13] A. Luther, I. Peschel, Phys. Rev. B12, 3908 (1975).

[14] B.M. Coy, Phys. Rev. 173, 531 (1968).

[15] E.R. Gagliano, E.D. Moreo, A. Moreo, F.C. Alcarez, Phys. Ref. B34, 1677 (1986).

[16] S. Liang, Phys. Rev. Lett., 64, 1597 (1990).

[17] K. Wilson, *Proceedings of the Midwest Conference on Theoretical Physics* (Notre Dame, April 1970), p.131.

[18] P. Ginsparg, *Fields, Strings and Critical Phenomena* (ed. E. Brézin and J. Zinn-Justin North-Holland, Amsterdam, 1990).

[19] I. Affleck, D. Gepner, H.J. Schulz, T. Ziman, J. Phys. A22, 511, (1989).

[20] F.D.M. Haldane, Phys. Rev. Lett. 60, 635 (1988).

[21] F.C. Alcarez, M.N. Barber, M.T. Batchelor, Phys. Rev. Lett. 58, 771 (1987); I. Affleck, J.B. Marston, J. Phys.C21, 2511 (1988).

[22] F.C. Alcarez, M. Baake, U. Grimm, V. Rittenberg, J. Phys. A21, L117 (1988).

[23] C.L. Kane, M.P.A. Fisher, Phys. Rev. Lett. 68, 1220 (1992).

[24] C.L. Kane, M.P.A. Fisher, Phys. Rev. B46, 15233, (1992).

[25] D. Clarke, T. Giamarchi, B. Shraiman, Phys. Rev. B48, 7070 (1993).

[26] P. Nozières, A. Blandin, J. de Phys. (Paris), 41, 193 (1980).

[27] I. Affleck, A.W.W. Ludwig, Phys. Rev. Lett. 68, 1046 (1992).

[28] I. Affleck, A.W.W. Nucl. Phys. B360, 641 (1991).

[29] I. Affleck, Phys. Rev. Lett. 56, 2763 (1986).

[30] S. Eggert, I. Affleck, M. Takahashi, Phys. Rev. Lett. 73, 332 (1994).

[31] J.C. Bonner, M.E. Fisher, Phys. Rev. 135, A640 (1964).

[32] I. Affleck, Nucl. Phys. B336, 517 (1990).

[33] See, for example P. Nozières, Proceedings of the 14^{th} Int.'l Conf. on Low Temp. Phys. (ed. M. Krusius and M. Vuorio, North Holland, Amsterdam, 1974) V.5, p. 339. and references therein; N. Andrei, Phys. Rev. Lett. 45, 773 (1980); P.B. Wiegmann, JETP Lett. 31, 364 (1980); P.W. Anderson, J. Phys. C3, 2346 (1970); K.G. Wilson, Rev. Mod. Phys. 47, 773 (1975).

[34] N. Andrei, C. Destri, Phys. Rev. Lett. 52, 364 (1984); P.B. Wiegmann, A.M. Tsvelick, J. Phys. C18, 159 (1985).

[35] A.W.W. Ludwig, I. Affleck, Phys. Rev. Lett., 67, 3160 (1991).

[36] TRIUMF Research Proposal, "Quantum Impurities in One Dimensional Spin 1/2 Chains" (1994), Spokesperson: R. Kiefl, Group members: I. Affleck, J.H. Brewer, K. Chow, S. Dunsinger, S. Eggert, A. Keren, R.F. Kiefl, A. MacFarlane, J. Sonier, Y.J. Uemura.

[37] R.F. Kiefl, G.M. Luke, S.R. Kreitzman, M. Celio, R. Keitel, J.H. Brewer, D.R. Noakes, Y.J. Uemura, A.M. Portis, V. Jaccarino, Phys. Rev. B35, 2079 (1987).

[38] J.H. Brewer, S.R. Kreitzman, D.R. Noakes, E.J. Ansaldo, D.R. Harshman, R. Keitel, Phys. Rev. B33, 7813 (1986).

[39] M.F. Collins, V.K. Tondon, W.J.L. Buyers, Intern. J. Magnetism 4, 17 (1973).

[40] R. Shankar, Summer Course on Low-Dimensional Quantum Field Theories For Condensed Matter Physicists, ICTP, Trieste, 24 August - 4 September 1992.

[41] For a review of the valence bond basis see: K. Chang, I. Affleck, G.W. Hayden, Z.G. Soos, J. Phys. 1, 153 (1989).

[42] M.Marcu, A. Wiesler, J.Phys.A 18, 2479 (1985).